PREPARATION OF CHIRAL ACID-FUNCTIONALIZED SCHIFF-BASE LIGANDS

AND THEIR COMPLEXATION WITH DIVALENT TRANSITION METALS:

THE STORY OF HELICES AND CUBANES

by

AZADEH LALEHZARI

B.S., Mälardalen University, 2002

AN ABSTRACT OF A DISSERTATION

submitted in partial fulfillment of the requirements for the degree

DOCTOR OF PHILOSOPHY

Department of Chemistry
College of Arts and Sciences

KANSAS STATE UNIVERSITY
Manhattan, Kansas

2007

Abstract

A series of chiral symmetrical and unsymmetrical acid-functionalized Schiff-base ligands were synthesized by condensation reactions between 3-formyl salicylic acid and the two diamines (1R,2R)-cyclohexyldiamine (CHDA) and (R)-[1,1'-binapthalene]-2,2'-diamine (BINAM). The addition of a weak base (TEA) to these Schiff-bases resulted in the formation of a partially deprotonated ligand while the addition of the strong base NaOMe, resulted in fully deprotonated ligands. Complexations were carried out using metal salts of Fe(II), Co(II), Ni(II), Cu(II), Cu(I) and Zn(II). The partially deprotonated unsymmetrical Schiff-base (CHDA as the backbone), resulted almost exclusively in the formation of double-stranded helices with M helices. The fully deprotonated ligand, on the other hand, formed cubane-type structures with Fe(II), Co(II) and Ni(II) in methanol. Similar cubane-type structures were also obtained after complexation of the symmetrical CHDA-based ligands with Fe(II) and Co(II) using NaOMe in methanol. Reactions involving Cu(II) and Cu(I) salts resulted in either mono-or dinuclear salen complexes, even if the unsymmetrical Schiff-base was used as the starting ligand. This type of ligand conversion is dependent of the metal salt concentration in the reaction. Unsymmetrical Schiff-base ligands have a higher tendency to undergo conversion to their symmetrical salen analogues if the metal salt is added is much excess.

PREPARATION OF CHIRAL ACID-FUNCTIONALIZED SCHIFF-BASE LIGANDS

AND THEIR COMPLEXATION WITH DIVALENT TRANSITION METALS:

THE STORY OF HELICES AND CUBANES

by

AZADEH LALEHZARI

B.S., Mälardalen University, 2002

A DISSERTATION

submitted in partial fulfillment of the requirements for the degree

DOCTOR OF PHILOSOPHY

Department of Chemistry
College of Arts and Sciences

KANSAS STATE UNIVERSITY
Manhattan, Kansas

2007

Approved by:

Major Professor
Christopher J. Levy

Abstract

A series of chiral symmetrical and unsymmetrical acid-functionalized Schiff-base ligands were synthesized by condensation reactions between 3-formyl salicylic acid and the two diamines (1*R,2R*)-cyclohexyldiamine (CHDA) and (*R*)-[1,1'-binapthalene]-2,2'-diamine (BINAM). The addition of a weak base (TEA) to these Schiff-bases resulted in the formation of a partially deprotonated ligand while the addition of the strong base NaOMe, resulted in fully deprotonated ligands. Complexations were carried out using metal salts of Fe(II), Co(II), Ni(II), Cu(II), Cu(I) and Zn(II). The partially deprotonated unsymmetrical Schiff-base (CHDA as the backbone), resulted almost exclusively in the formation of double-stranded helices with *M* helices. The fully deprotonated ligand, on the other hand, formed cubane-type structures with Fe(II), Co(II) and Ni(II) in methanol. Similar cubane-type structures were also obtained after complexation of the symmetrical CHDA-based ligands with Fe(II) and Co(II) using NaOMe in methanol. Reactions involving Cu(II) and Cu(I) salts resulted in either mono-or dinuclear salen complexes, even if the unsymmetrical Schiff-base was used as the starting ligand. This type of ligand conversion is dependent of the metal salt concentration in the reaction. Unsymmetrical Schiff-base ligands have a higher tendency to undergo conversion to their symmetrical salen analogues if the metal salt is added is much excess.

Table of Contents

List of Figures

List of Tables

Acknowledgements

Dedication

To my grandparents

CHAPTER 1 - Introduction

1.1 Introduction

Chemists constantly try to find ways to mimic the fascinating biological systems surrounding us. One important aspect in succeeding with this task is to increase the knowledge of how different systems tend to form and recognize the forces directing and determining the specific outcomes. Within this understanding lies an increased knowledge of molecular self-assembly,[1-6] metal-ligand complexation[3,7] and disposition of metal binding sites.[8] By mastering these areas, new improved systems related to the fields of catalysis[1,7,9], supramolecular chemistry[5,6,10,11] and bioengineering[3,6] can be achieved.

Generally speaking, metal-ligand complexation depends on three different factors; the nature of the ligand,[8,12-15] the geometrical preferences of the metal[8,13,16,17] center and the solvent polarity/basicity.[18-20] Of these factors, the nature of the ligand has turned out to have the most impact on the self-assembly of the metal-organic products. A ligand system for complexation studies should be easily modified to change its chelating abilities as well as its framework flexibility. Additionally, a relatively uncomplicated ligand synthesis and inexpensive reactants are desired for the investigated system. Salens and related Schiff-base compounds fit the descriptions very well. A condensation reaction between salicylic aldehyde and a diamine yields the tetradentate salen ligand. Condensations of salicylic aldehyde with a monoamine on the other hand result in the formation of a Schiff-base ligand. Both salens and Schiff-bases are well known for being

easily synthesized from inexpensive starting materials.[21] Also, the simple yet extensive reaction conditions promotes the synthesis of a wide variety of Schiff-base compounds with different chelating abilities and framework flexibility.[22-24]

Complexation of salen/Schiff-base ligands has received considerable attention during recent years. As a result, a large pool of unique and interesting metal-organic structures has been established. Though there are many different molecular architectures that can be explored and investigated, the focus of our work has been exploring the coordination chemistry of *acid functionalized* Schiff-base/ salen ligands.

Figure 1.1. General structure of salen and Schiff-base ligands

salen   *Schiff-base*
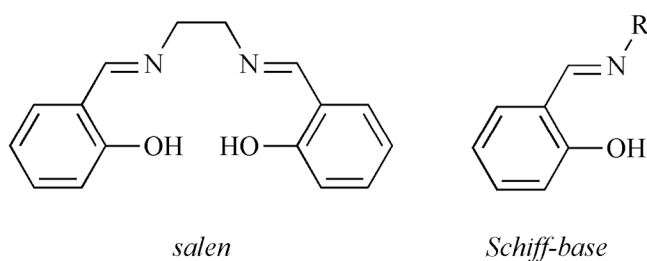
1.2 Macrocyclic complexes

Since the great success of Lehn, Cram and Pedersen in the synthesis of crown-ethers, significant attention has been devoted to the investigation and improvement of these compounds and related systems in the field of host-guest chemistry.[25] Other forms of macrocyclic systems have not received attention to the same degree, though they have shown to be of great use in the understanding of molecular processes in biochemistry, catalysis, encapsulation, transportation and separation chemistry.[24] Systems of particular

interest are Schiff-base and salen based macrocycles. These cycles have excellent abilities in molecular recognition,[24-26,27] catalysis[24,28] and as molecular magnets.[29-31]

Figure 1.2. Schiff-base ligands with host-guest abilities.
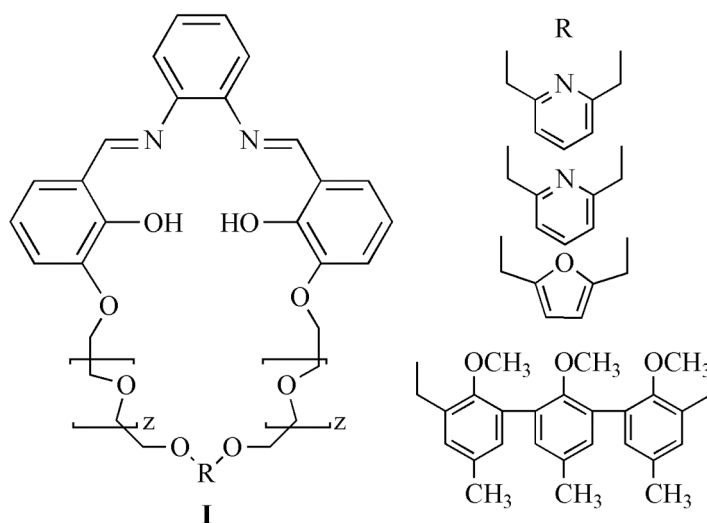
Complex **I** (Figure 1.2) is as an example of a Schiff-base catalyst with host-guest chemistry abilities. The uranyl(VI) complex holds four water molecules, three are located in the cavity and the fourth in the axial position of the metal.[24] Work done by Kim *et al* shows Mn(III) and Co(II) complexes of the Schiff-base macrocycle **II** (Figure 1.3) are catalysts for the asymmetric epoxidation of olefins and borohydride reduction of ketones, respectively.[28] These complexes exhibited a high conversion and a moderate enantioselectivity.

Figure 1.3. Mn(III) and Co(II) complexes of **II** catalyzes asymmetric epoxidation and borohydride reductions.

II
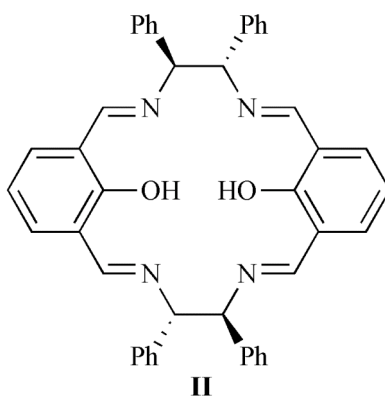
Similar salen macrocycles were also reported by Okawa *et al.* (Figure 1.4).[29-33] Beside the catalytic properties of these salen macrocycles, the magnetic exchange properties of the complexes were also investigated in both homo- and hetero dinuclear complexes.

Figure 1.4. Macrocycles reported by Okawa.
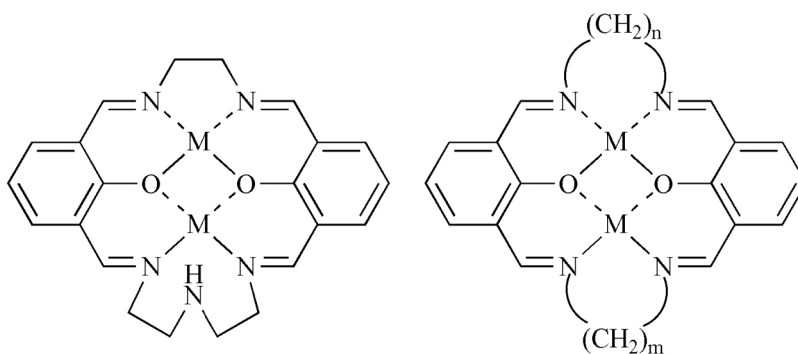
1.3 Acyclic complexes

1.3.1 Diimine complexes

Schiff-base macrocycles and their complexes are relatively rigid since the cyclic configuration does not allow for much fluctuation. Acyclic ligands are less strained and are therefore possess a higher degree if flexibility. Unlike salen based macrocycles, the acyclic salen complexes have been explored extensively in the past decades. With excellent abilities for catalyzing a wide range of both symmetric and asymmetric reactions, the list of examples of salen complexes is long indeed.

Fernandez *et al.* have investigated the Schiff-base Mn(III) complexes **III**, and the effect of the counterions on their dimeric self-assembly.[34] It was shown that chloride and perchlorate anions can induce self-assembly through hydrogen-bonded interactions (Figure 1.5).

Figure 1.5. Stick diagram of salen complex **III** showing hydrogen bonding between $[MnL(H_2O)_2]_2^{2+}$ units through perchlorate anions.
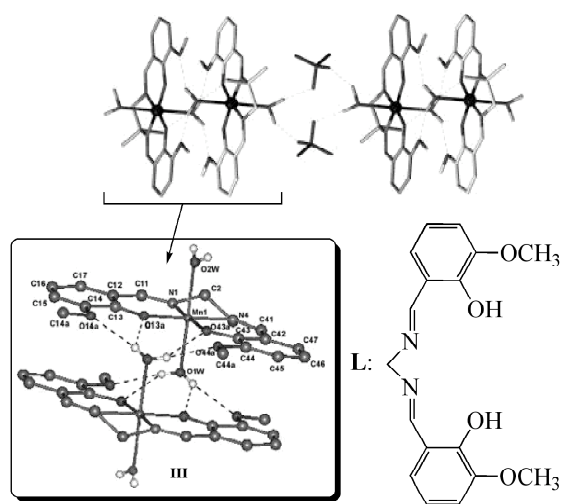
Figure 1.6. Different complexation mode depending on hydrogen bonding ability of the diimine.
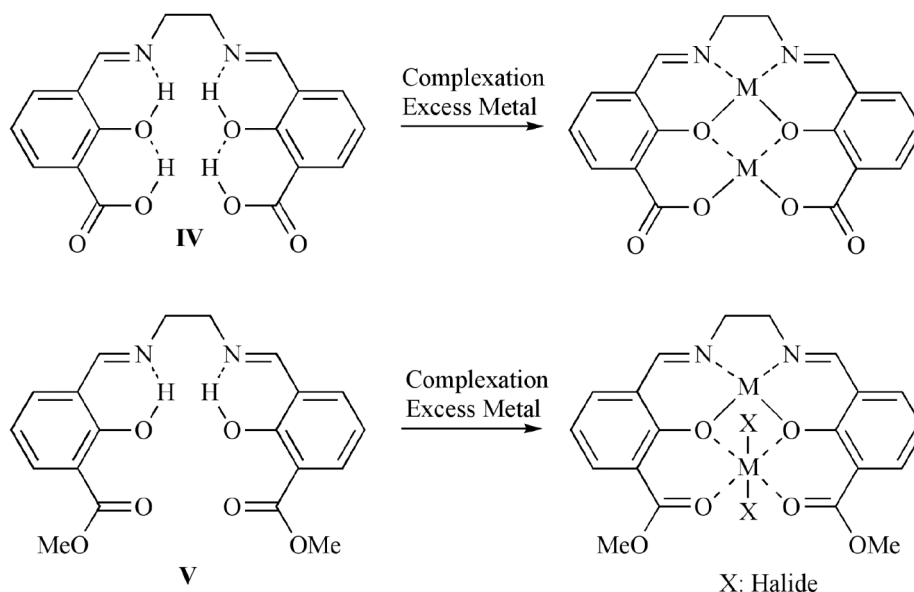
Other examples, illustrating the effects of hydrogen bonding on complexation, can be seen in the two similar ligands **IV** and **V** (Figure 1.6). The acidic hydrogens on the carboxylic moiety in **IV** can participate in further hydrogen bonding while in ligand **V** this bonding is not possible. Though both ligands form dinuclear salen complexes upon complexation with excess metal ions, they will bind in slightly different ways since their deprotonated forms are significantly different. **IV** will bind two metal ions, one in the traditional salen pocket and the second in the O_4-site between the two phenoxide oxygens and the deprotonated oxygens from the carboxylates. **V** will also bind through the salen pocket and an O_4-site. However, the latter is from the oxygens generated from the phenoxide oxygens and the carbonyl oxygens of the ester moiety.[35-36]

In the previous examples the nature of the diamine backbone is a key factor determining the complexation ability of the ligand. Changing the electron donor/acceptance characteristics of the backbone can result in a significant change in the

properties of the salen pocket.[37] Generally speaking, a more electron-donating backbone will increase the reactivity of the chelating pocket as there will be more electron density available for an nucleophilic attack on the (usually) positively charged metal ion. An electron-withdrawing backbone will have the opposite effect. Figure 1.7 shows some examples of salen complexes where the electron-withdrawing BINAM backbone was utilized.[18,38]

Figure 1.7. Salen complexes based on the electron-withdrawing BINAM backbone.
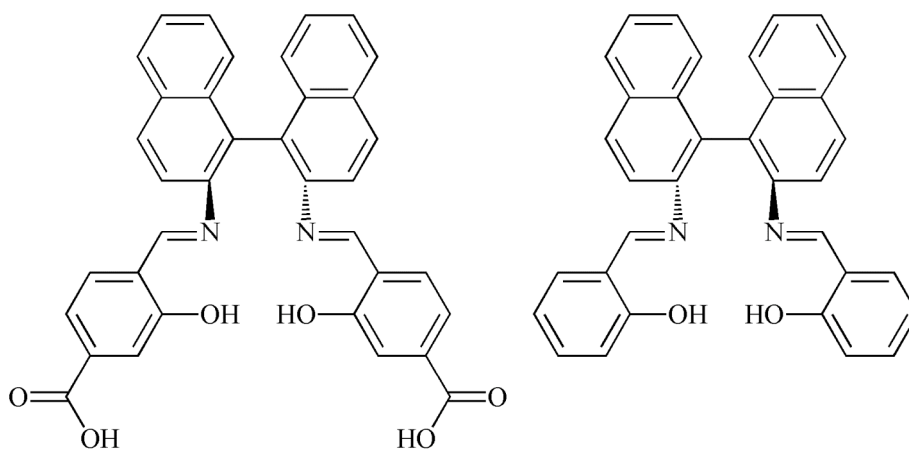
1.3.2 Monoimine complexes

An increased degree of coordination flexibility can be achieved by replacing the salen ligand with a ligand that only has one imine linkage. In general, Schiff-base ligand synthesis results from the condensation of a monoamine and an aldehyde. Although the syntheses of these ligands are very straightforward, they have not being studied as extensively as their diimine analogues. Complexation can result in the formation of both mono- or dinuclear complexes depending on the number of chelating groups provided by

the ligand. Furthermore, in reactions with transition metals, the formed complexes can have either a one or two coordinated ligands (Figure 1.8).[17,20,39-42]

Figure 1.8. General reaction scheme for the formation of monoimine ligands and the synthesis of complexes with one or two coordinating ligands.
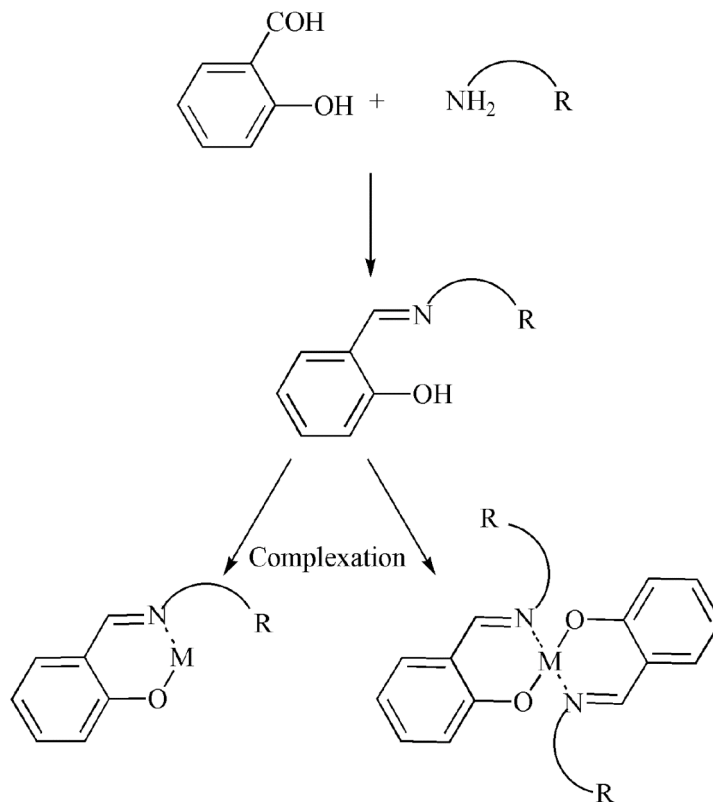
Whether one or two ligands will coordinate to the metal center is highly dependent on the pH of the solution. Erxleben *et al.* have demonstrated that the simple Schiff-base ligand **VI**, can be directed to form both complexes by controlling the reaction pH and solvents (indirect effect on the pK_a's of the functional groups). The two structures are shown in figure 1.9.[20] The reason for the formation of the complex with one coordinated ligand was given to be due to presence of hydrogen bonding between the carboxylic hydrogen and the phenoxide oxygen.

Figure 1.9. Controlling the complexation outcome by changing the pH/solvent.
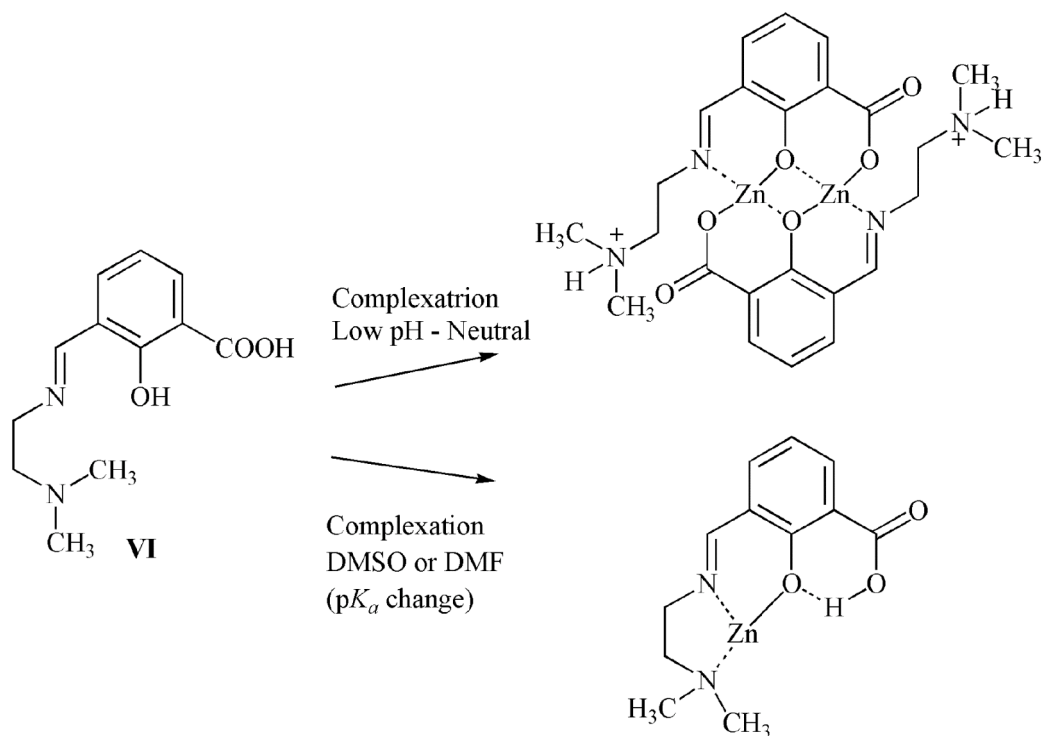
Hydrogen bonding abilities of the ligand have also been shown to have an impact on the orientation of the two ligands. In most cases, the two ligands show a preference toward binding *trans* to each other. However, ligands with hydrogen bonding abilities on either the amine moiety or the carboxylate moiety have been shown to favor the formation of the *cis* isomer. Ligand **VII** will usually bind in a *trans* fashion, however the partially deprotonated ligands have strong preference for hydrogen bonding and will therefore promote the formation of a *cis* configuration (figure 1.10).[43,44]

Figure 1.10. Formation of *cis* or *trans* complexes depending on the hydrogen bonding ability of the deprotonated ligand.
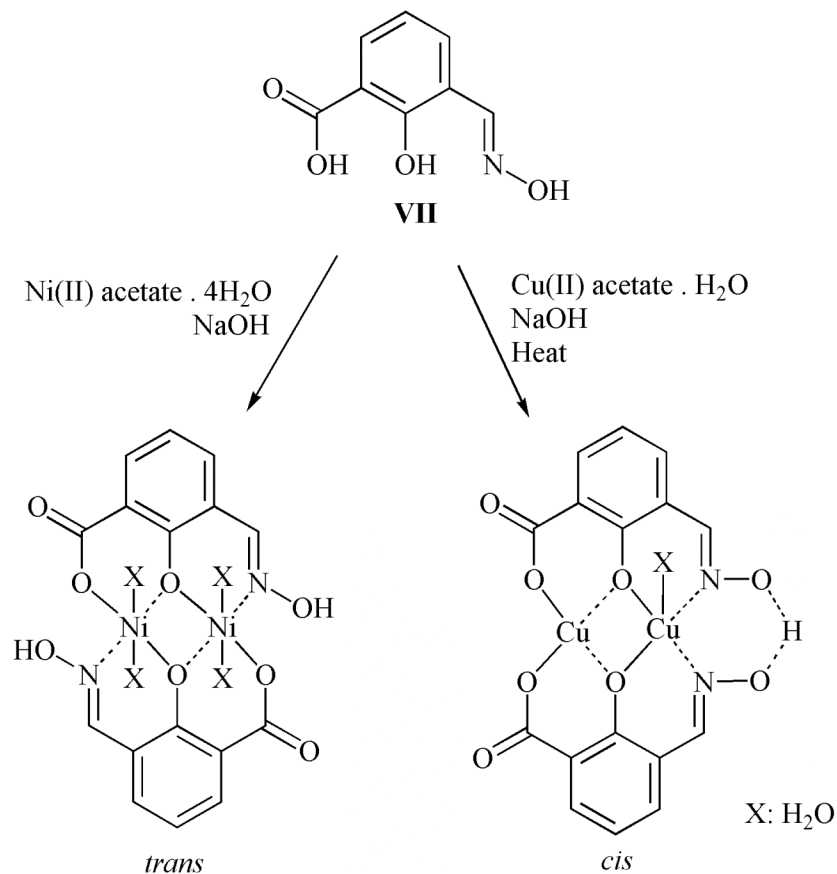
There have been few cases where the imine moiety of the acid-functionalized Schiff-base has an additional chelating group (fourth donor). In these cases, the metals bind in the phenoxide/imine/(fourth donor) pocket of the combined ligands. In **VIII** (Figure 1.11), the fourth donor is a thiol, and the metal binds to the thiol/imine/phenoxide pocket of two adjacent ligands. Usually, the two ligand stands bind *trans* to each other.[45]

Figure 1.11. Acid-functionalized Schiff-base ligands with a thiol as the fourth donor group.

VIII
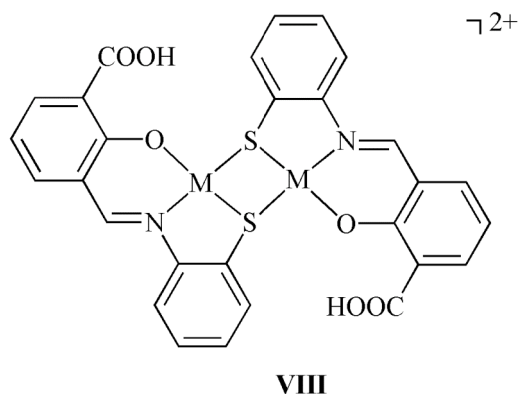
1.3.3 Helicates/ Helices

Helicates are compounds that consist of two or more metal centers. If only one metal center is present in the complex, the systems are referred to as helices or monohelices instead. As the names suggest, these complexes have highly twisted, spiral shaped molecular configuration that can either be left handed (or minus, *M*) or right handed (or plus, *P*).[46] Few classes of compounds have the same impact as helical molecules. In nature, their configuration can be seen in many biological systems (DNA, proteins, enzymes).[47-51] Supramolecular chemists are interested in understanding the self-assembly process of helical formation[49,50] and in catalysis they have been shown to be excellent for asymmetric reactions.[49,50,52]

Of the two forms, helicates are the group that has received most attention. The word helicates was first introduced by John-Marie Lehn in 1987.[49] Though its meaning has changed slightly since then, it initially referred to polymetallic helical complexes with two ligands strands. Over the years, the definition expanded to include both double and

triple stranded polynuclear complexes. The most common form of helicates involves a doubly chelating ligand coordinating to two metal centers (Figure 1.12).[50]

Figure 1.12. Formation of double and triple stranded helicates.

double stranded   *triple stranded*
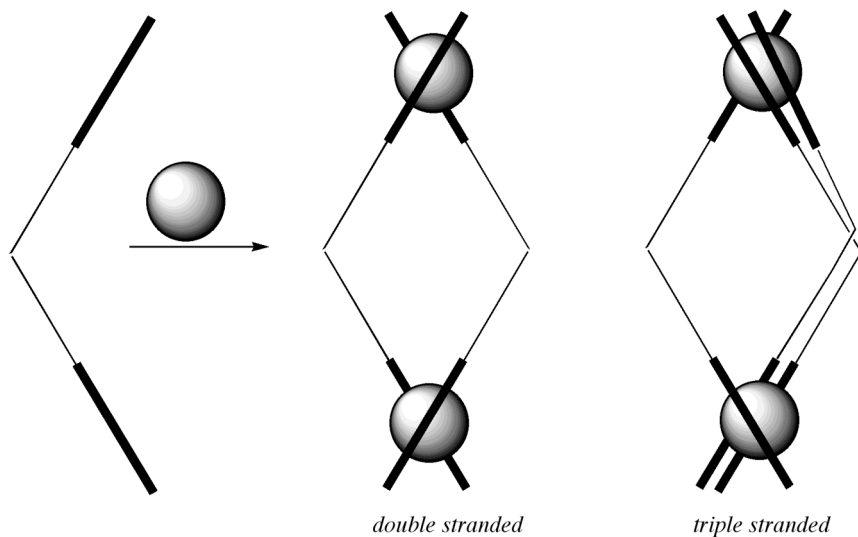
In a similar fashion, two ligand straps can bind to one metal center to form helices (Figure 1.13).

Figure 1.13. Formation of double stranded helices.

double stranded
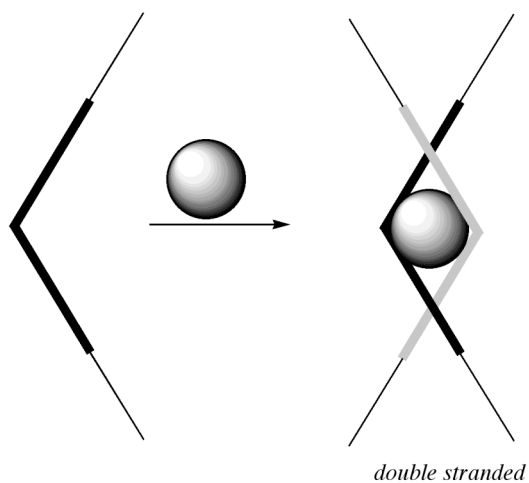
For acid-functionalized Schiff-base complexes, there are only a few cases of complexation resulting in the formation of helical complexes. Most cases give rise to flat dinuclear complexes. In order to achieve a helical structure, the ligand must be either very flexible or have its chelating groups carefully placed to fit the geometry of the metal ion.

1.4 Cubanes

Metal-organic cubanes can be found in nature as the active site of electron-transferring (ET) enzymes.[53] Also, these type of materials are good candidates as single molecule magnets (SMMs).[54-57] Often, four transition metals (usually divalent Mn, Fe, Co, Ni or Zn) are connected through oxygen or nitrogen linkers to form a cube.

Most ligands used in the formation of these cubanes are small oxygen or nitrogen containing compounds. However, there are few examples where a more advanced organic framework has been used to create cubane-like structures (Figure 1.14).[58]

Figure 1.14. Cubane structures of the two Schiff-base ligands sae^{2-} and sap^{2-}.

$$sae^{2-} \xrightarrow[\text{Methanol}]{\text{FeCl}_2 \cdot 4H2O \quad \text{TEA}} [Fe_4(sae)_4(MeOH)_4]$$

$$sap^{2-} \xrightarrow[\text{Methanol}]{\text{FeCl}_2 \cdot 4H2O \quad \text{TEA}} [Fe_4(sap)_4(MeOH)_4]$$
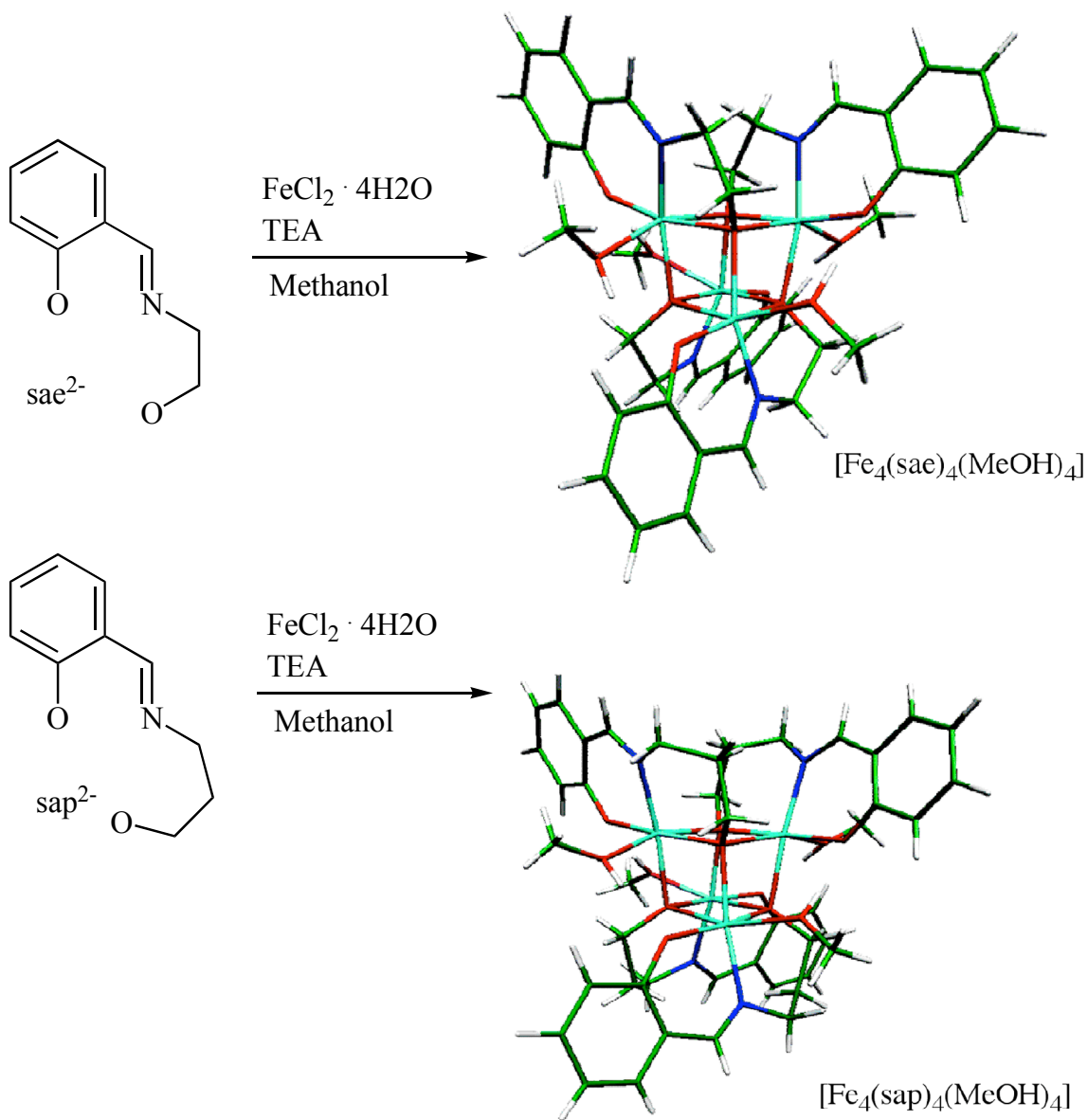
1.5 Prediction of complexation

The following three examples illustrate how one can, by changing the reaction conditions, control the outcome of some simple complexation reactions.

In the first examples, Leznoff and coworkers investigate the effects of metallation base, reaction solvent and metal counterions. Complexation is performed using the simple ligands **IX** and Co(II) salts (Figure 1.15).[19] In the absence of added base helical complexes could be isolated. The key step to helicate formation is the hydrogen bonding ability of the ligand. The absence of base will keep the ligands protonated, and the acidic phenol protons are still present. These protons participate in non-covalent bonding with an adjacent phenol oxygen and this further stabilizes the helicates. In the presence of the strong base NaOH, a cubane structure was achieved. Four cobalts occupy four corners of the cubane and are connected through four phenoxide oxygens. The strong coordination of the phenoxides is the force behind cubane formation. Furthermore, the complex is stabilized through π-π* interactions between two adjacent ligands. When the less aggressive base triethylamine (TEA)is used, the outcome is slightly different. Here, a defect face-shared double cubane is the result. Changing the solvent to DMSO (rather than methanol) favors the formation of bowl type structure instead. Finally, as the metal counterion was change to the dianionic SO_4^{2-} (rather than monoanionic Cl^- and NO_3^-), a coordination polymer was formed.

Figure 1.15. Different complexation mode of **IX** depending on solution pH, solvent and metal salt.
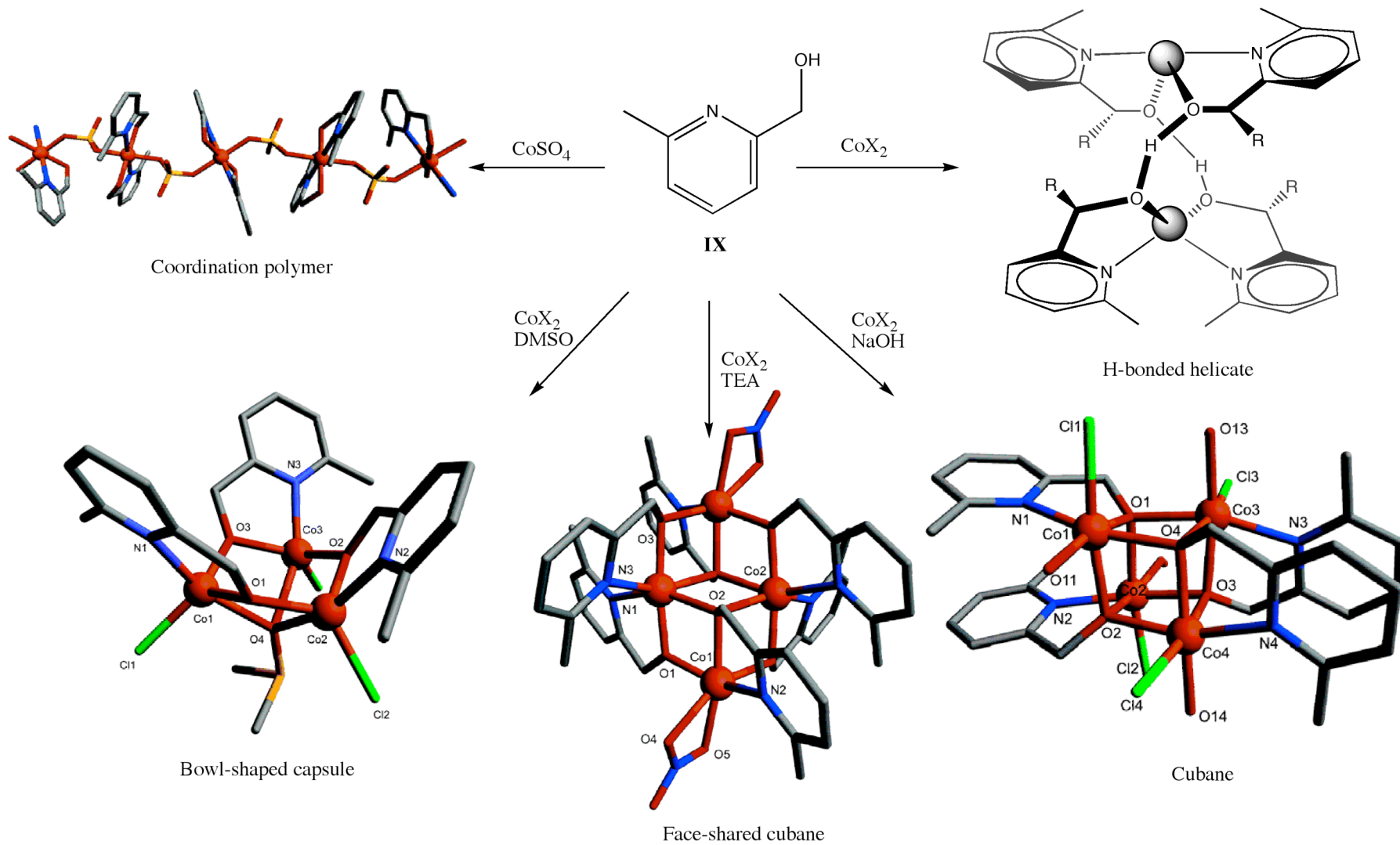
Figure 1.16. Complexation of BINAM based Schiff-base ligands; the effect of solvent.
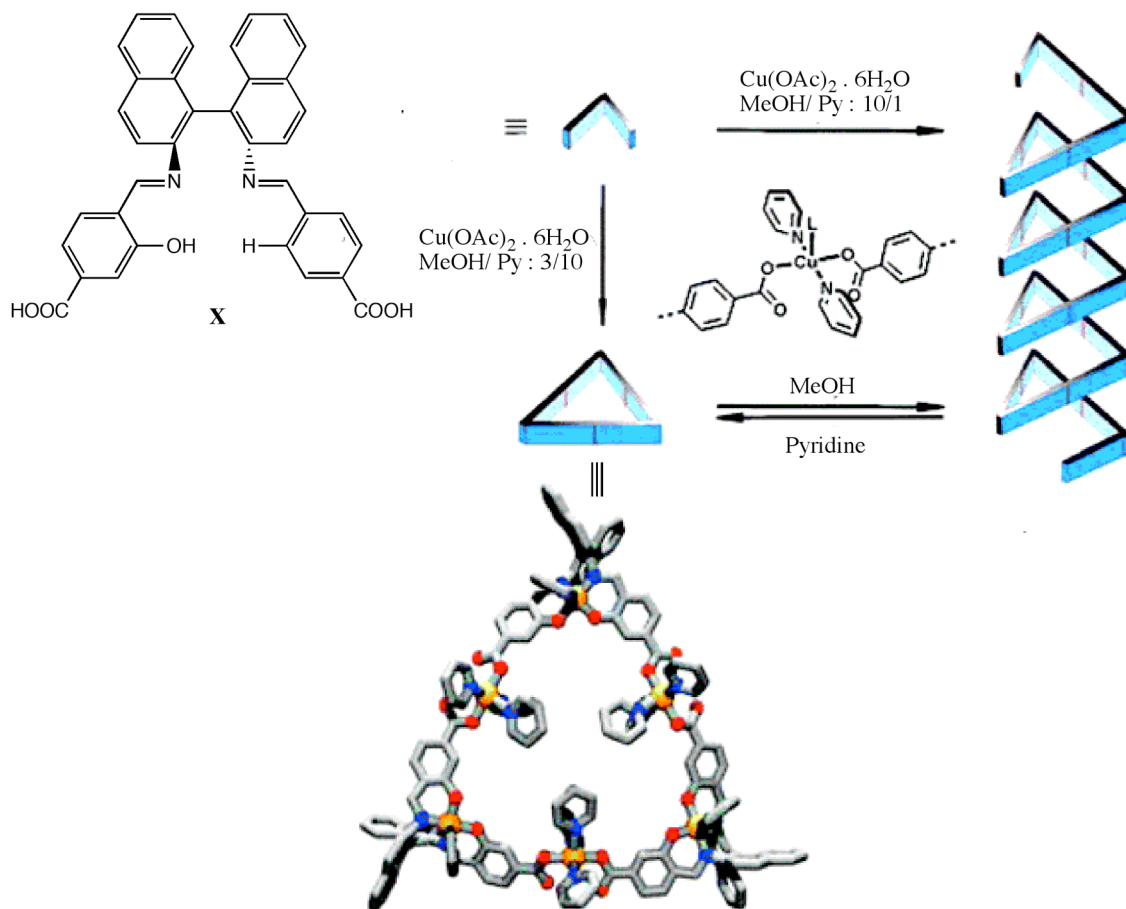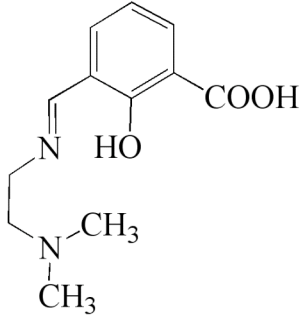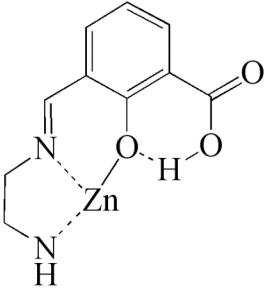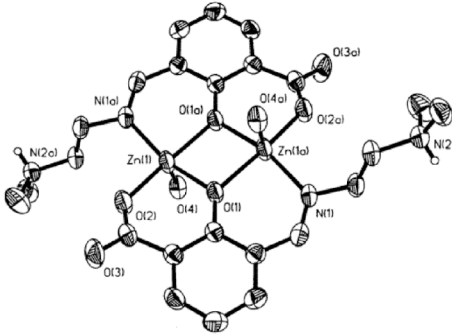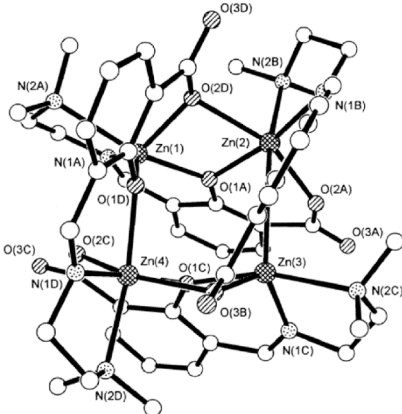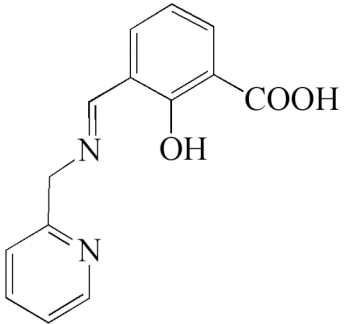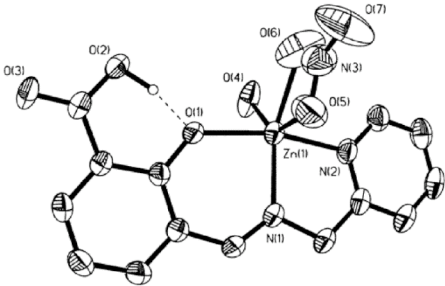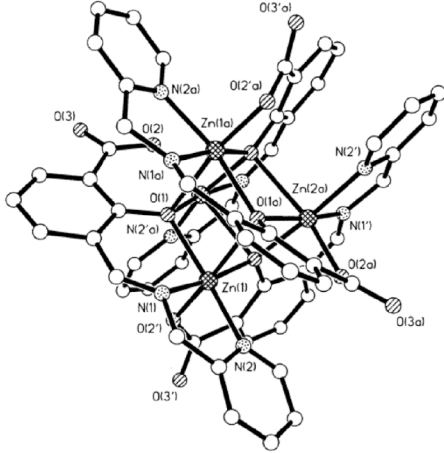
In work done by Mirkin and coworkers, it was shown that the solvent can have a huge effect on the outcome of the self-assembly process of the formed complexes.[18] BINAM based acid-functionalized Schiff-base ligand **X** was exposed to Cu(II) salts in a mixture of methanol/pyridine. At a methanol/pyridine ratio of 3:10, metal-organic prisms were detected as the major product. Changing the ratio to 10:1 methanol/pyridine resulted in the formation of helical coordination polymers instead. It was also illustrated that the two forms can interconvert with each other, as the addition of methanol will convert the molecular prisms to helicates. In similar fashion, molecular prisms could be reformed upon the addition of pyridine to the helical polymers (Figure 1.16).

17

In another study on acid-functionalized Schiff-base ligands, Erxleben demonstrated the effect of reaction pH on the complexation outcome.[20] Here the focus was on the solution pH and the effect of solvents on the pK_a of the functional groups of the ligand. Also, the basicity of the amine group (fourth donor) on the complexation outcome was investigated (Figure 1.17). Complexation was carried out using divalent Zn salts with ligands **XI** and **XII**. Both ligands have the potential of acting as tetradentate ligands if fully deprotonated. There is a significant difference in basicity between the amine and pyridine nitrogens, with the latter being less are less basic. In acidic solution, ligand **XI** forms dinuclear complexes with two coordinating ligands. The two metal ions are located in the pseudo-salen pocket of the two ligands and the O_4-pocket created by the two deprotonated carboxylic acid moieties. The amine groups are protonated to form ammonium ions and do not partake in the metallation process. The two ligand strands are binding in a *trans* fashion. Metallation of **XII**, under similar conditions resulted in a mononuclear complex with one coordinated ligand. The difference in the two morphologies was explained as due to the lower basicity of the pyridine nitrogen. In **XII**, the pyridine group is not basic enough to deprotonate the carboxylic acid. As a result the acid remains protonated and does not coordinate to the metal center. The metal bonds to the N,N,O pocket of the ligand. When a stronger amine is present as in **XI**, the complex has a deprotonated carboxylate moiety and an ammonium group. It was illustrated that by changing the polarity of the solvent, the pK_a of both the amine group and the carboxylic acid can be changed to either coordinate one or two ligands to the metal center. Lastly, in the presence of a strong base (NaOH), metallation of both ligands resulted in the formation of cubane type structures.

Figure 1.17. Affect of Ph on complexation of acid-functionalized Schiff-base ligands **XI** and **XII**.

1.6 Research Strategy

Based on the information provided above, the following conclusions can be made.

1.6.1 The ligand

The structure of the ligand is by far the most important factor in the prediction and control of the complexation process. A cleverly designed ligand should be versatile and capable of forming a wide variety of complexes, yet be restricted enough to maintain one structure without interconverting between the different forms. Furthermore, it is of a great importance to be able to modify the ligand to fine tune its properties such as steric bulk, electron withdrawing/donating abilities, acid-base properties, non-covalent bonding abilities, etc. and hence change its abilities for complexation and self assembly. Also, it should have donating/chelating groups that are suitable for metal centers with different size, acidities and geometrical preferences. Moreover, protic functional groups of the ligand should be of different pK_a so they can be systematically deprotonated. This will change the chelating abilities of the ligand and produce a more versatile system.

The structures described in this chapter have been shown to have high catalytic activities. Helicates and helices are of chiral nature and do not require the use of a chiral ligand. However, introducing chirality by using a chiral ligand has shown to increase the control of asymmetry and the formation of one handiness (*M* or *P* only). Furthermore, by using a chiral ligand, twisted macrocycles, helical salen complexes and chiral cubanes can also be achieved.

Acid-functionalized Schiff-base/salen ligands have shown great versatility for complexation with transition metals. The oxygen and nitrogen donor groups are suitable

for a wide variety of transition metals. Also, these are good candidateS for the formation of cubane type structures. Additionally, the carboxylic acid can contribute to intra- and intermolecular hydrogen bonding. The presence of non-covalent bonding, such as H-bonding and π-π interactions, can have a great effect on the formation and stabilization of helical structures.[12,19] Furthermore, the three chelating groups all have different pK_as. As Erlxelben demonstrated, the carboxylic acids can be utilized more efficiently if an additional amine group is present in the molecule.[20] This amine functionality can also act as a fourth donor group. Additionally, this amine can be further reacted to give new functional groups. The same is true for the carboxylic moieties.

Simply put, the components needed to carry out this study are a carboxylic acid group, a phenol, an aldehyde, and a diamine. 3-formylsalicylic acid (3-fsa) is a great candidate for introducing the first three functional groups. Varying the ratios and the reaction conditions of 3-fsa with the diamine can result in the formation of a macrocycle, a diimine or a monoimine ligand as shown in figure 1.18.

Figure 1.18. Formation of macrocycles, salen and Schiff-base ligands based on 3-formylsalicylic acid and a chiral diamine.
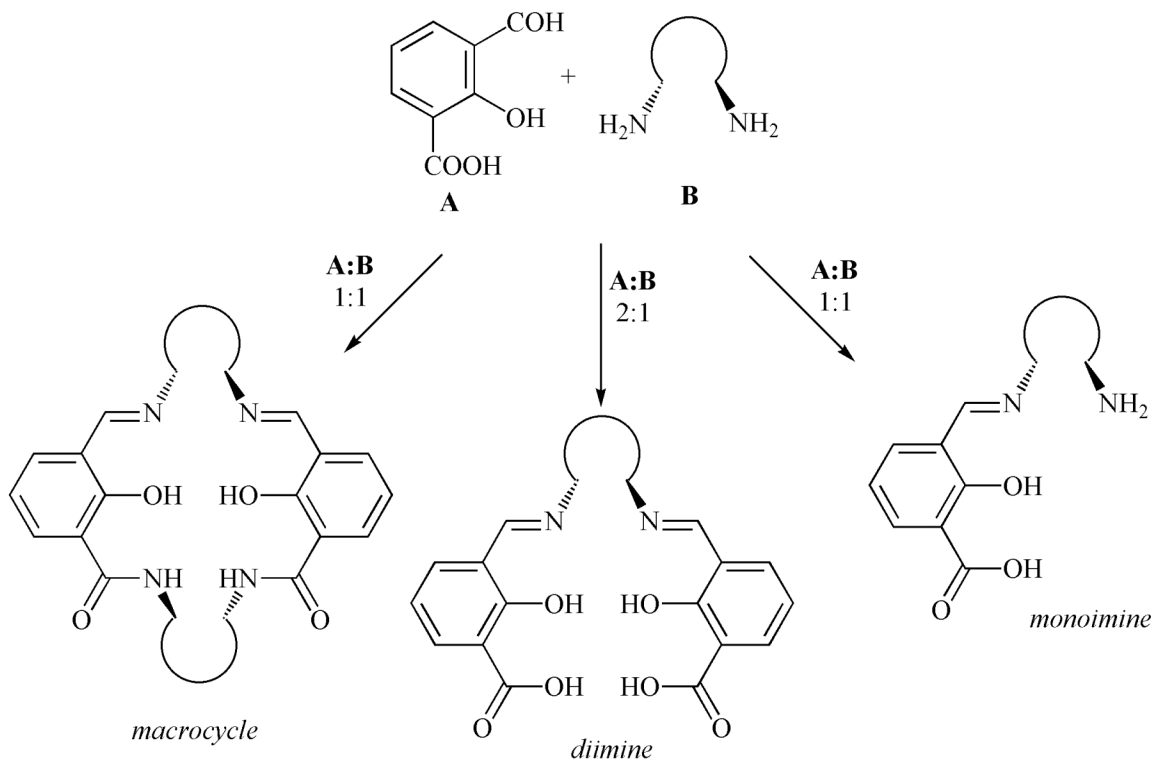
The use of a chiral diamine is a great way of elegantly introducing chirality to the ligand. There is a wide range of chiral diamines available both commercially and synthetically (figure 1.19). In addition to introducing chirality, the backbone can act as a tool in the modification of the ligand properties. As we move to the right in figure 1.19, the diamines increases in steric bulk, decrease in basicity, and flexibility. The two backbones chosen for this project are as indicated the (1*R*, 2*R*)-diaminocyclohexane and (*R*)-1,1'-binaphthyl-2,2'-diamine.

Figure 1.19. Commercially and synthetically available chiral backbones.

Increasing steric bulk
Increasing twist (dihedral angle) between chelating donors in the metal complexes
Decreasing basicity of amine groups
Decreasing flexibility
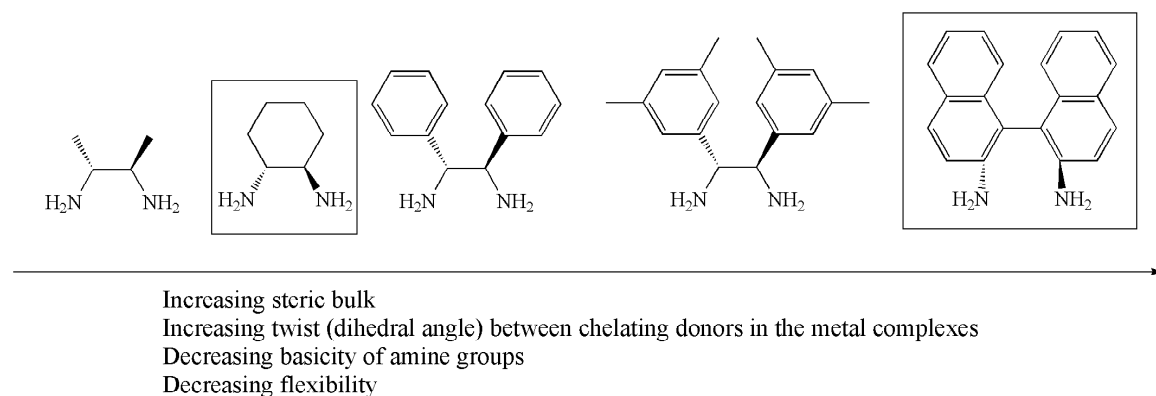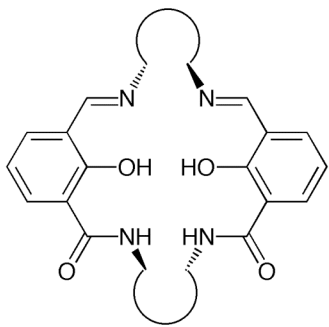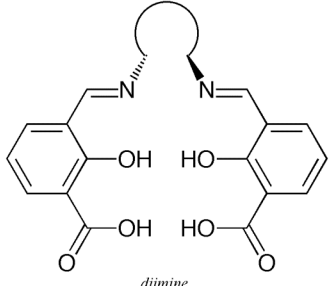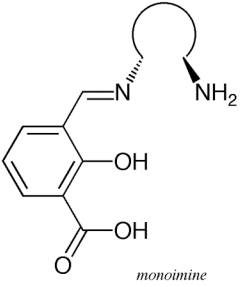
1.6.2 Metal salt and base

Most transition metals are good candidates for this study. However, the later transition metals are of interest due to their richer coordination chemistry. Also, as most biological systems of this kind involves Fe(II), Co(II), Ni(II) and Cu(I)/ (II) and Zn(II) complexes, special attention has been devoted to these metals.

The complexation base used should have the ability to at least deprotonate the phenolic hydrogens. TEA is a widely used, mild base that is of great interest in this work. The fairly bulky base is strong enough to deprotonate the phenols but not basic enough for the deprotonation of the carboxylic acids. NaOMe, on the other hand, is a very harsh base that is usually used to fully deprotonate ligands of this kind. The reason this base was chosen over KOH or NaOH (the most common bases used for deprotonation of acid-functionalized salen ligands), is to reduce the formation of OH⁻ (H_2O) as the Schiff-base ligands are slightly moisture sensitive.

In conclusion, the combined ligands and their anticipated complexation structure are shown in figure 1.20.

Figure 1.20. Prediction of complexation of the suggested Schiff-base ligands.

Ligand	Weak Base (TEA)	Strong base (NaOMe)	Fully deprotonated ligand Solvent: Methanol
macrocycle	M(II) is expected to bind to the salen pocket of the macrocycle. TEA is not basic enough to deprotonate the carboxylic acids.	M(II) is expected to bind to the both the salen and the salan pocket of the macrocycle.	—
diimine	M(II) is expected to bind to the salen pocket of the macrocycle. TEA is not basic enough to deprotonate the carboxylic acids.	M(II) is expected to bind to the both the salen and the salan pocket of the macrocycle.	A fully deprotonated ligand in methanol have the potential of forming a cubane.
monoimine	Considering the pKa's of the functional groups, it is believed TEA will only deprotonated the phenolic hydrogen. However, in the case of CHDA, the amine have the potential of deprotonation the carboxylic acid creating an ammonium ion and a carboxylate. CHDA: M(II) is expected to bind to the phenoxide/carboxylic acid pocket of two cis located (H-bonding ability) ligands. BINAM: M(II) is expected to bind to the phenoxide/imine/amine pocket of two cis located ligands. The chirality of the backbone is believed to promote the formation of helices.	A fully deprotonated ligand of this kind is expected to form a dinuclear, double stranded complex. There are two possibilities for hydrogen bonding; between two adjacent amines or between an amine and a carboxylate. The later is believed to be more likely since the carboxylate has a higher pKa than an amine. Therefore it is predicted the final double strand will have a trans configuration.	A fully deprotonated ligand in methanol have the potential of forming a cubane.

CHAPTER 2 - Synthesis and characterization of acid-functionalized salen ligands

2.1 Introduction

Acid-functionalized salen ligands have great potentials as versatile ligands that can produce a variety of coordination environments for metal ions. Their two metal binding pockets (Figure 2.1) have significantly different binding abilities; the salen pocket, consisting of two imine-nitrogen donors and two phenoxide donors, can be activated by the addition of a mild base while the phenoxide/carboxylate pocket requires a stronger base for deprotonation. Both binding pockets are suitable for coordinating to transition metals of different geometries. Additionally, salen ligands are easily synthesized from inexpensive starting materials.

Figure 2.1. Acid-functionalized salen ligands and their complexation using strong and weak base.
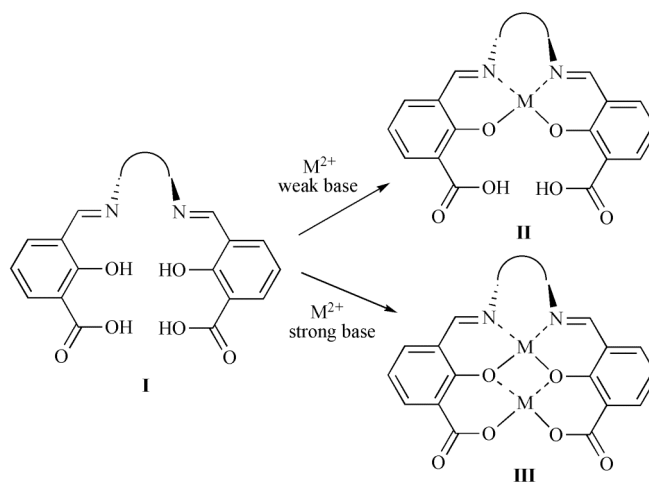
The two ligands of interest are the (1*R,2R*)-cyclohexyldiamine (CHDA) and (*R*)-[1,1'-binaphthalene]-2,2'-diamine (BINAM) based salen ligands (*R,R*)-**4** and (*R,R*)-**5** (Figure 2.2). The ligands possess chirality from the non-racemic diamines used to produce them and have the potential of forming stepped single-stranded mono helices if the right reaction conditions are met. In designing these ligands for this outcome, several factors need to be considered. The helicity depends on *i)* the disposition of metal coordination sites, *ii)* the flexibility and bulkiness of the ligand framework and *iii)* the coordination geometry of the metal center.

Figure 2.2. CHDA and BINAM based acid-functionalized salen ligands.
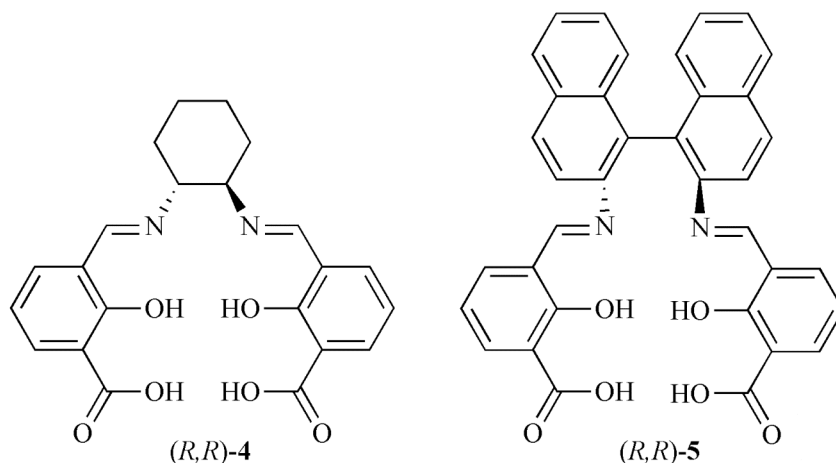
When tetradentate ligands coordinate to a single octahedral metal center, three different complex morphologies can be formed, depending on the disposition of the metal coordination sites. Figure 2.3 shows the three different geometries. When all four of the donor groups bind to the metal on the same plane, the complex has the *trans* configuration. Consequently, the remaining two monodentate ligands (often the counter ions or solvent molecules) are located *trans* to each other. When the monodentate ligands

are *cis*, two configurations are possible; the *α-cis* and *β-cis*, depending on the position of the donor groups of the salen ligand. In *α-cis* there are two donors from the tetradentate ligand in each metal coordination plane, while in the *β-cis* three donors coordinate in the same plane while the forth is coordinated axial to this plane.

Figure 2.3. The combination of tetradentate ligand to an octahedral metal center.

trans   *α-cis*   *β-cis*
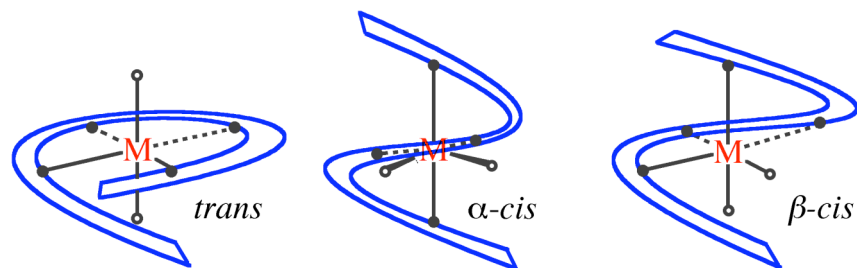
The nature of the chiral backbone is critical for establishing helical structures. Chirality can be introduced into salen ligands by choosing enantiopure diamines with different sizes, flexibilities, shapes and basicity. In this work the focus has been on the two diamines (1*R,2R*)-cyclohexyldiamine (CHDA) and (*R*)-[1,1'-binapthalene]-2,2'-diamine (BINAM) in figure 2.4.

Figure 2.4. Structures of (1*R,2R*)-cyclohexyldiamine (CHDA) and (*R*)-[1,1'-binapthalene]-2,2'-diamine (BINAM**)**

CHDA   BINAM
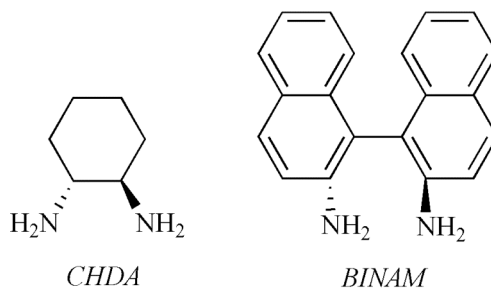
Between the two, BINAM is both bulkier and has a larger dihedral angle between the two chelating donors when metallated. This has a distinct effect in the complex structure. Due to BINAMs high degree of "twistedness", complexation with divalent metal salts usually creates a system with binaphthyl groups roughly perpendicular to the planes of the ligand arms (Figure 2.5). CHDA on the other hand is less twisted and will keep the complex structure roughly in one plane (Figure 2.5, blue plane, there is a twist in the chiral complex).[59]

Figure 2.5. Space filling models of square planar Zn(II) complexes showing the effect of backbone bulkiness and the final product.
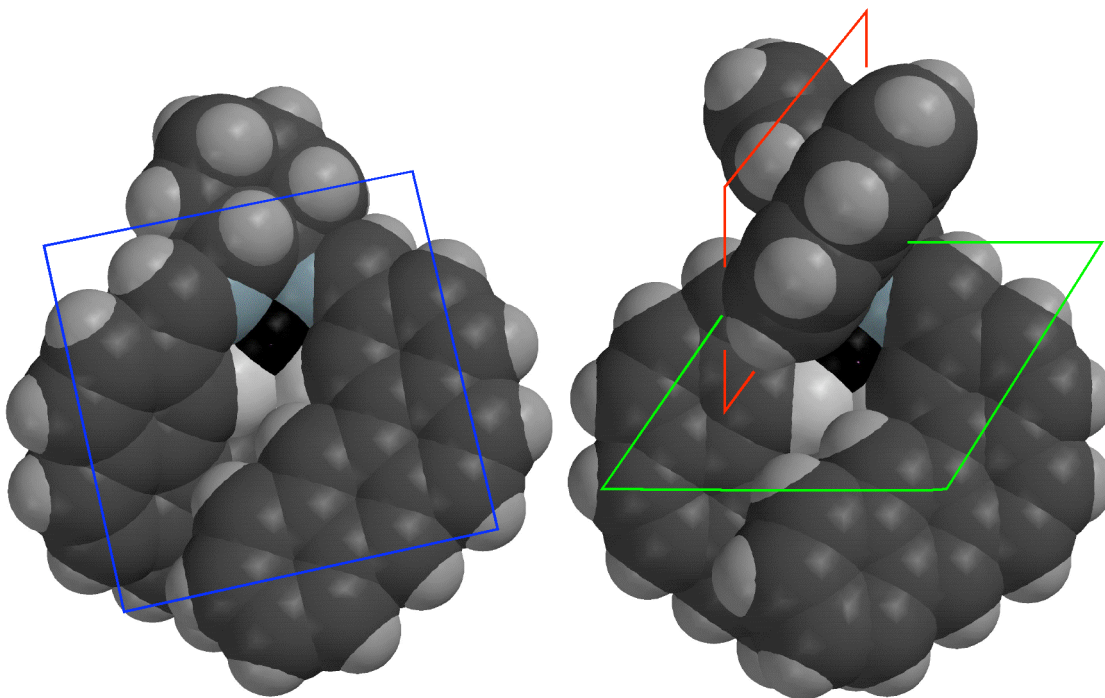
Figure 2.6 shows result based on molecular modeling (MMFF calculations on McSpartan) of complexation of (*R,R*)-**4** in combination with square planar Zn(II). Unlike regular salens, which only have one metal binding site, acid functionalized salens can in

addition bind metals through their phenolic/carboxylate coordination pocket. Binding to two metals will, however, prevent the complex from adopting a stepped configuration. As shown in figure 2.6, the dinuclear complex will not be a twisted while the mononuclear complex shows a stepped configuration.

Figure 2.6. Molecular modeling based on MMFF calculation of (*R,R*)-**4** and square planar Zn(II). Top and side view of mono- and dinuclear acid functionalized salen complexes.

Top view

Side view
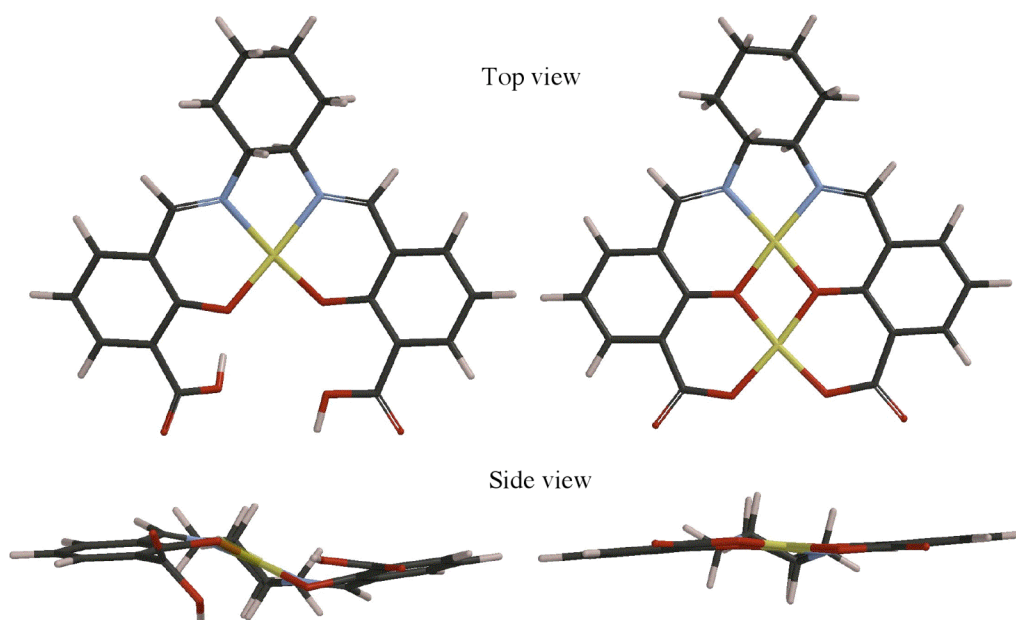
There are no known examples of complexes of (*R,R*)-**5**, however, Merkin *et al* recently presented the very similar 4-formylsalicylic based salen ligand and its Cu(II) complexes (Figure 2.7).[18]

Figure 2.7. Complexation of (*S*)-BINAM based acid-functionalized salen ligands with Cu(II) salts.
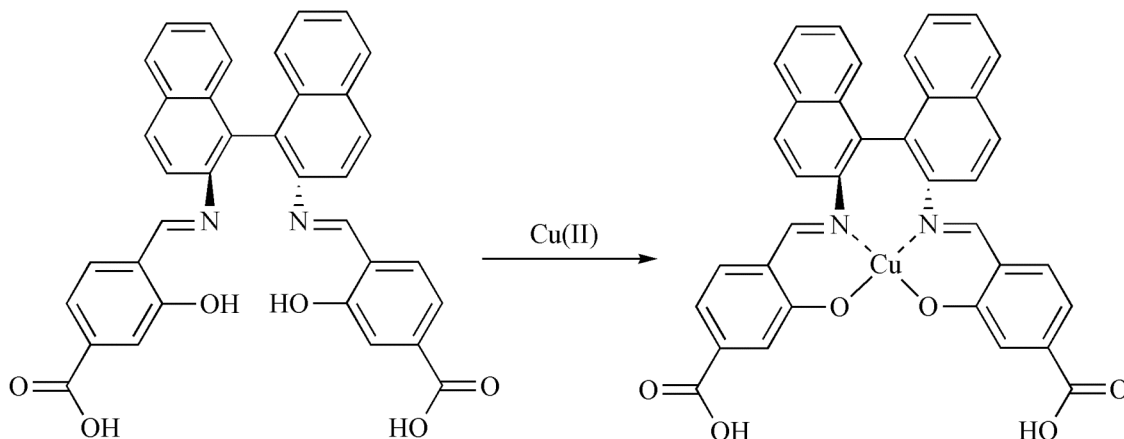
Salen (*R,R*)-**4** has been previously synthesized. The aim of the studies involving (*R,R*)-**4** has been to synthesize compartmental ligands that can hold two or more metal centers closely related to each other. Therefore, complexation of this ligand has mostly concerned the coordination of two similar/ dissimilar metal centers (Figure 2.8). Okawa and coworkers did the most thorough investigation of acid-functionalized salen ligands in late 70's.[60,61] However, during recent years, a new wave of researchers has started to investigate these systems.[62] Almost all of the attention has been on the synthesis of flat dinuclear complexes (Figure 2.8). The dinuclear complexes have been synthesized by adding an excess amount of metal salts to the fully deprotonated ligand. The deprotonation is usually carried through the addition of the strong bases KOH and NaOH.

Figure 2.8. Examples of existing CHDA based complexes.

M, M': Cu(II), Fe(II),
Ni(II), Zn(II)
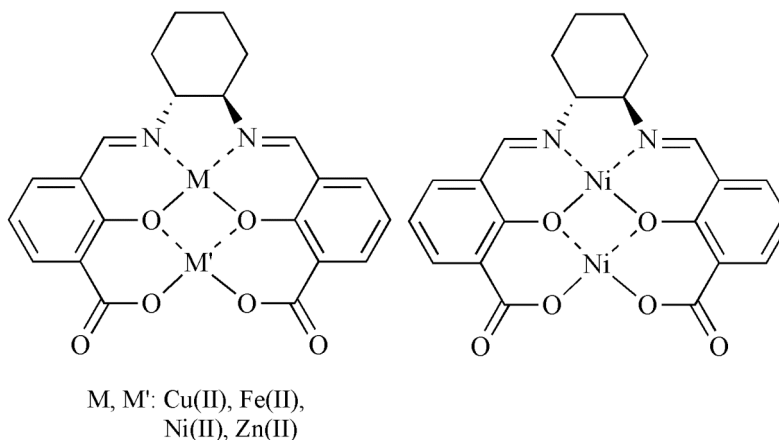
A twisted, mononuclear complex can be formed if only the salen pocket becomes deprotonated and metalated. This requires the use of a much weaker base. In the following two chapters, results from the synthesis and metallation of these salen ligands with dinuclear transition metals using both a strong base (sodium methoxide) and a weak base (triethylamine) is reported.

2.2 Synthesis of acid-functionalized salen ligands

Chiral diamines (1R,2R)-cyclohexyldiamine (R,R)-**1** and (R)-[1,1'-binaphthalene]-2,2'-diamine (R)-**2** (Figure 2.9) are commercially available, however due to ease of preparation and relatively inexpensive starting materials they were synthesized following well documented procedures.[63] The 3-formylsalicylic acid **3** is not commercially available and was prepared according to the methods of Duffs and Bills with some minor modifications.[64] In general, the synthesis of 3-formylsalicylic acid Schiff base ligands involves a condensation reaction between the diamine and two equivalents of 3-formylsalicylic acid (Figure 2.9). (R,R)-**4** has been previously reported, but lack of

detailed synthetic and characterization information lead us to investigate a new synthesis rout. By doing so, the preparation method and the reaction yield were improved significantly.

Reflux in protic solvents such as ethanol or methanol gives the desired Schiff bases (*R,R*)-**4** and (*R,R*)-**5**, after only a few hours. The reflux results in the precipitation of the products in high purity without any further purification. However, as the Schiff bases are slightly soluble in boiling methanol/ethanol, highly concentrated reaction conditions are recommended for a high reaction yield. Solution of (*R,R*)-**4** and (*R,R*)-**5** show sensitivity to moisture and should therefore be handled under dry atmosphere. The solids are mildly hydroscopic and can be stored on the bench top.

Figure 2.9. Synthesis of the salen ligands.
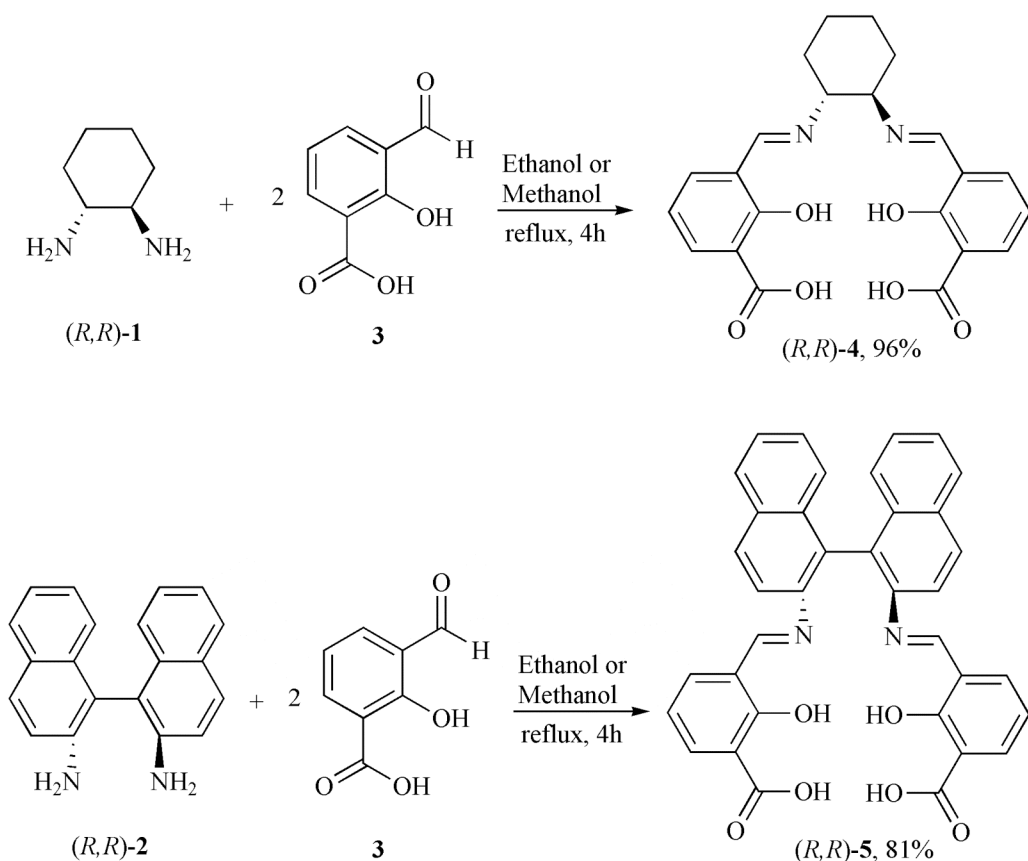
2.3 NMR spectroscopy of Schiff base ligands

Figure 2.10 and Table 2.1 show the 1D-NMR spectrum of (*R,R*)-**4** along with the specific peak assignments in different deuterated solvents. The number of peaks depicted in the NMR spectra is half the number of possible resonances, indicating the presence of a C_2-symmetrical molecule. In chloroform-d_1, the imine peak appears at 8.86 ppm as a singlet, corresponding to two hydrogens (Figure 2.10a). The benzyl hydrogens located *ortho*, *meta* and *para* to the imine bond appear as a doublet, triplet, doublet at 7.39, 6.58 and 8.21 ppm respectively. The cyclohexyl backbone hydrogens appear as broadened multiple peaks in the aliphatic region. This is believed to be due to fluctuation of the ring and second order effects. The NMR spectra also show the presence of two broad singlets at 13.55 and 16.81 ppm. Although visible in $CDCl_3$, these two peaks are no longer detectable in protic solvents such as methanol-d_4 (Figure 2.10c). This is due to rapid hydrogen exchange processes between the phenol (13.55 ppm) and a carboxylic acid (16.81 ppm) with the solvent deuterons (Figure 2.10 a). The spectrum in methanol-d_4 is consistent with literature data.[62]

Figure 2.10. NMR spectra of (*R,R*)-**4** (a) ^{1}H (400 MHz) in CDCl$_3$ (b) ^{13}C (50 MHz) in CDCl$_3$ (c) ^{1}H (400 MHz) in CDCl$_3$.

c

Chemical Shift (ppm)

b

Chemical Shift (ppm)

a

Chemical Shift (ppm)
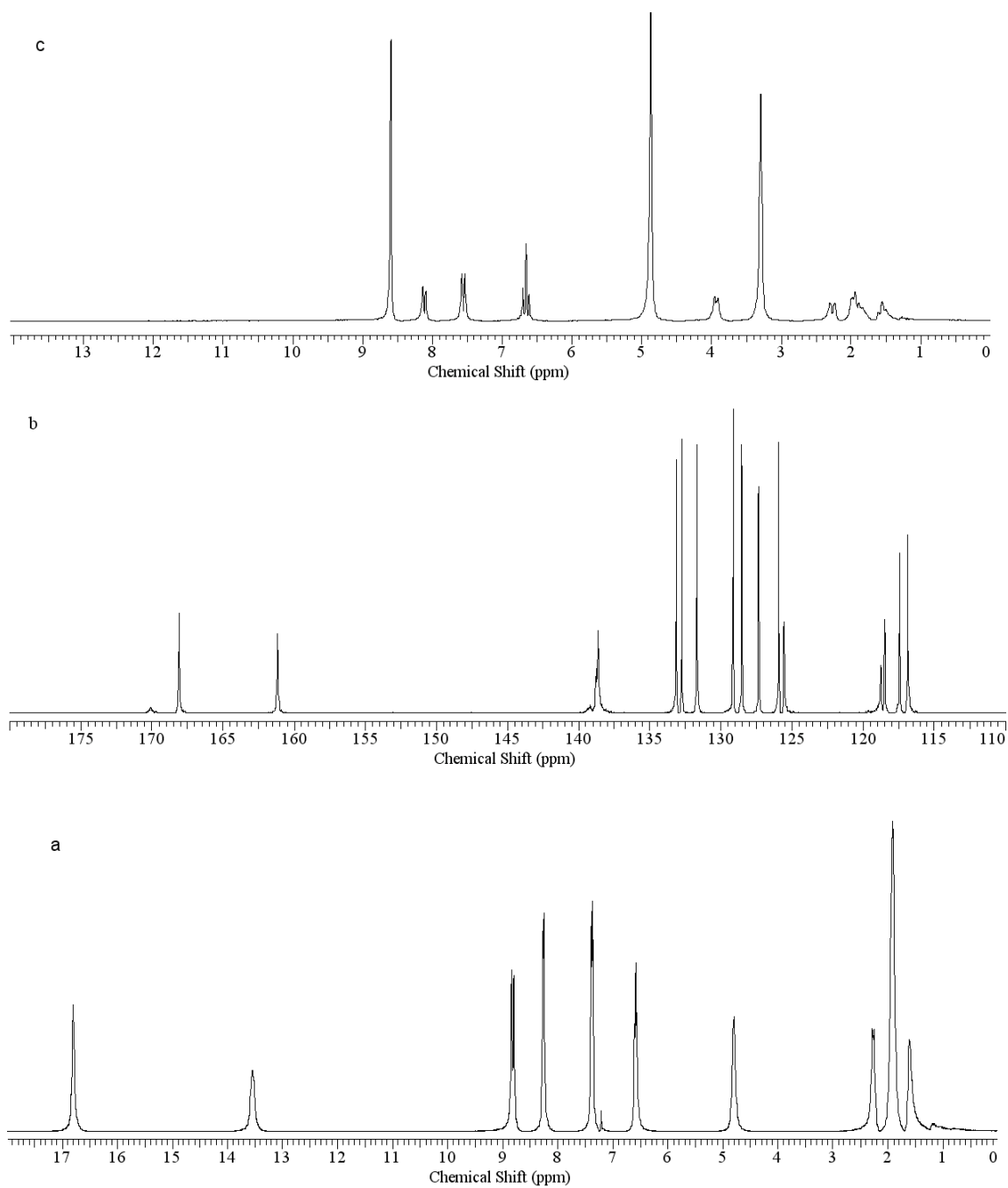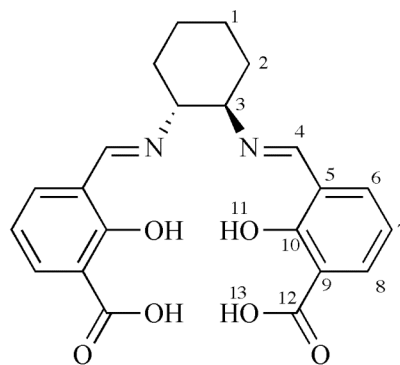
Table 2.1. Peak assignments of (*R,R*)-4 in CDCl$_3$, DMSO-d_6, CD$_3$OD

	CDCl$_3$		DMSO-d_6	CD$_3$OD
#	^{1}H	^{13}C	^{1}H	^{1}H
1	1.60, 1.91	24.18	1.40, 1.83	1.53, 1.92
2	1.91, 2.26	33.34	1.83, 2.18	1.92, 2.25
3	4.80	64.80	4.26	3.91
4	8.86	169.98	8.76	8.62
5	-	119.88	-	-
6	7.39	~140	7.64	7.57
7	6.58	114.95	6.66	6.65
8	8.21	~ 140	8.03	8.10
9	-	115.78	-	-
10	-	181.02	-	-
11	13.55	-	13.11	N/A
12	-	176.71	-	-
13	16.81	-	15.98	N/A

Figure 2.11. Possible intramolecular hydrogen bonding.
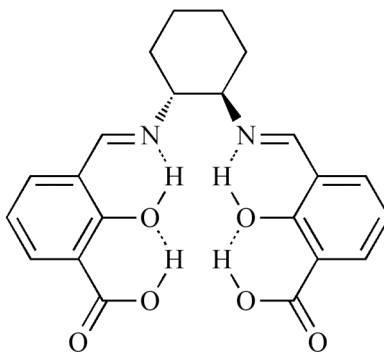
The molecule is set up for facile hydrogen bonding between the phenolic hydrogens, the imine nitrogens and the carboxylate oxygens (Figure 2.11). Hydrogen bonded phenols/carboxylates usually appear as sharp signals in the ^{1}H NMR spectrum as the proton exchange process is restricted in the presence of such bonding.[65] The two peaks at 13.5 and 16.8 ppm in figure 2.10a are significantly sharper that regular phenol and carboxylic acid peaks, indicating the presence of hydrogen-bonding between these functional groups. Furthermore, the COSY spectra show a strong correlation between the phenolic hydrogens at 13.55 ppm and the imine hydrogens at 8.86 ppm (figure 2.12). This indicates that, in addition to the phenol/carboxylic acid interactions, there is hydrogen bonding present between the imine nitrogen and the phenol.

Figure 2.12. COSY spectrum (400 MHz) of (*R,R*)**4** in CDCl₃.
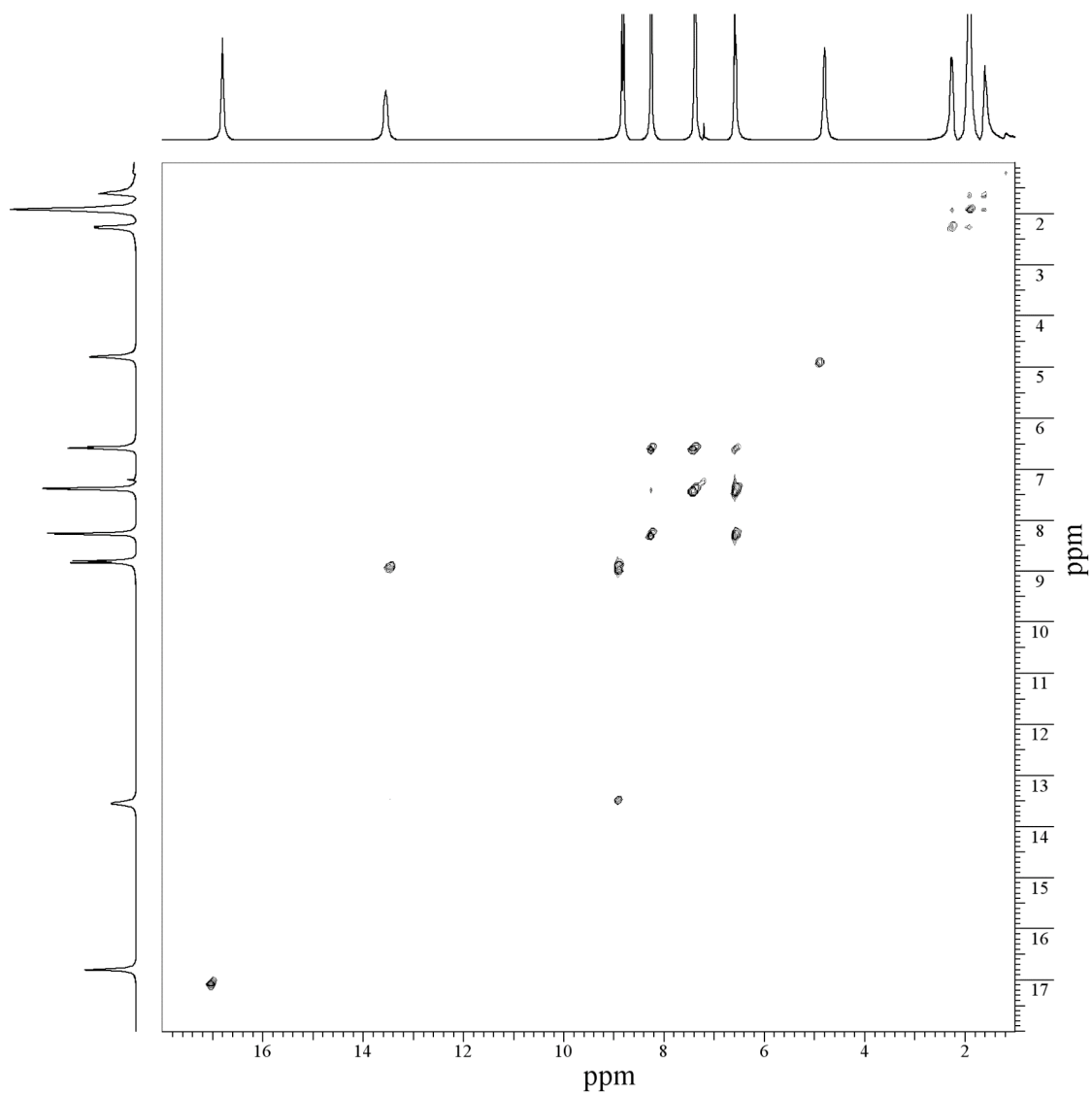
Figure 2.13. a)^{1}H NMR (800 MHz) of (*R,R*)-5 in DMSO-d_6 b) ^{13}C NMR (200 MHz) of (*R,R*)-5 in DMSO-d_6
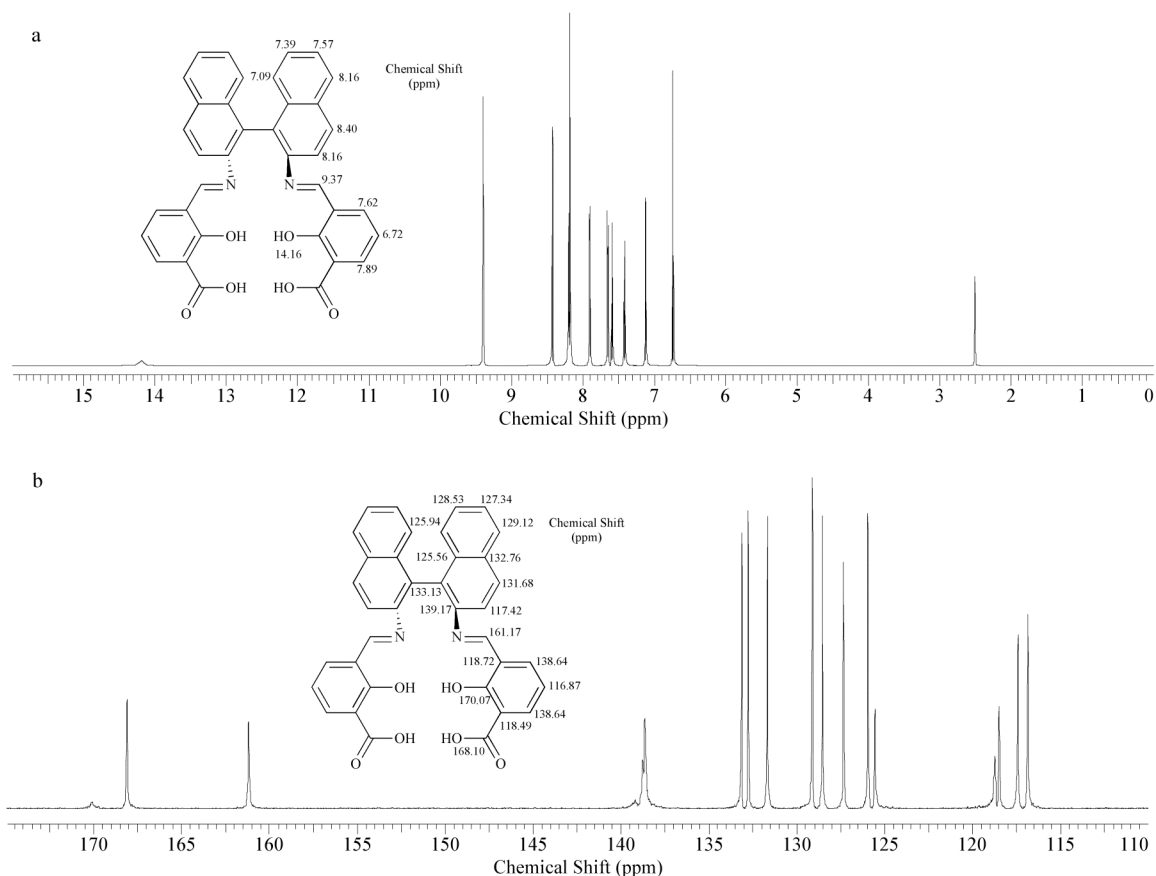
Similar 1D and 2D NMR analyses were done for ligand (*R,R*)-**5**. Figure 2.13a shows the ^{1}H NMR spectra along with the peak assignments. Again, the number of resonances indicates the presence of a C_2-symmetrical molecule. The only singlet in the molecule is the highly distinguishable imine hydrogen, which appears at 9.37 ppm. The only triplet in the spectrum is due to the phenyl proton located *meta* to the imine functional group. The two phenyl protons next the triplet were assigned to 7.62 and 7.89 ppm respectively (NOESY, Figure 2.14). NOESY also showed NOE between the resonance at 7.62 ppm and the imine hydrogen (Figure 2.14). The hydrogens *ortho*, *meta* and *para* to the imine functional group were assigned to 7.62, 6.72, and 7.89 ppm

38

respectively (Figure 2.14). Furthermore, NOESY showed NOE between the imine hydrogen and a doublet at 8.16 ppm, corresponding to one the hydrogens on the binaphthyl moiety. Using NOESY(Figure 2.14), HMQC (Figure 2.15) and HMBC (Figure 2.16) the total hydrogen and carbon assignment of (*R,R*)-**5** was deciphered (Figure 2.13). One noteworthy comment regards the appearance of the binaphthyl carbon resonance located adjacent to the imine nitrogen (Figure 2.13b). Due to the quaterinary effect of the ^{14}N nuclei and the lack of NOE from ^{1}J-coupled protons, this resonance is significantly broader than the others.

Figure 2.14. NOESY spectrum (800 MHz) of (*R*,*R*)-5 in DMSO-*d*₆
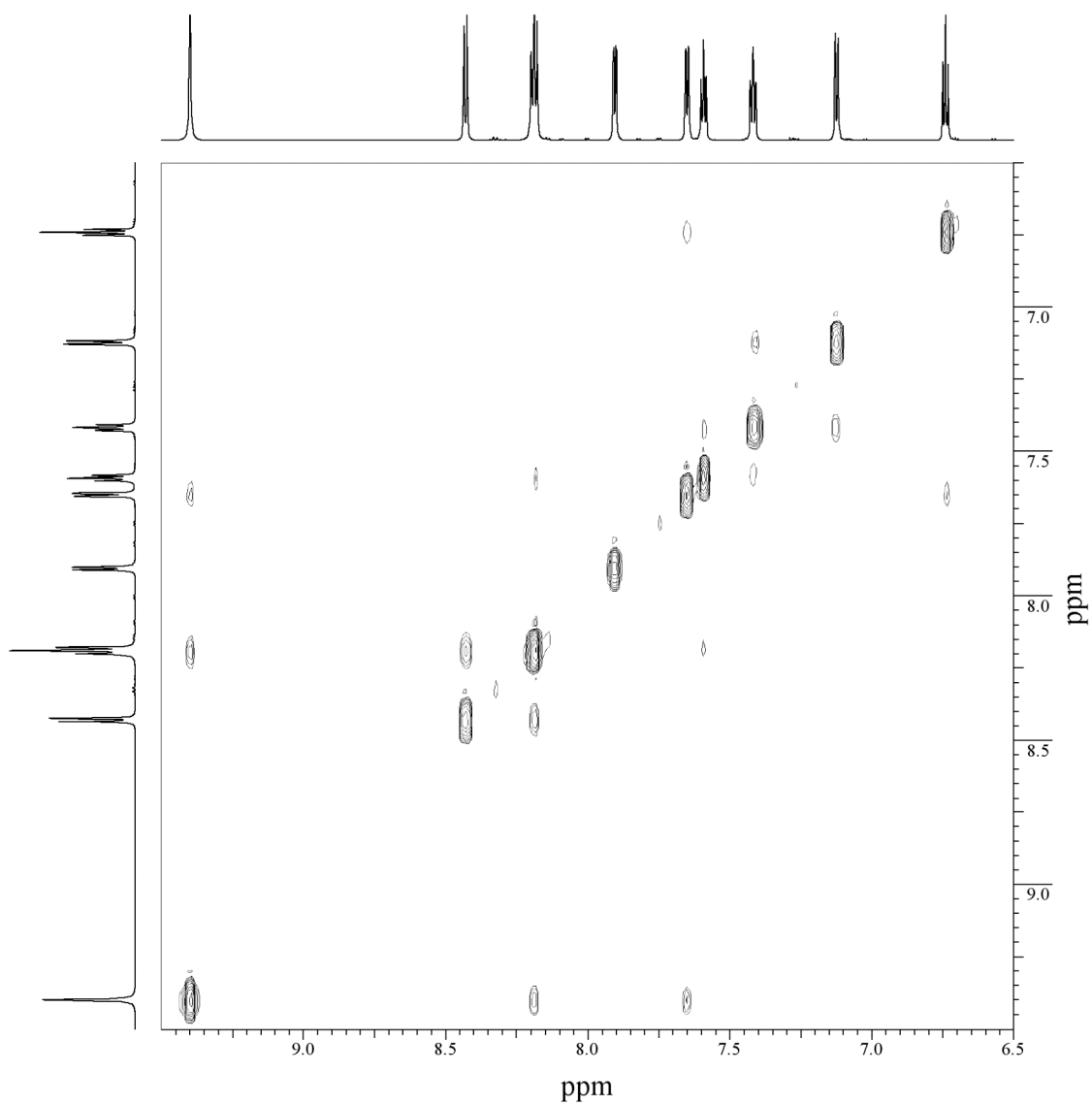
Figure 2.15. a) HMQC spectrum (800 MHz for ^{1}H) of (*R,R*)-5 in DMSO-*d*$_6$
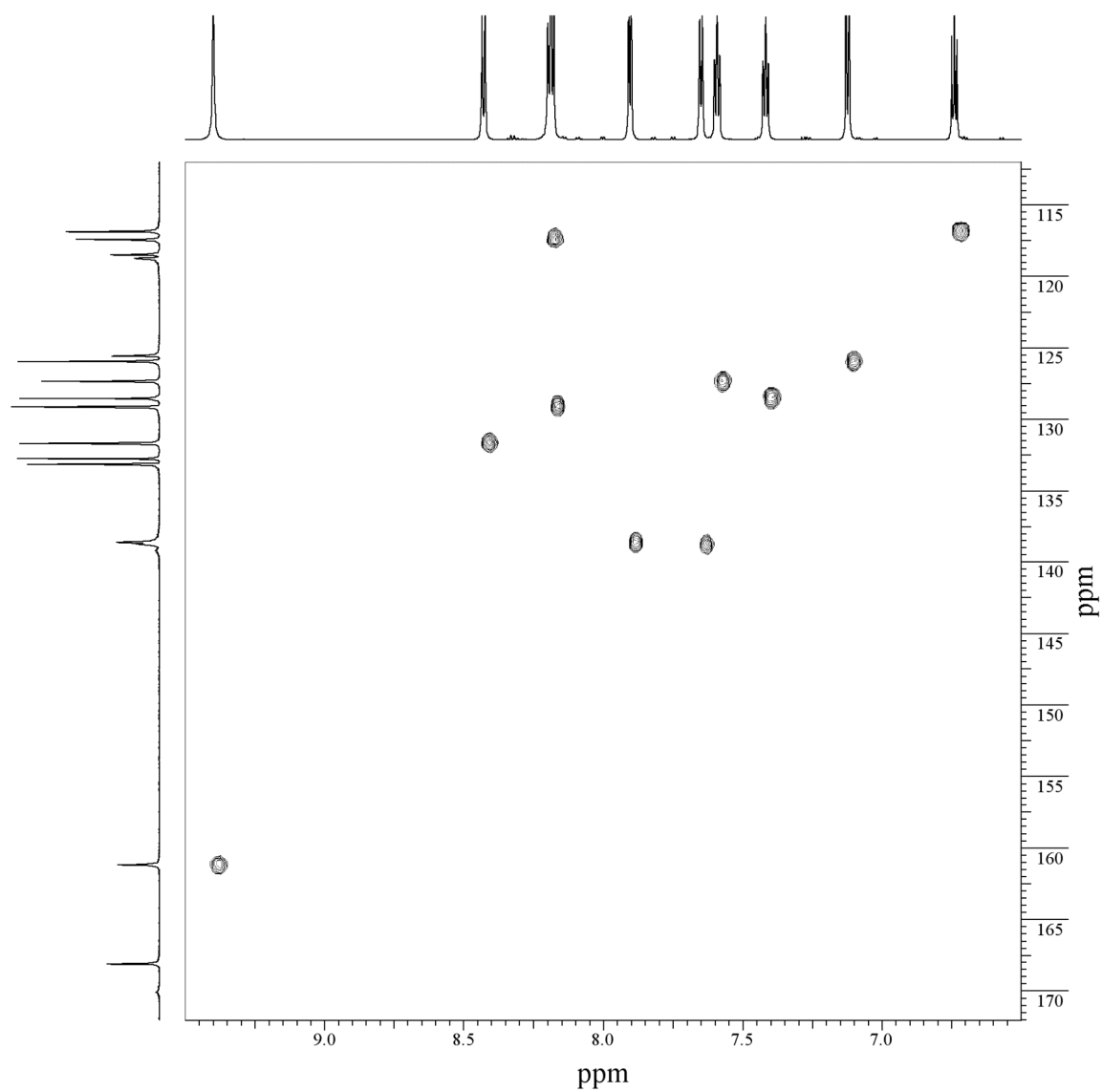
Figure 2.16. HMBC Spectrum (800 MHz for ^{1}H) of (*R,R*)-5 in DMSO-*d*$_6$
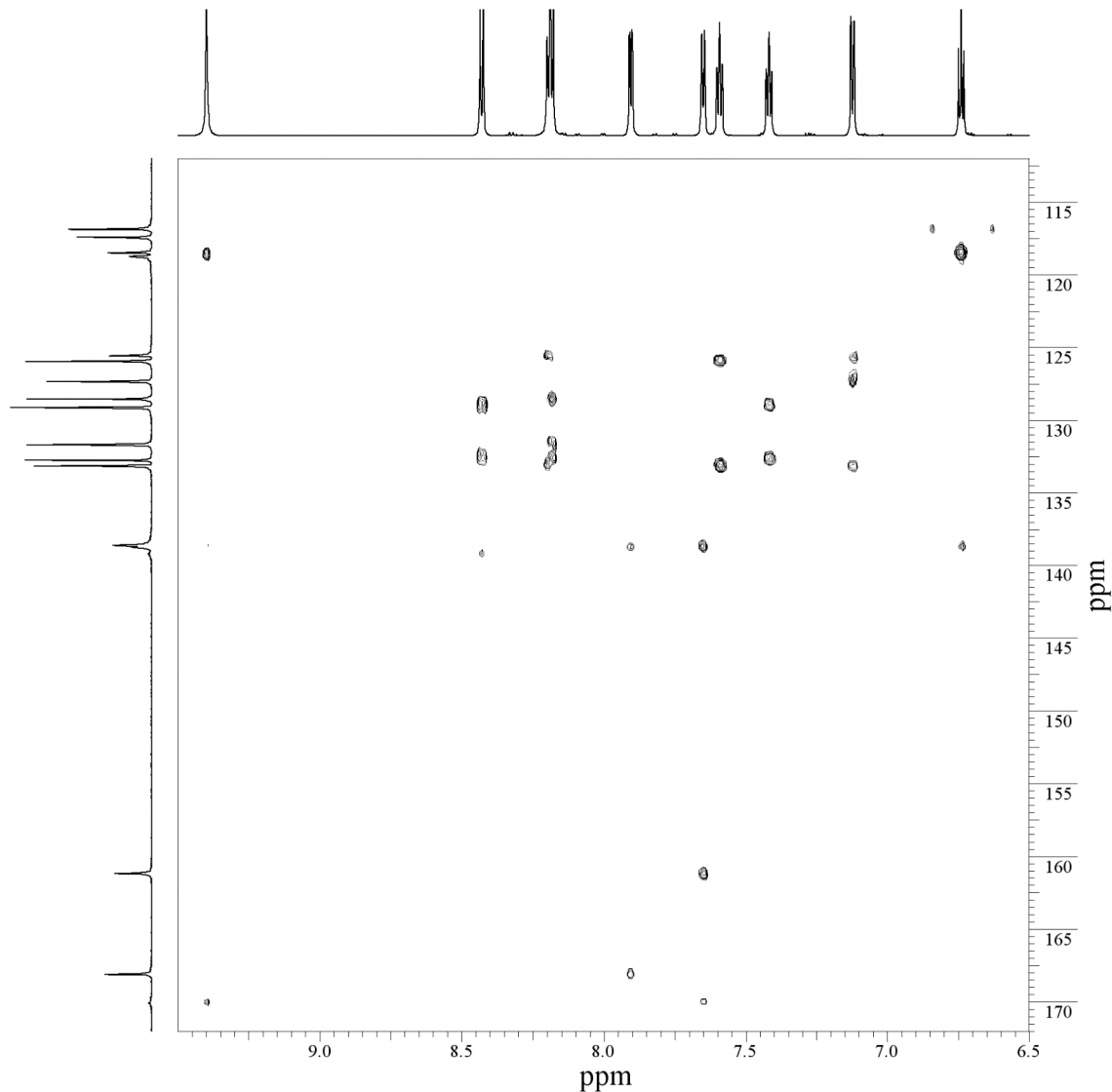
The carbon NMR spectrum shows the presence of a phenolic carbon at 170.07 and a carboxylic carbon at 168.10 ppm (Figure 2.13b). However, in the RT ^{1}H NMR spectrum, both the phenolic and the carboxylic protons appear as one broad singlet at 14.16 ppm. The peak integrates to approximately four hydrogens. When CDCl$_3$ is used as the solvent, both phenolic and carboxylic hydrogens are visible at 13.1 and 15.7 ppm respectively. It is believed that in DMSO-*d*$_6$ (wet) the two protons undergo rapid

intramolecular exchange and appear as an averaged signal. Figure 2.17 shows the result of the addition of DMSO-d_6 to a sample of (R,R)-5 in CDCl$_3$. As the concentration of DMSO increases, the two resonances merge to give one broad singlet at around 14 ppm (Figure 2.17 a-c). Figure 2.17d shows the spectrum in pure DMSO-d_6.

Figure 2.17. a) ^{1}H-NMR of (R,R)-5 in CDCl$_3$. b-c) addition of DMSO-d_6 (wet) d) ^{1}H-NMR of (R,R)-5 in DMSO-d_6.
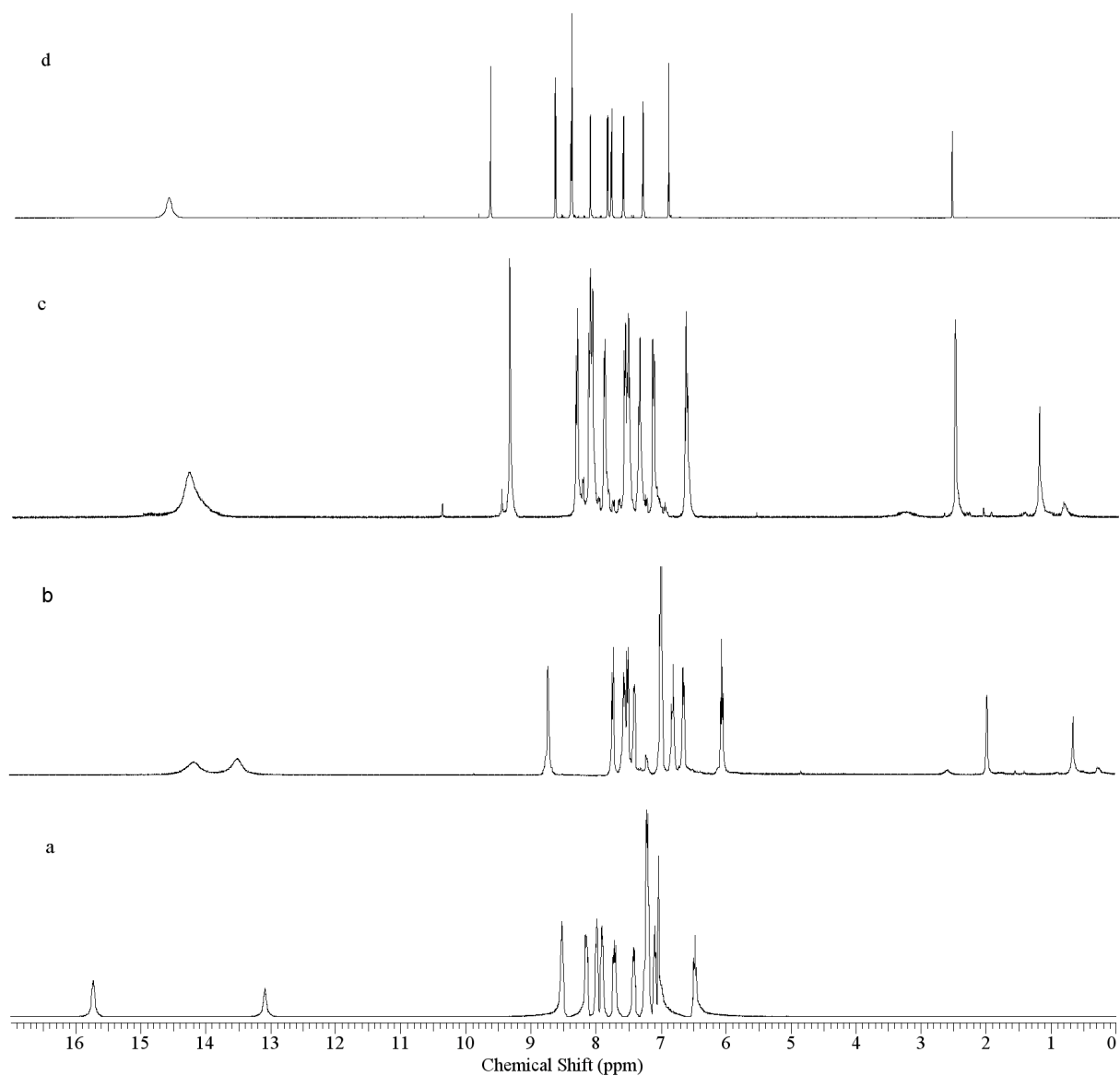
2.4 Solid state structure of the Schiff base ligands

Single crystals of (*R,R*)-**4** were grown via heating-cooling crystallization technique from ethanol (Figure 2.18). Though the molecule has been previously reported, the crystal structure has not. X-ray analysis reveals the ligand exists as a zwitterion in the solid state with iminium and phenoxide functional groups. The phenoxide is hydrogen bonded to both the iminium and carboxylate hydrogens. Table 2.2 and 2.3 show selected bond lengths, bond angles and hydrogen bonded properties of (*R,R*)-**4**.

Crystals of (*R,R*)-**5** were grown via solvent diffusion. Suitable crystals were obtained from a methylene chloride/ ether solution. Figure 2.19 show the crystal structure of (*R,R*)-**5**. The naphthalene part of the binaphthyl moiety and one of the ligand arms are located on the same plane resulting in two independently conjugated sections. The ligand arms are oriented away from each other. Similar to (*R,R*)-**4**, the ligand exist as a zwitterion in the solid state. However, the proton exchange forms an iminium and a carboxylate. The phenols remain protonated and act as a hydrogen bond donors and acceptors for the two ionic moieties; the phenol oxygen is an acceptor for the iminium hydrogen and the phenol hydrogen is a donor to one of the carboxylate oxygens. Table 2.4 and 2.5 show selected bond lengths, bond angles and hydrogen bonded properties of (*R,R*)-**5**.

Figure 2.18. Thermal ellipsoid plot (50% probability) and tube representation of (*R*,*R*)-4.

(*R*,*R*)-**4**
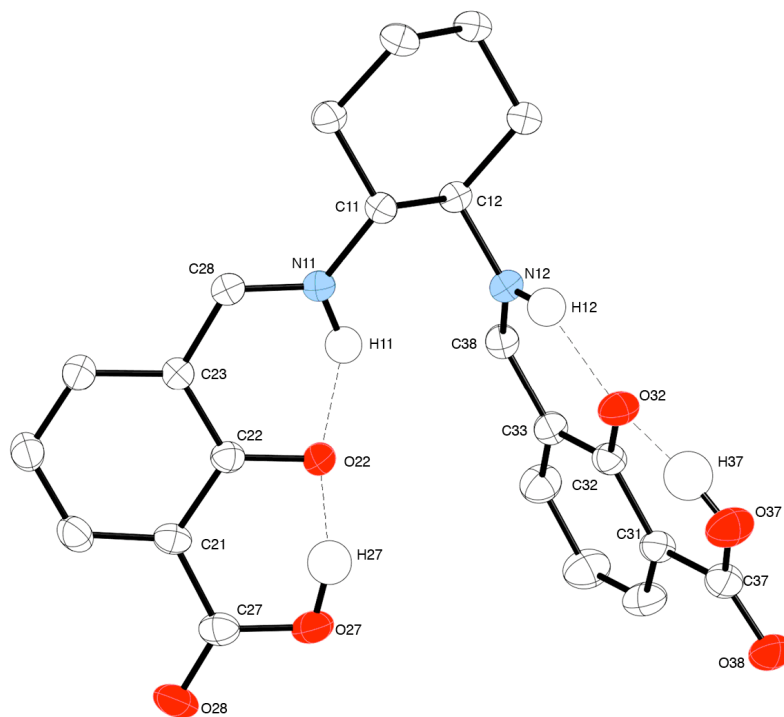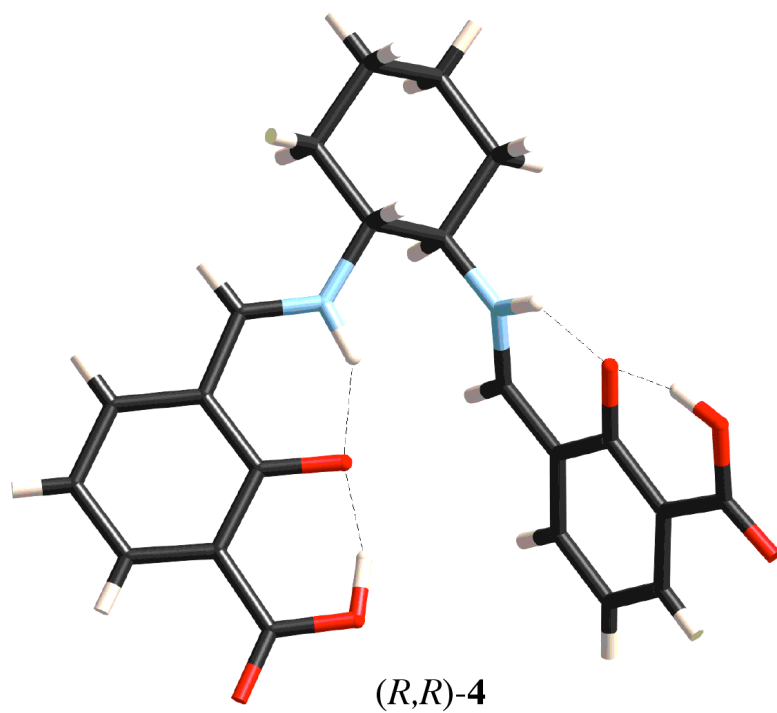
Table 2.2. Selected bond lengths (Å) and bond angles (°) for (*R,R*)-4

Bond lengths	C(11)-N(11)	1.4596(15)
	N(11)-C(28)	1.2936(16)
	C(12)-N(12)	1.4659(15)
	N(12)-C(38)	1.3007(17)
	C(22)-O(22)	1.3023(15)
	C(27)-O(28)	1.2169(16)
	C(27)-O(27)	1.416(11)
	N(23)-C(48)	1.3254(18)
	C(32)-O(32)	1.2973(15)
	C(37)-O(38)	1.2166(17)
	C(37)-O(37)	1.3257(19)
Bond angles	N(11)-C(11)-C(12)	108.41(10)
	C(28)-N(11)-C(11)	127.72(11)
	N(12)-C(12)-C(11)	108.58(10)
	C(38)-N(12)-C(12)	125.17(11)
	O(28)-C(27)-O(27)	121.13(13)
	O(38)-C(37)-O(37)	121.40(14)

Table 2.3. Selected hydrogen bond lengths (Å) and bond angles (°) for (*R,R*)-4

D-H...A	d(D-H)	d(H...A)	d(D...A)	<(DHA)
N(11)-H(11)...O(22)	0.949(18)	1.696(18)	2.5392(13)	146.2(17)
N(12)-H(12)...O(32)	0.901(19)	1.826(18)	2.5905(14)	141.2(16)
O(27)-H(27)...O(22)	0.97(2)	1.54(2)	2.4793(13)	160(2)
O(37)-H(37)...O(32)	0.95(2)	1.58(2)	2.4794(14)	157(2)

Figure 2.19. Thermal ellipsoid plot (50% probability) and tube representation of (*R,R*)-5.

(*R,R*)-**5**
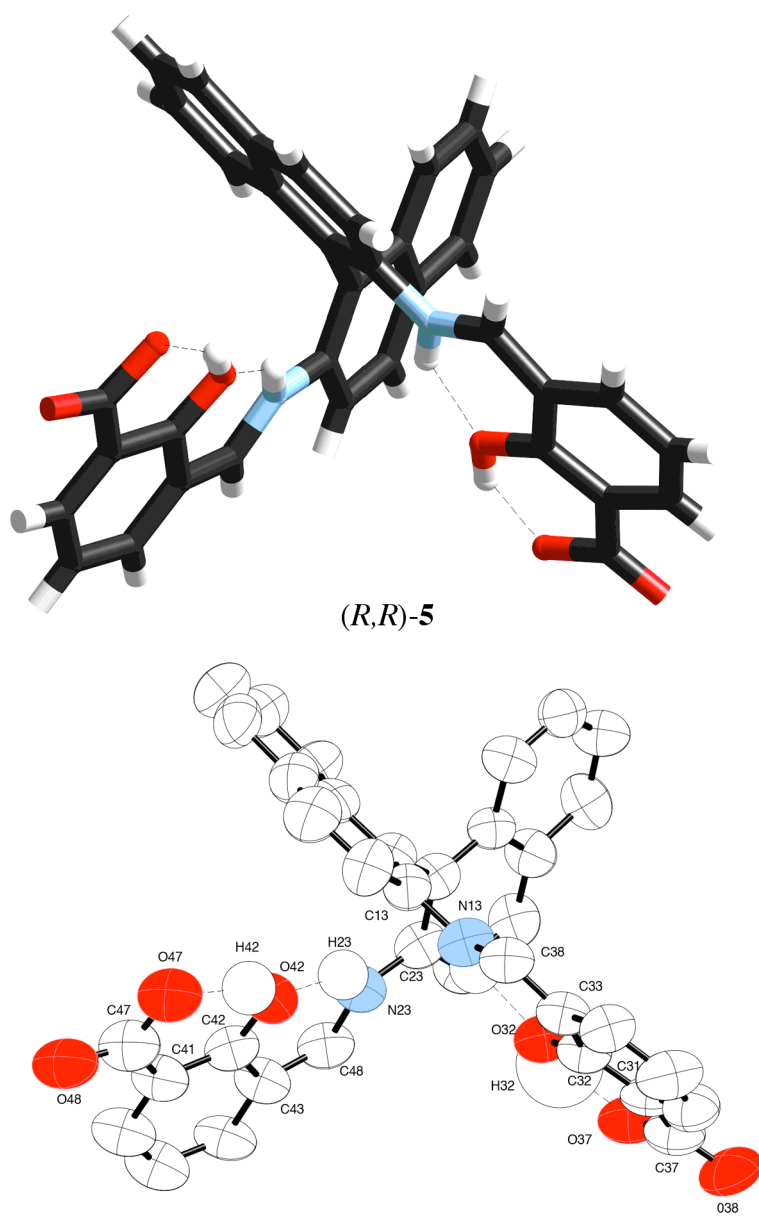
Table 2.4. Selected bond lengths (Å) and bond angles (°) for (*R*,*R*)-5

Bond lengths	C(12)-C(13)	1.356(12)
	C(12)-C(22)	1.483(11)
	C(13)-N(13)	1.422(12)
	N(13)-C(38)	1.286(11)
	C(22)-C(23)	1.394(11)
	C(23)-C(24)	1.402(11)
	C(23)-N(23)	1.416(11)
	N(23)-C(48)	1.284(10)
	C(31)-C(37)	1.487(12)
	C(32)-O(32)	1.298(10)
	C(37)-O(38)	1.204(13)
	C(37)-O(37)	1.332(13)
	C(41)-C(47)	1.460(11)
	C(42)-O(42)	1.283(10)
	C(47)-O(48)	1.242(13)
	C(47)-O(47)	1.310(12)
Bond angles	C(12)-C(13)-N(13)	118.3(7)
	C(14)-C(13)-N(13)	118.6(8)
	C(38)-N(13)-C(13)	128.6(7)
	C(22)-C(23)-N(23)	115.9(7)
	C(24)-C(23)-N(23)	121.1(8)
	C(48)-N(23)-C(23)	128.9(7)
	O(38)-C(37)-O(37)	121.4(9)
	O(48)-C(47)-O(47)	120.6(8)

Table 2.5. Selected hydrogen bond lengths (Å) and bond angles (°) for (*R*,*R*)-5

D-H...A	d(D-H)	d(H...A)	d(D...A)	<(DHA)
N(13)-H(13)...O(32)	0.88	1.83	2.553(9)	138.2
O(32)-H(32)...O(37)	0.84	1.72	2.477(9)	148.2
N(23)-H(23)...O(42)	0.88	1.76	2.499(9)	139.5
O(42)-H(42)...O(47)	0.84	1.71	2.465(8)	48.3

CHAPTER 3 - Synthesis and characterization of zwitterionic Schiff-base ligands

3.1 Introduction

Schiff bases derivates of 3-formylsalicylic acid (Figure 3.1) can easily be modified to give a wide variety of symmetric and unsymmetric multidentate ligands[35,40,66] and the terminal acid groups can be further functionalized or act as directing groups for the formation of supramolecular arrays.

Figure 3.1. General structure of a 3-formylsalicylic acid derived Schiff-base.
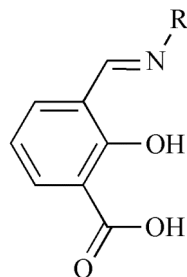
Studies by Okawa,[35,41,43] Khan[40] and Dey[42,67] on metallation by tridentate ligands of this type show that they can form mono- or dinuclear complexes with divalent metals (figure 3.2) in when activated by bases; weak bases result in the formation of the mononuclear complexes, while strong bases such as KOH almost exclusively yield the dinuclear complex as the final product. In mononuclear complexes, the imine and phenoxide donors coordinate to the metal, while the carboxylic acid remains free (figure

3.2, **I**). In dinuclear complexes, the metals occupy both the imine/phenoxide as well as the phenoxide/carboxylate pockets of the ligands, (figure 3.2, **II**). Neither the mono- or dinuclear complexes have shown helical structures, but instead have a planar arrangement of the donors at the metal center.

Figure 3.2. Structure of previously reported complexes based on Schiff base derivates of 3-formylsalicylic acid

M = divalent metal ion
R = alkyl, aryl group
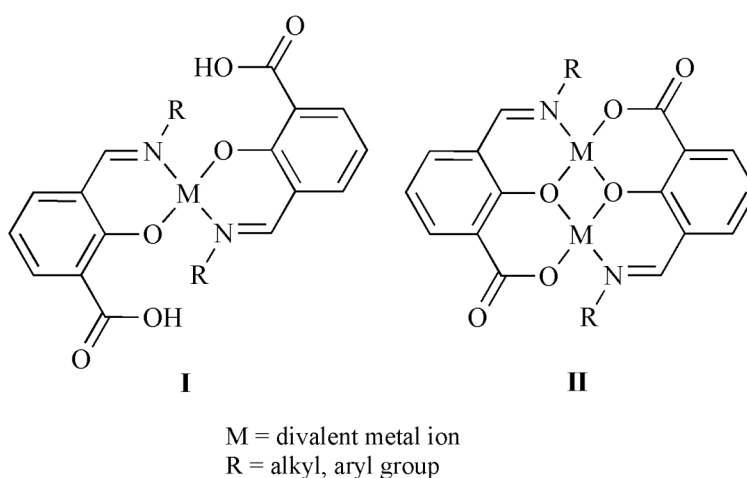
For the formation of helicates, two strands have to bind to one metal only and be twisted with respect to one another. The use of a weak base, such as triethylamine, will promote the formation of such complex since it can selectively form singly-deprotonated ligands. Furthermore, the presence of additional chelating groups on the ligands can direct the complex to adopt a more twisted conformation. An additional donor creates a tridentate ligand that has the potential to form a double-stranded complex. If the new linker is chiral, then double-stranded helices of only one handedness can be achieved. Furthermore, if a flexible linker is applied, then *facial* isomers are possible (e.g. **III**, figure 3.3). There are 11 possible *facial* isomers, but the situation is much simpler if a

more rigid linker is employed since only *meridional* isomers can be formed (e.g. **IV**, figure 3.3). In this case only two isomers are possible, the minus (*M*) and plus (*P*) helical forms (alternately Λ and Δ, respectively). When one configuration of a chiral ligand is employed, then the two isomers are diastereomers, and the possibility exists that helices of only the most stable complex can be isolated.

Figure 3.3. The addition of a third chelating group to the ligand can form two different complex types; *facial* or *meridional.*
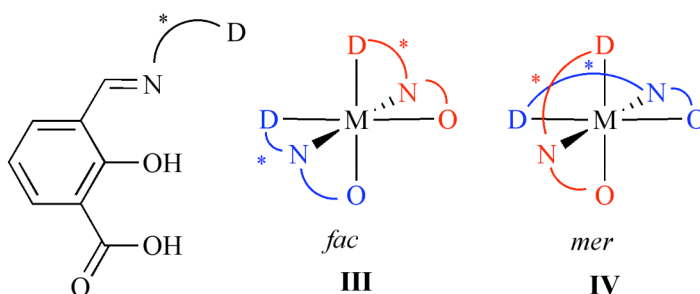
Zwitterionic acid functionalized Schiff-bases possess qualities that are of use both in complexation reactions as well as in the synthesis of new chelating salen ligands. The four donor groups; amine, imine, phenol/phenoxide and carboxylic acid/carboxylate, can be used as tools in the investigation and understanding of complexation and the disposition of metal binding sites. By changing the reaction conditions (nature of the added base and/or hydrogen bonding ability of the solvent) these ligands can easily be modified to act as bi-, tri- or multidentate chelates and binding different modes to the metal center(s). A systematic change of the reaction conditions will change the binding mode of the ligand and allow for investigation of the coordination chemistry of different complexation modes of the systems. Additionally, the self-protected zwitterions used in

this work can elegantly be converted to a wide variety of unsymmetrical Schiff-base and Schiff-base related ligands simply by a condesation reaction with a second amine group.[68]

Despite their unique qualities, zwitterionic Schiff-base ligands are extremely rare. In fact, the only other related system is reported by Mirkin *et. al,* where the 4- and 5-substituted acidaldehydes were utilized (Figure 3.4).[68] However, having the carboxylate further away from the reaction pocket (*pseudo*-salen pocket) reduces the possibility of its participation in the metal binding process.

Figure 3.4. Similar zwitterionic acid functionalized Schiff bases based on 4- and 5- substituted acidaldehydes**.**
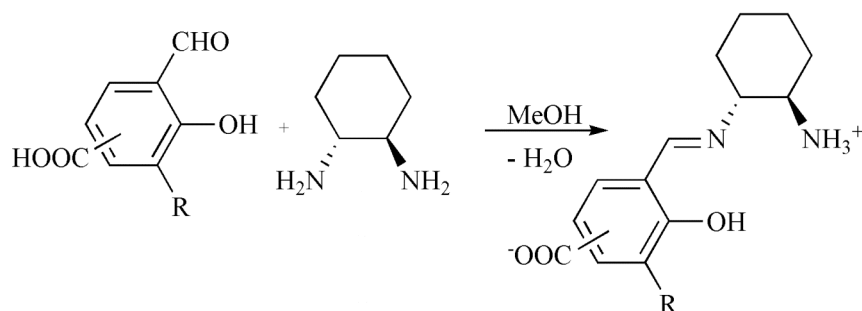
Chiral diamines, (*R,R*)-**6** and (*R,R*)-**7** (Figure 3.5) can serve as excellent linkers in these new Schiff base ligands. While one amine group participates in the imine bond formation, the other remains as a free amine and can act as the third chelating group to a metal. Furthermore, the rigidity of the linker can easily be modified by the use of diamines with different sizes, flexibility and basicity. Finally, these diamines can introduce chirality to the ligand and increase the chances of forming helices of a predetermined configuration.

Figure 3.5. CHDA and BINAM derived Schiff-bases used in this work.
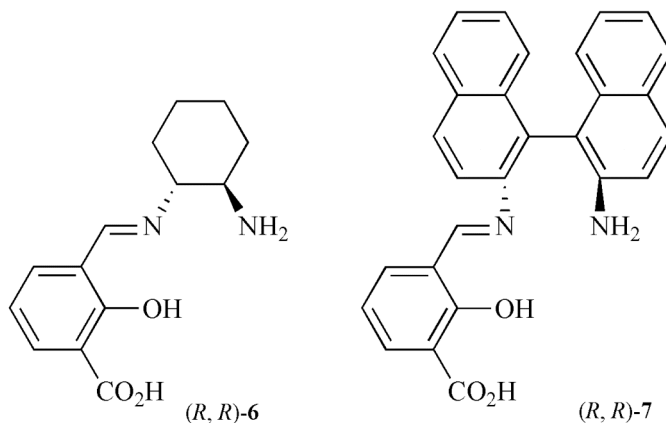
3.2 Synthesis of 3-formylsalicylic acid based ligands

The addition of an equimolar amount of (1R,2R)-cyclohexyldiamine (R,R)-**1** and (R)-binaphthyldiamine (R)-**2** to the symmetrical salen ligands (R, R)-**4** and (R,R)-**5**, yield the unsymmetrical ligands (R, R)-**6** and (R, R)-**7** as a white and a bright red solid, respectively (Figure 3.6). In solution, both Schiff-bases exist as an equilibrium mixture of their neutral and zwitterionic forms. NMR studies revealed that in DMSO and at room temperature, the predominant products are the zwitterionic component of (R,R)-**6** and a the neutral component of (R,R)**7** (Figure 3.6). The use of a protic solvent, in this case methanol, and control of the temperature in the 40–50 ˚C range are crucial for the formation and isolation of these products. In aprotic solvents such as pyridine and DMSO the Schiff-base does not form, and reaction temperatures higher than 50 ˚C reduces the yield significantly. The highest yields are achieved when the reactions are done at high concentrations with reaction times under 6 h. The starting materials (R, R)-**4** and (R,R)-**5**, are soluble in warm methanol while the products, (R, R)-**6** and (R,R)-**7**, require boiling

53

methanol to fully dissolve. A one-pot synthesis of both products from 3-formylsalicylic acid and the diamine is possible, but delivers lower yields and product mixtures. Given the high yield and purity of the two-step process and the necessity for tight control of the reaction conditions in the second step, the two-step process is preferable. Solutions of both unsymmetrical acid functionalized Schiff-base ligands show sensitivity to moisture and they should therefore be handled under a dry atmosphere. The solids are only mildly hygroscopic and can be stored on the benchtop.

Figure 3.6. Synthesis of unsymmetrical Schiff-base ligands.
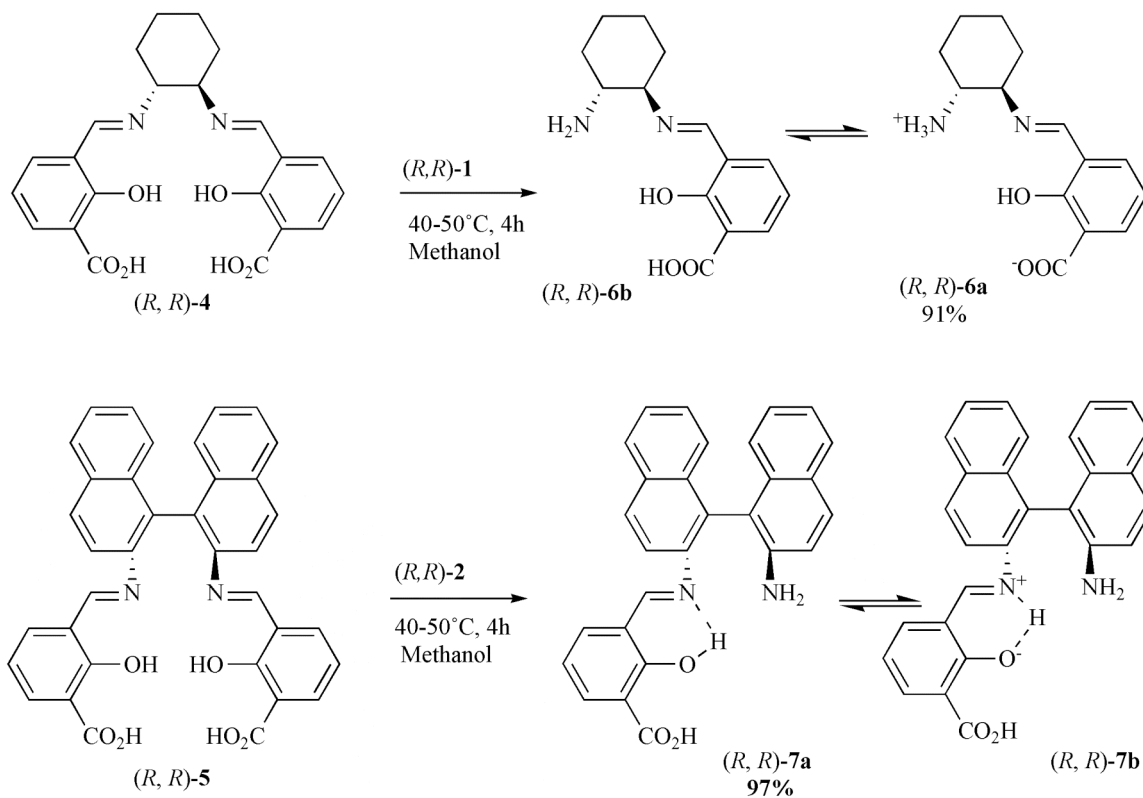
3.3 NMR spectroscopy of the CHDA derived unsymmetrical Schiff base ligand

Figure 3.7 shows the 1D-NMR ^{1}H spectrum of (R, R)-**6** in DMSO-d_6 at 25 ^{o}C. There are two sets of peaks; a major set corresponding to (R,R)-**6a** (*, Figure 3.7), and a minor set from (R,R)-**6b** (^, Figure 3.7) with a ratio of 1:6.7 (15% minor). Both sets show signals compatible with imine hydrogens, aromatic hydrogens and cyclohexyl hydrogens at 8.75 (8.61), 6.58-7.82 (6.50 – 7.71) and 1.32-3.16 (1.15-3.2) ppm respectively (data in parenthesis indicates the shifts for the minor set). In the major set, the phenol proton appears as a broad singlet at 18.02 ppm, which is consistent with a hydrogen bonded phenol.[65] The spectrum also has a broad singlet at 7.2 ppm corresponding to approximately 3 hydrogens. This is consistent with reported chemical shifts of ammonium hydrogens.[65] No protons in the characteristic carboxylic acid region could be observed at either temperature. The minor set of signals shows one broadened singlet at 4.1 ppm. This is assignable to the amine hydrogens of (R,R)-**6b**. All attempts to purify (R,R)-**6** so that a single component was observed in solution, failed. This suggests that there is a solution equilibrium between the two components, and not an impure material.

Figure 3.7. ^{1}H NMR spectra (400 MHz) of (R,R)-6 in DMSO-d_6 at 25 ^{o}C. The peaks at around 2.5 and 5.6 ppm is due to DMSO-d_6. The major (*) and minor (^) peaks are shown for the aromatic and exchangeable hydrogens
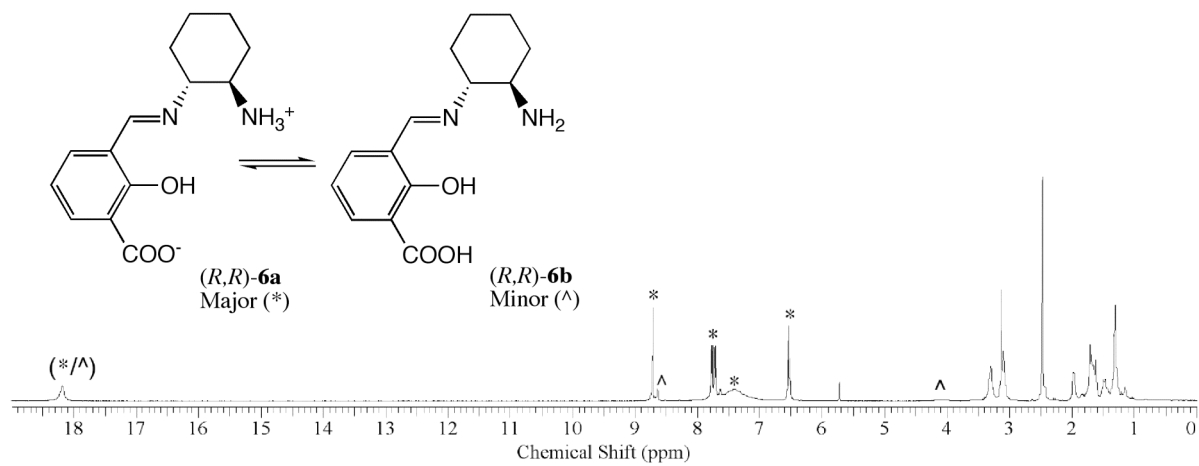
Figure 3.8. Variable Temperature (VT) experiment. ^{1}H NMR (400 MHz) of (*R,R*)-6 in DMSO-d_6/ CD$_2$Cl$_2$ at 0 - 70 ^{o}C. The singlets at 2.5 ppm, 5.6 ppm and 8.3 ppm are due to proton residues from the NMR solvents
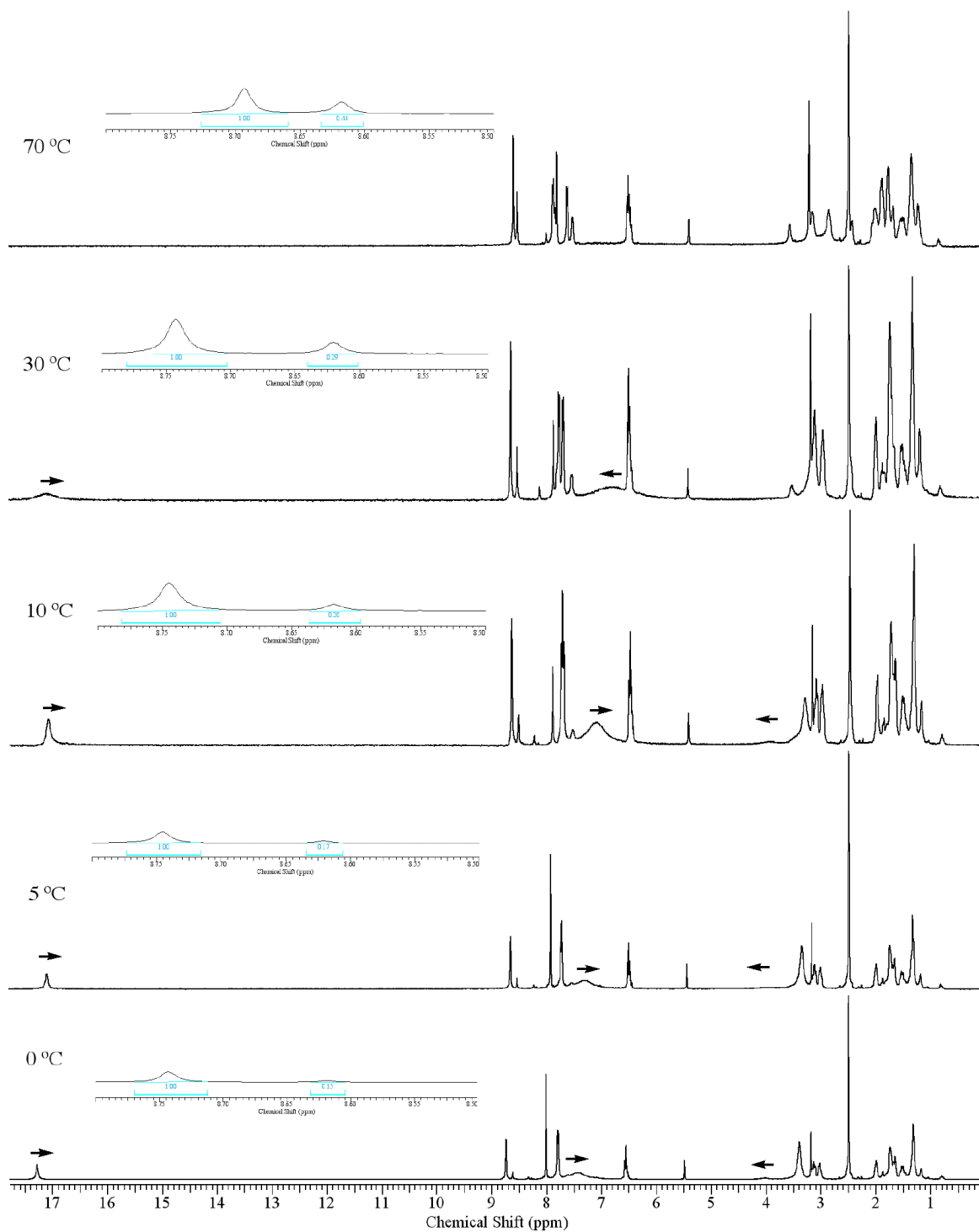
VT-NMR studies (Figure 3.8) revealed that the fraction of (R,R)-**6b** is temperature dependent and increases with increased temperature. In order to study the system below the freezing point of DMSO (18 $^{\circ}$C), NMR spectra were taken in a mixture of DMSO-d_6 and CD$_2$Cl$_2$ (3:2).

The spectrum at 0° C shows the presence of 15% of the minor component (**6b**). Integration of both the aliphatic and the aromatic region indicates the presence of additional peaks consistent with this assessment. As the temperature rises, so does the percentage of (R,R)-**6b**. At 70°C, the imine peak has increased to 44%. Also visible are the two doublets and a triplet in the aromatic region and a more complex looking aliphatic region (integration also indicate a 31% contribution).

3.3.1 Exchange process

The VT experiment suggests a complicated exchange process between the two components. At 0 $^{\circ}$C, The broadened peak at around 17.2 ppm integrates to two protons, the peak at around 7.4 ppm to three protons and the broadened peak at 4.1 ppm integrats to two protons. The peaks were assigned to phenol/carboxylate of (R,R)-**6a**/**6b**, the ammonium protons of (R,R)-**6a** and the amine hydrogens of (R,R)-**6b**, respectively. All the acidic protons are in exchange with each other (Figure 3.9).

Figure 3.9. Graphic interpretation of the observed ^{1}H NMR spectra in the VT experiment.
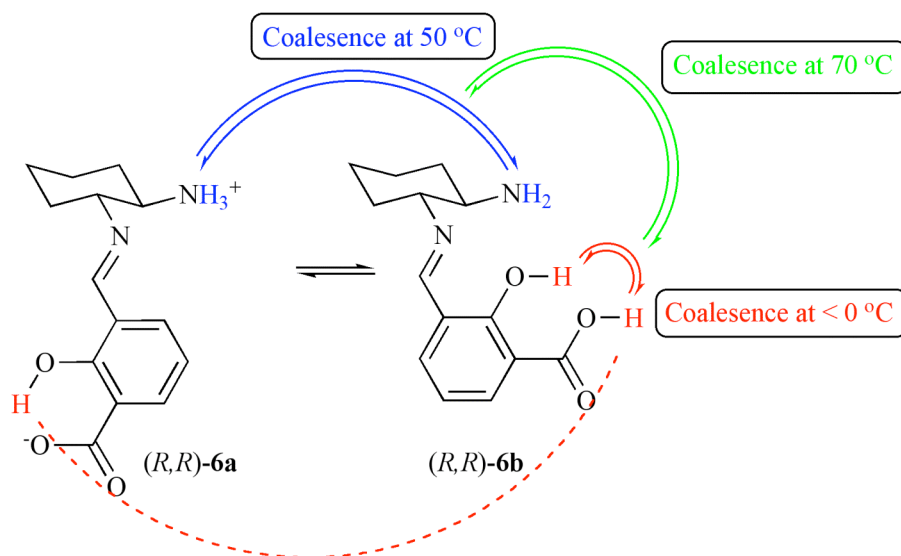
3.3.2 Phenol (6a)-phenol (6b)-carboxylate exchange

At 0 $^{\circ}$C, all phenol and carboxylic acid protons (one from (R,R)-**6a** and two from (R,R)-**2b**) appear as one broadened singlet at 17.2 ppm, suggesting that they are in fast exchange with one another. A decrease in temperature will slow this exchange process and separate the three peaks. However, as the freezing point of the NMR solvent is around 0 $^{\circ}$C, an attempt to reach this condition was not possible (Figure 3.9, red).

3.3.3 Ammonium-amine exchange

As the temperature rises, the ammonium proton signal from (R,R)-**6a** shifts upfield and the amine protons from (R,R)-**6b** shifts slightly downfield. This movement suggests an exchange process between the two protons. At 50 ^{0}C, the amine protons are no longer visible, which indicates that this is the coalescence temperature for the exchange process. The broadened peak at around 7.1 ppm corresponds to the ammonium/amine protons (Figure 3.9 blue).

3.3.4 Phenol-ammonium-amine exchange

The phenol peak is also moving upfield as the temperature rises, suggesting exchange with ammonium and/or amine protons. However, since the ammonium and amine protons are closer to each other in chemical shift, their broadening will be predominant at lower temperature for similar exchange rates. The exchange process between the phenol and ammonium-amine protons is detectable after the coalescence temperature of the ammonium-amine protons. After 50 $^{\circ}$C, the ammonium-amine peak shifts downfield as a result of the exchange process with the phenol protons. At 70 $^{\circ}$C none of the peaks are visible, which indicates that this is near the coalescence temperature for all exchangeable protons (Figure 3.9, green).

3.3.5 Exchange mechanism

Figure 3.10 shows a possible mechanism for the observed exchange process. At low temperature, (*R,R*)-**6** exists predominantly as a zwitterion with an ammonium group, hydrogen bonded phenoxide group and a carboxylate group (Figure 3.10a). As the temperature rises, the hydrogen exchange process will occur where two hydrogens are shuffled around the molecule forming the neutral analogue of (*R,R*)-**6** containing amine, phenol and carboxylic acid groups (figure 3.10b). This can also be seen in the slight upfield movement of the ammonium hydrogens in the ^{1}H-NMR. As the hydrogen transfer is completed (Figure 3.10c), the phenolic and carboxylic acid hydrogens will undergo rapid exchange with each other.

Figure 3.10. Hydrogen exchange process of (*R,R*)-6. Suggested mechanism.

a   b   c
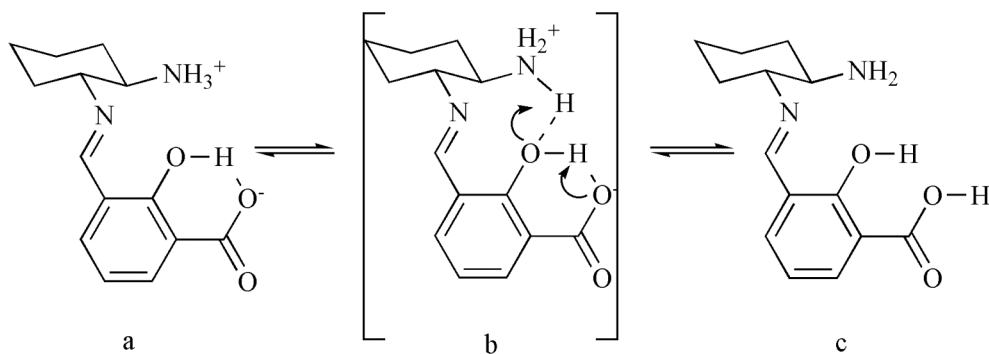
To explain the change of the interaction modes between the amine hydrogens and the phenol/carboxylic acid pocket, it is likely that the cyclohexyl backbone undergoes chair/chair interconversion to create either the equatorial/equatorial (*R,R*)-**6a** or the axial/axial (*R,R*)-**6b** (Figure 3.11). An eq/eq configuration (figure 3.11a) will bring the three groups closer to each other favoring hydrogen exchange while the axial/axial configuration (figure 3.11b) will prohibit an intramolecular hydrogen exchange between the amine hydrogens and the phenol/carboxylic acid.

Figure 3.11. Interconversion of the cyclohexyl backbone can be an underlying reason to the observed hydrogen exchange process.

a   b
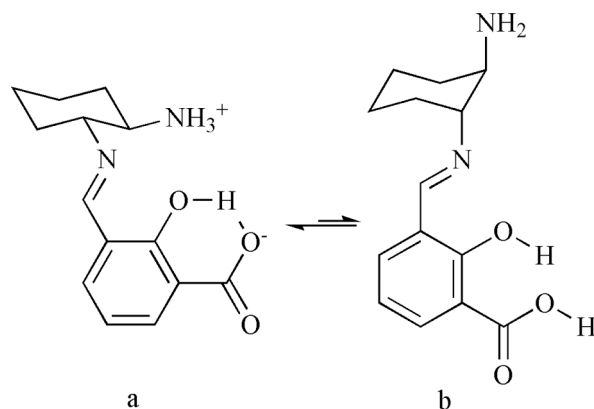
Figure 3.12 shows the effect of concentration on the exchange process. The formation of (*R,R*)-**6b** is favored at lower concentration.

Figure 3.12. The effect of concentration on the exchange process. ^{1}H NMR (400 MHz) of (*R,R*)-6 in DMSO-d_6.
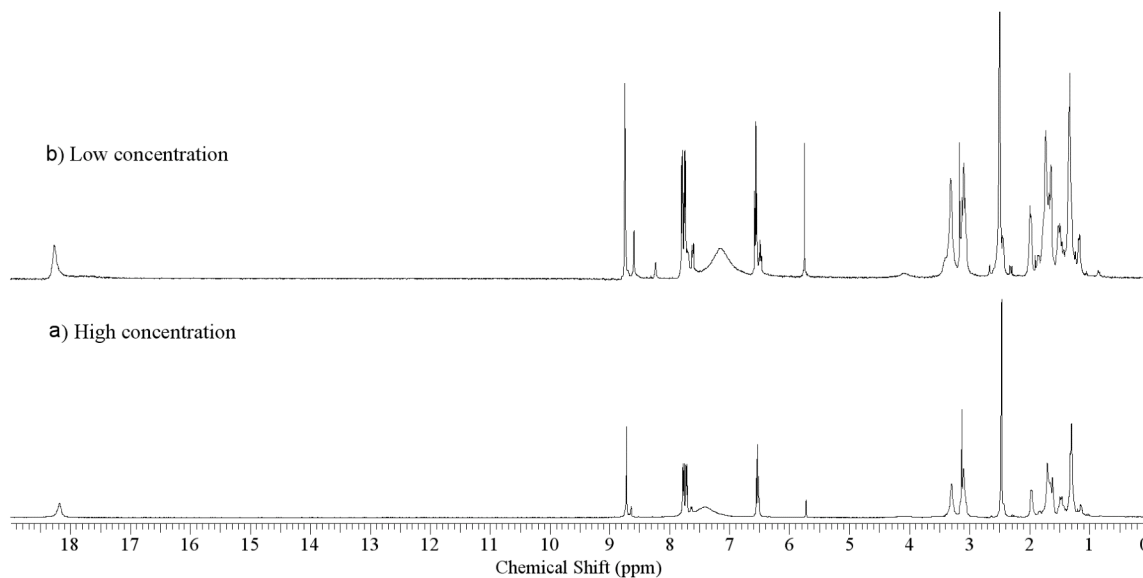
As the solution concentration decreases, the concentration of the minor peak (*R,R*)-**6b** increases indicating that it is favored when there are few intermolecular interactions.

3.4 NMR spectroscopy of the BINAM derived unsymmetrical Schiff-base ligand

Figure 3.13 shows the ^{1}H and ^{13}C NMR spectra of (*R,R*)-**7** in DMSO-d_6 and pydine-d_5. The ^{1}H NMR spectrum shows twice as many aromatic peaks as expected, based on C_2 symmetry. However, there are no visible amine, phenol or carboxylic acid hydrogens.

Interestingly, when the sample is taken in DMSO-d_6 (Figure 3.14) the number of resonances stays the same, but the peak integrals change significantly and the spectra resembles that of a product mixture with a ratio of approximately 1:4. Furthermore, there are two broad peaks present at approximately 4.7 ppm and 15 ppm.

Figure 3.13. 1D-NMR of (*R,R*)-7 in a) ^{1}H-NMR (400 MHz) in pyridine-d_5, b) ^{1}H-NMR (800 MHz) in DMSO-d_6, c) ^{13}C-NMR (200 MHz) in DMSO-d_6.
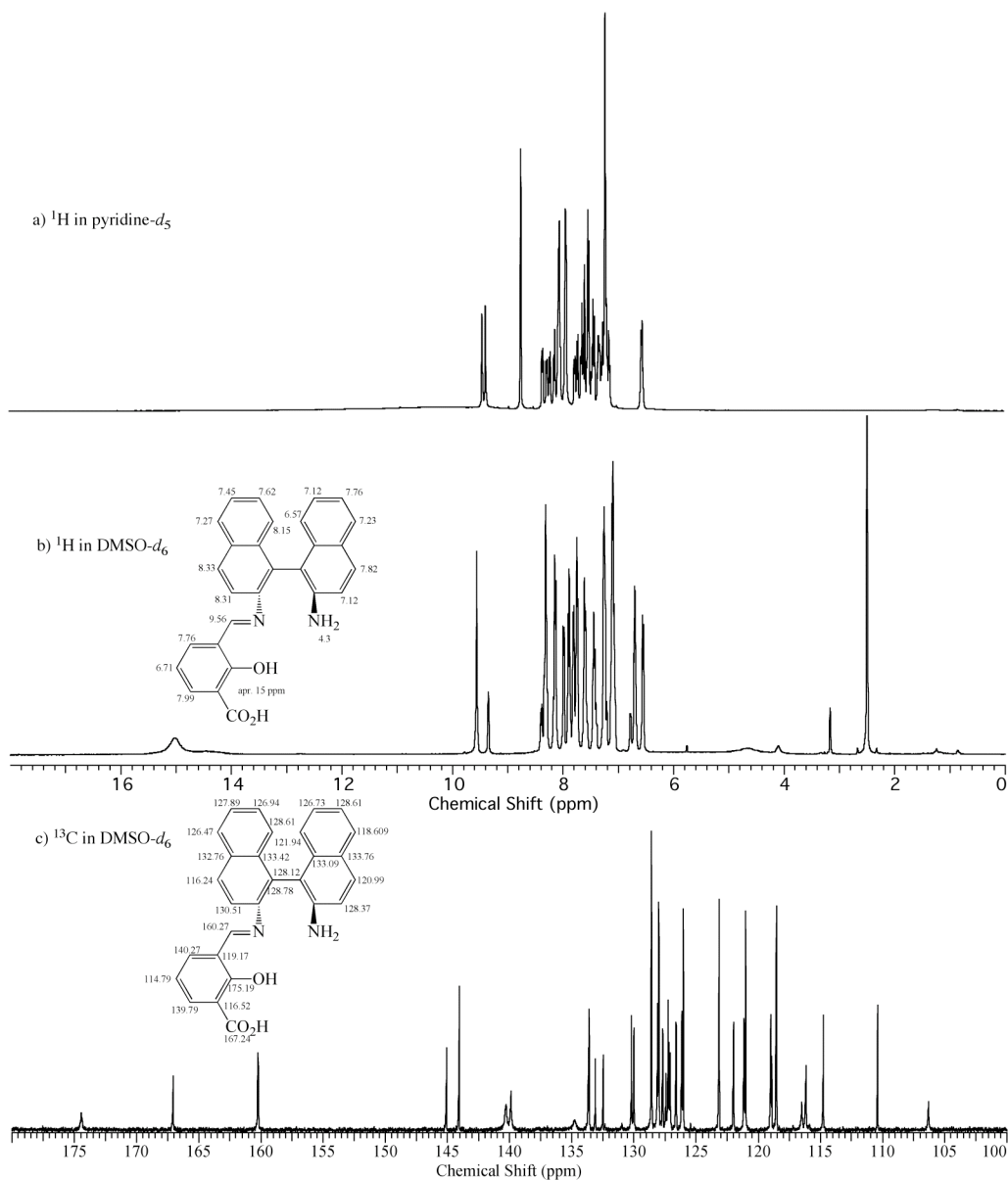
Figure 3.14. ^{1}H NMR of (R,R)-6 in DMSO-d_6 (800 MHz) and pyridine-d_5 (400 MHz).

a) ^{1}H in pyridine-d_5

1.00 1.05

b) ^{1}H in DMSO-d_6

1.00   0.30

9.5   9.0   8.5   8.0   7.5   7.0   6.5   6.0

Chemical Shift (ppm)
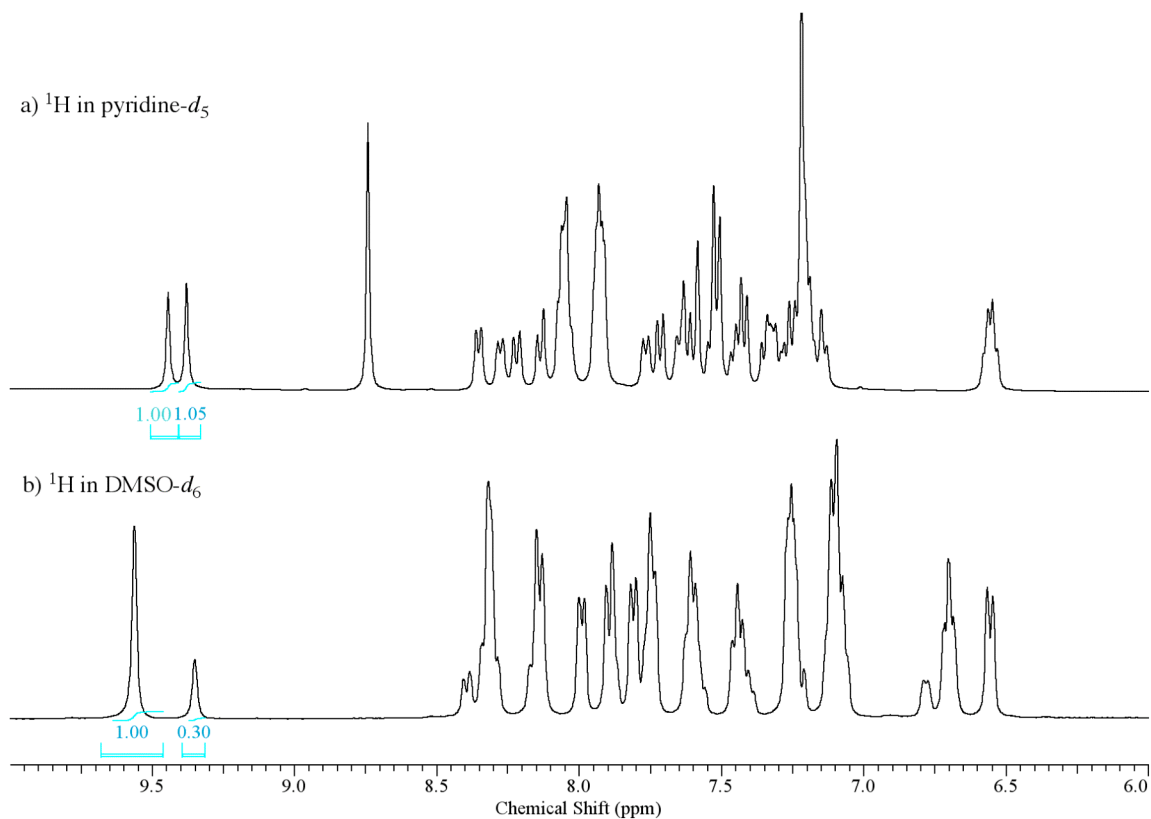
2D-NMR techniques (COSY, NOESY, HMBC and HMQC) helped determine the structure of the major signals in DMSO-d_6 (Figures 3.15 -3.18.). Starting with the known imine resonance at 9.56 ppm, COSY (Figure 3.15) could help identify the doublet, triplet, doublet pattern of the phenyl arm (7.76, 6.71 and 7.99 ppm). NOESY (Figure 3.16) showed NOE between the imine hydrogen and the proton located α to the imine moiety on the binaphthyl backbone at 8.33 ppm. The remaining peak assignment for the binaphthyldiamine backbone were determined by combining information from HMQC (Figure 3.17) and HMBC (Figure 3.18), along with comparisons with NMR data from the free binaphthyldiamine and the salen ligand (R,R)-**5**. A complete peak assignment for the major component is shown in figure 3.8b (^{1}H) and 3.8c (^{13}C). The broad singlet at 15

ppm resembles that of the hydrogen exchanged resonance of the salen ligand (*R,R*)-**5** where the phenolic and the carboxylic hydrogens are in exchange with each other (Figure 2.13b). The broadened singlet at 4.3 ppm correlates to the amine hydrogens of the binaphthyldiamine and is therefore indicating the presence of a free amine. However, the amine protons are participating in exchange processes, which is indicated by the broadness of the peak (this exchange will be explained later in this chapter). It should be mentioned that although there are many similarities with both binaphthyldiamine and the salen ligand (*R,R*)-**5**, there is no evidence of the presence of these two species in the NMR spectra based on the chemical shifts.

Figure 3.15. COSY NMR (800 MHz) spectum of (*R*,*R*)-7 in DMSO-*d*₆.

Figure 3.16. NOESY NMR (800 MHz) spectrum of (*R,R*)-7 in DMSO-*d*₆
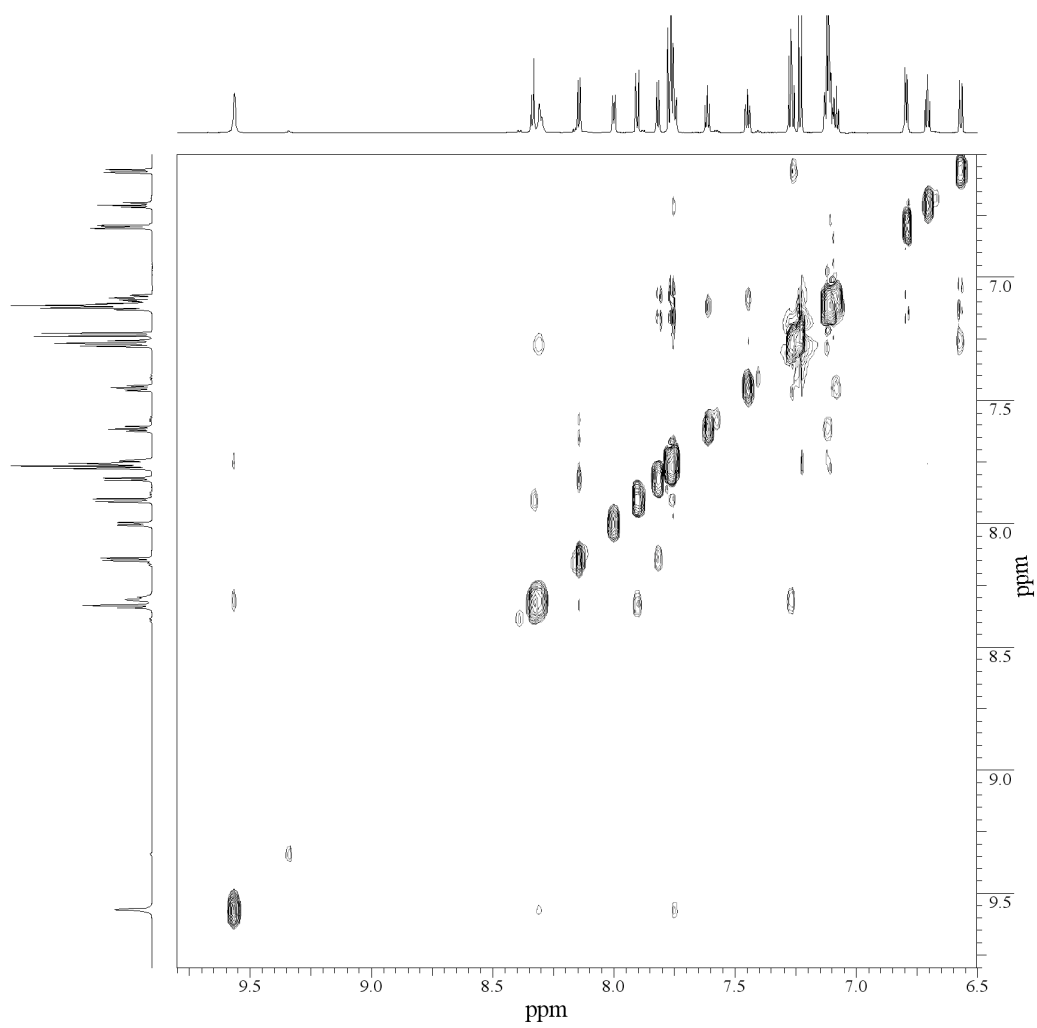
Figure 3.17. HMQC NMR (800 MHz for ^{1}H) spectrum of (*R*,*R*)-7 in DMSO-*d*$_6$.
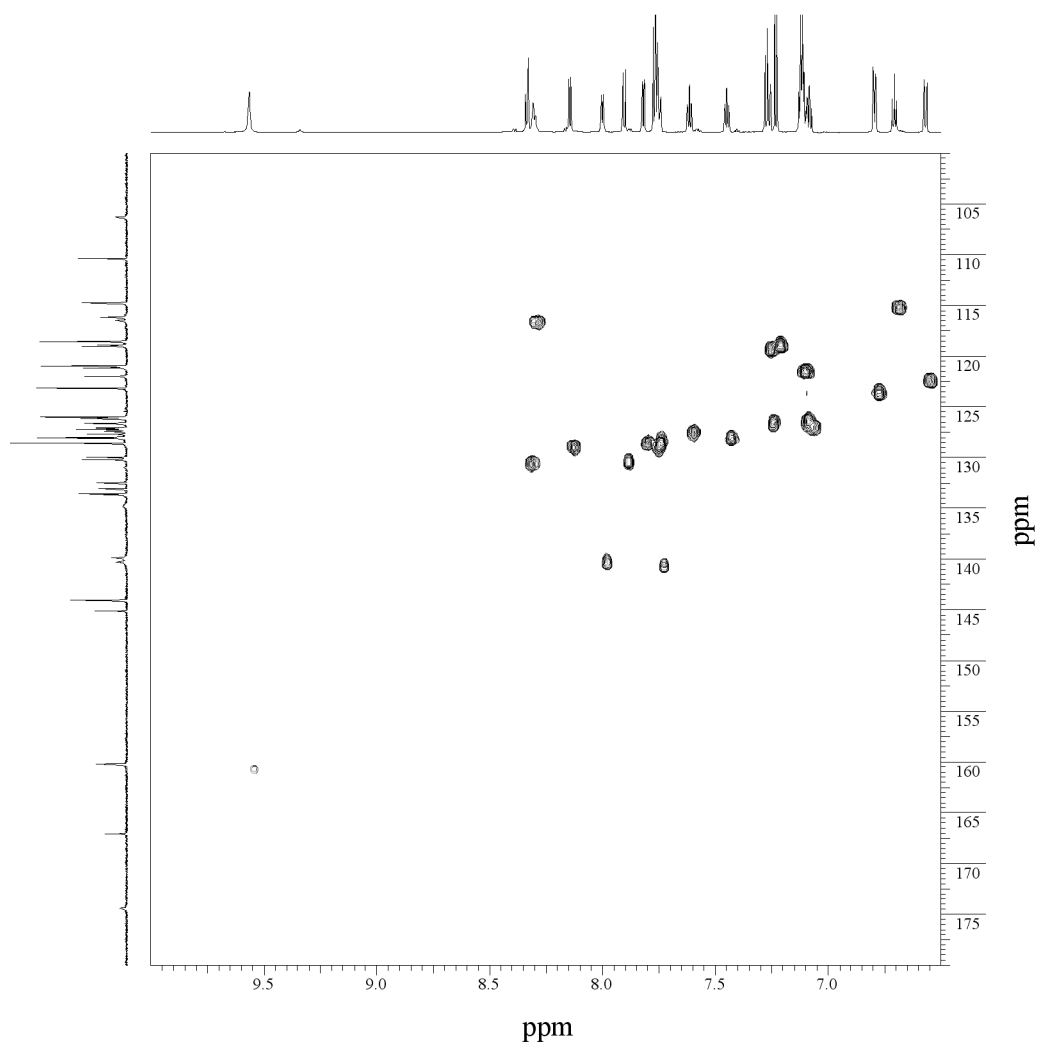
Figure 3.18. HMBC NMR (800 MHz for ^{1}H) spectrum of (*R,R*)-7 in DMSO-*d*$_6$.
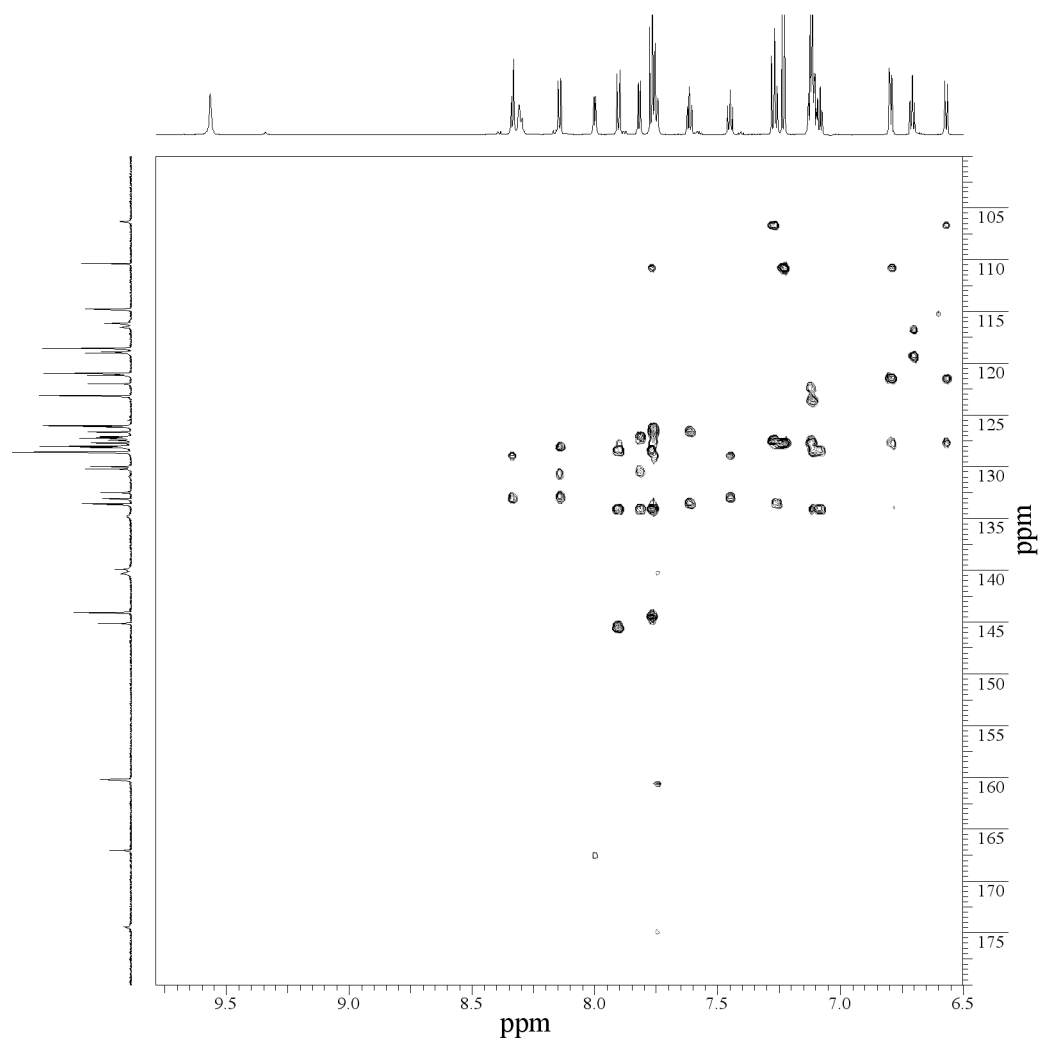
Based on the preceding analysis, the major set of resonances was determined to be the neutral unsymmetrical acid functionalized salen ligand (*R,R*)-**7a** (Figure 3.19). Although the assignment of the major peak was fairly straightforward, the analysis of the minor peak resulted in some uncertainties. The aromatic region (both peak numbers, integrals and appearances) shows the same molecular skeleton as (*R,R*)-**7a**. However, due to the low intensity of the peaks, the exchanging protons could not be detected, leaving us with questions about intramolecular hydrogen bonding and proton exchange processes. The

aromatic amine present in the molecule is not basic enough to deprotonate the carboxylic acid. Therefore, the formation of an ammonium ion and carboxylate is not likely. However, crystal structures of this ligand showed a somewhat different arrangement. (*R,R*)-**7b** in figure 3.19 shows the zwitterion obtained from X-ray analysis. There is an iminium hydrogen and a phenoxide present in the molecule. A proton transfer of this kind has been reported previously for the solution states of salen ligands with similar structures.[59b,69] There, it was suggested that the compound undergoes an enol-imine/keto-amine tautomerization is shown in figure 3.19. The formation of a iminium/phenoxed ion can result in the same tautomerization process.

Figure 3.19. Hydrogen exchange process for (*R,R*)-**7**

(*R, R*)-**7a**

(*R, R*)-**7a**   (*R, R*)-**7b**

enol-imine   *keto-amine*
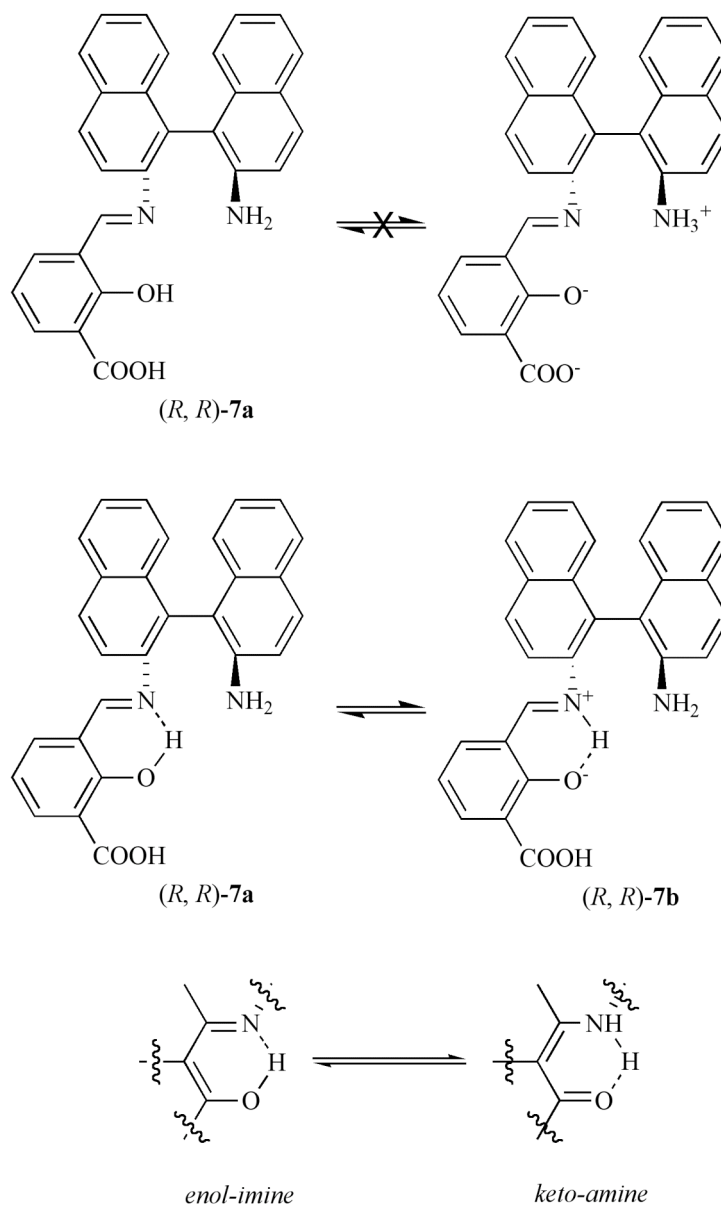
The VT-NMR analysis of (*R,R*)-**7** in pyridine-d_5 is shown in figure 3.20. There is no change in the ratios of the two imine peaks as the temperature is varied. This indicates that an increase in temperature does not affect the position of the equilibrium between the two components. However, there is a significant shift in the ppm of the two imine (HC=N) protons. This shift is much more significant that for (*R,R*)-**6** which suggests the

imine group in (R,R)-**7** is more directly involved in the exchange process. The formation of an iminium/phenoxide would have a larger impact on the imine hydrogens compare to an ammonium/carboxylate formation as in the case for the cyclohexyldiamine based zwitterion. Furthermore, as the temperature increases, a broadened signal at around 9.5 ppm starts to appear. In the few cases where iminium hydrogens have been detected by NMR, they appear at similar chemical shifts (9-11 ppm).[70] Referring back to the ^{1}H NMR spectra of (R,R)-**7** in DMSO-d_6 (Figure, 3.13b), it is clear the three protons at 15, 14,6 and 4.4 ppm (carboxylic acid, phenol and amine) are in exchange with each other since they are significantly broadened.

Figure 3.20. Variable Temperature (VT) experiment. ^{1}H NMR (400 MHz) of (R,R)-7 in pyridine-d_5 at 25 - 85 ^{o}C.
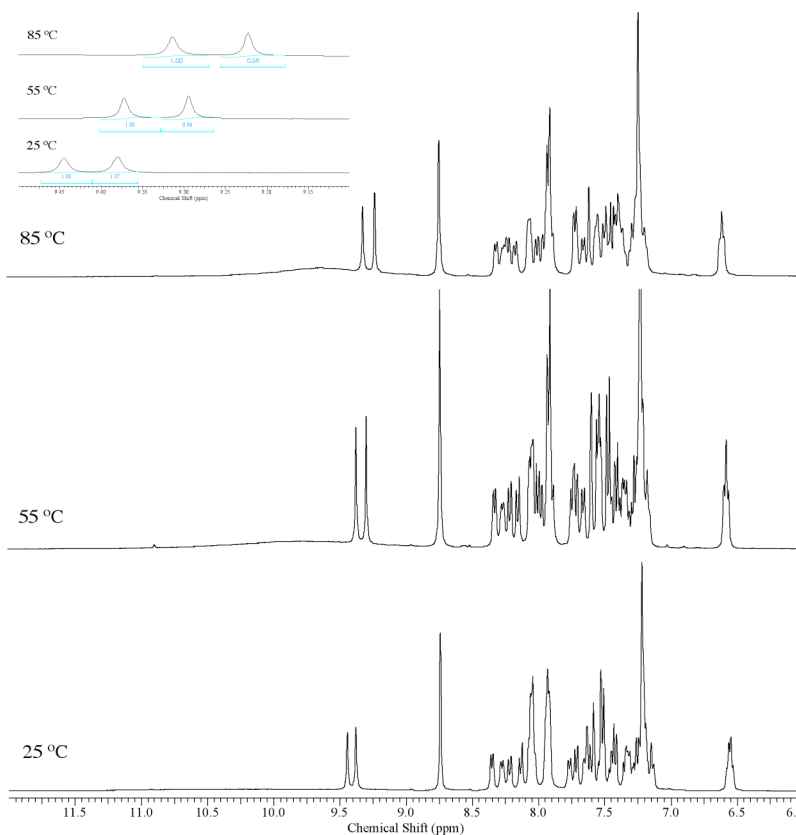
3.5 Solid state structure of unsymmetrical Schiff base ligand

Component (*R*, *R*)-**6** exists as a zwitterion (Figure 3.21) with a primary ammonium ion and a terminal carboxylate that participates in an intramolecular hydrogen bond with the phenol proton. In the crystal lattice, each molecule is hydrogen-bonded in a zigzagged, head-to-toe fashion with two adjacent molecules (Figure 3.22a). This forms a pleated hydrogen bonded sheet (Figure 3.22b). Table 3.1 and 3.2 show selected bond lengths, bond angles and hydrogen bonding properties of (*R*,*R*)-**6**.

Figure 3.21. Thermal ellipsoid plot (50% probability) and tube representation of (*R,R*)-**6**

(*R,R*)-**6**
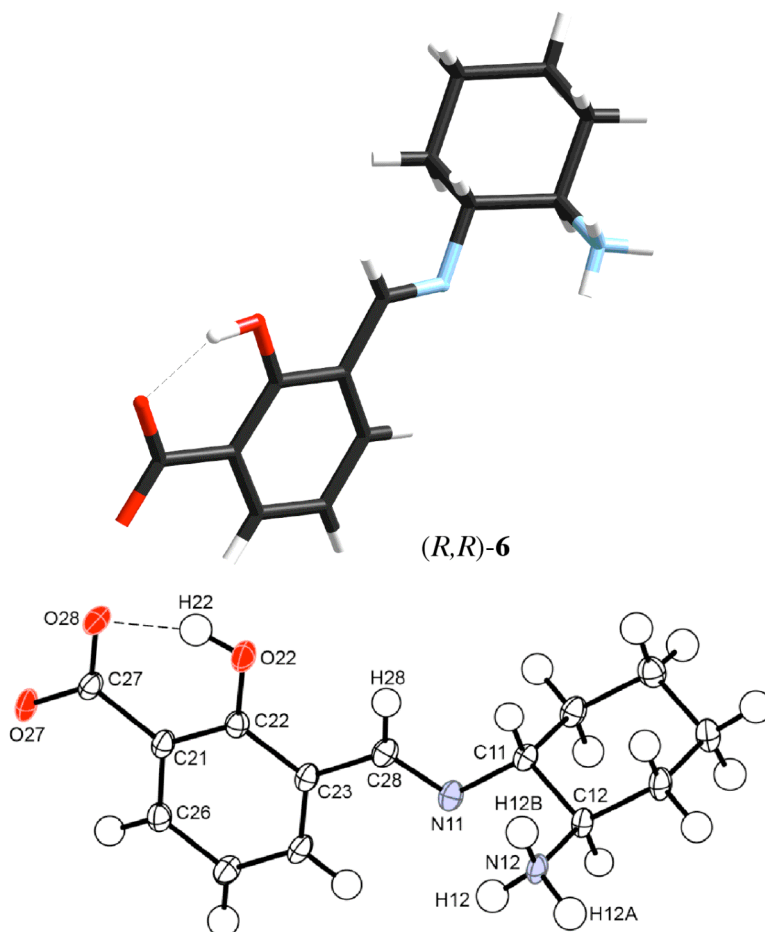
Figure 3.22. Crystal packing structure of (*R,R*)-6. a) viewed down a, b) viewed down b.

a

b
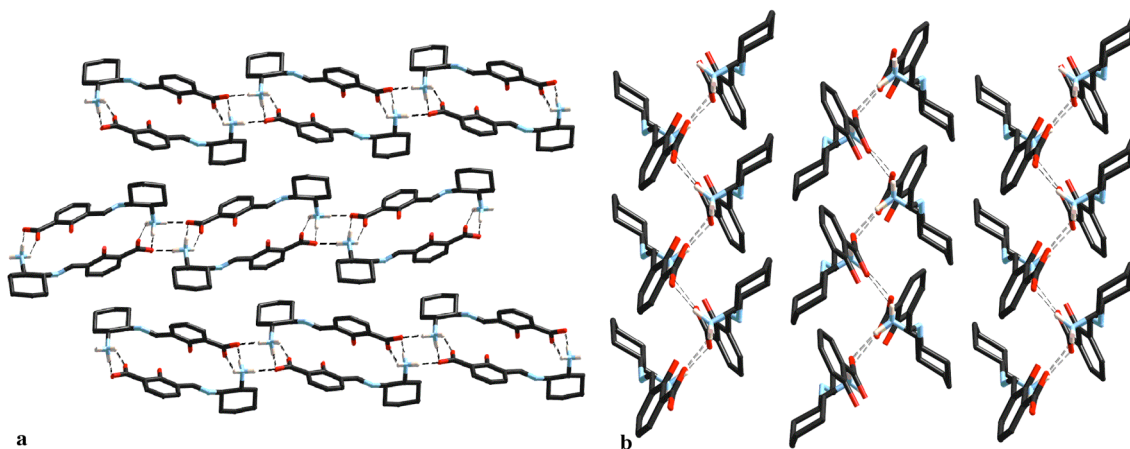
Table 3.1. Selected bond lengths (Å) and bond angles (°) for (*R,R*)-6.

Bond lengths	C11-N11	1.459(3)
	C12-N12	1.496(3)
	C28-N11	1.270(3)
	C22-O22	1.338(3)
	C21-C27	1.501(3)
	C27-O27	1.268(3)
	C27-O28	1.265(3)
Bond angles	N11-C11-C12	110.53(19)
	C11-C12-N12	110.08(16)
	C11-N11-C28	115.4(2)
	N11-C28-C23	122.3(2)
	O27-C27-O28	123.7(2)

Table 3.2. Selected hydrogen bond lengths (Å) and bond angles (°) for (*R,R*)-6

D-H...A	D-H (Å)	H...A (Å)	D...A (Å)	DHA (°)
O(22)-H(22)...O(28)	0.88(3)	1.73(3)	2.540(2)	152(3)
N(12)-H(12')...O(27) (B)	0.93(3)	1.79(3)	2.719(2)	176(3)
N(12)-H(12")...O(27) (B)	1.01(3)	1.80(3)	2.793(3)	169(2)
N(12)-H(12"')...O(28) (C)	0.90(3)	2.17(3)	2.942(3)	144(2)

The crystal structure of (*R,R*)-**7** is shown in figure 3.23. In the solid state, the phenolic hydrogen has been transferred to the imine nitrogen to form an iminium cation and a phenoxide. The phenoxide is participating in hydrogen bonding between both the iminium hydrogen and the carboxylic hydrogen. Weak non-covalent interactions in form of π-π* stacking are present between the aromatic groups of two molecules (Figure 3.24). However, the distance of 6.77 Å, indicates there are not strong π-π* interactions between adjacent ligands; the distance is approximately twice as long as observed for strong π-π* interactions.[71] Table 3.3 and 3.4 show selected bond lengths, bond angles and hydrogen bonding properties of (*R,R*)-**7**.

Figure 3.23. Thermal ellipsoid plot (50% probability) and tube representation of (*R,R*)-7

(*R,R*)-**7**
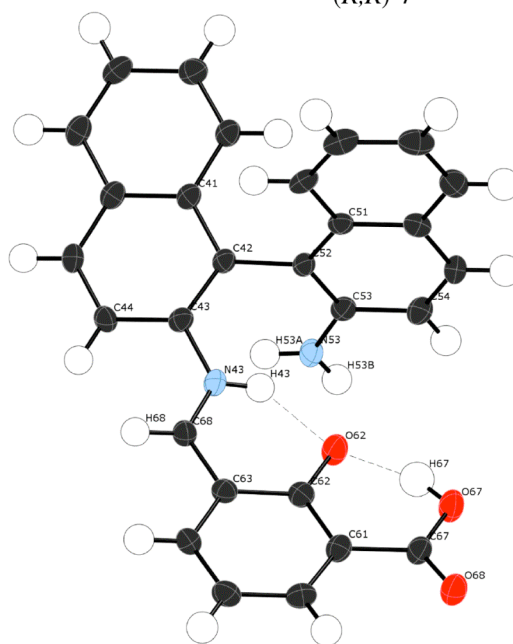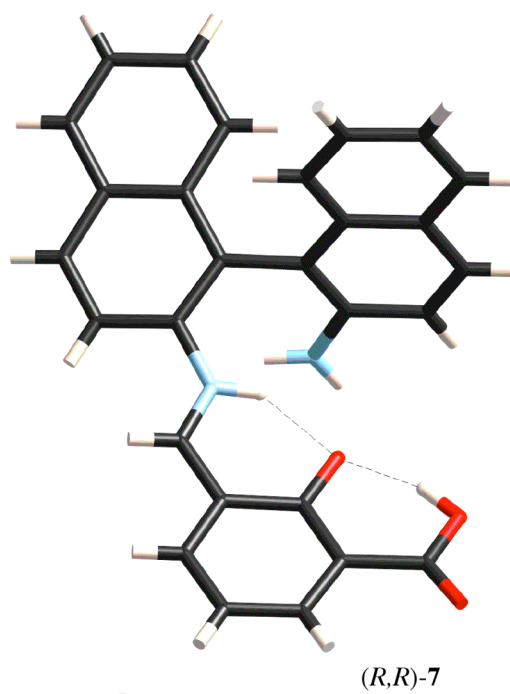
Figure 3.24. Crystal packing of (*R*,*R*)-7.

6.77 Å
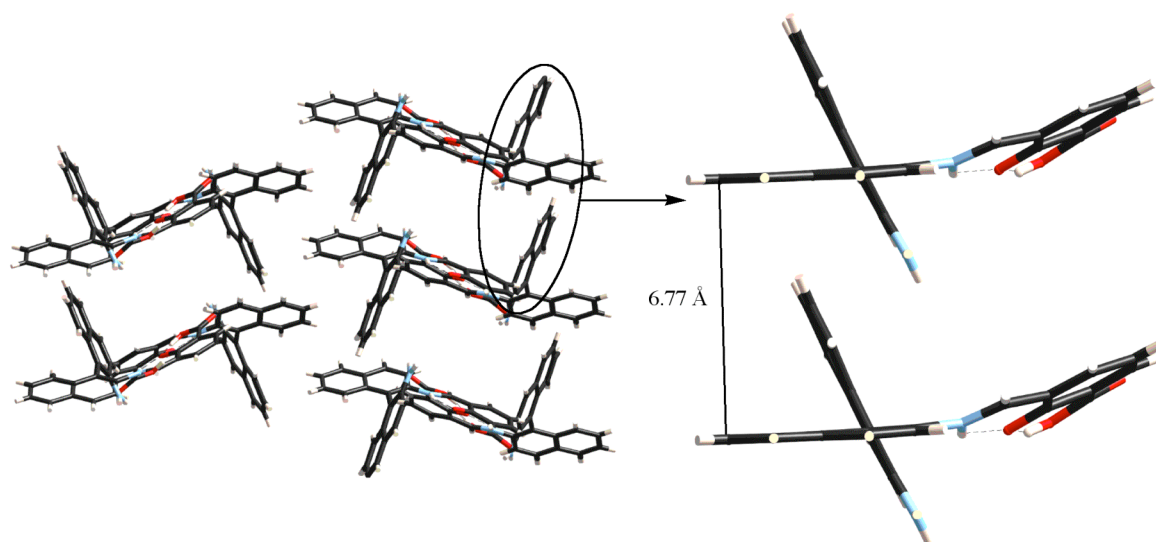
Table 3.3. Selected bond lengths (Å) and bond angles (°) for (*R*,*R*)-7.

Bond lengths	C(43)-N(43)	1.421(3)
	N(43)-C(68)	1.306(3)
	C(53)-N(53)	1.367(3)
	C(62)-O(62)	1.289(2)
	C(61)-C(67)	1.494(3)
	C(67)-O(68)	1.213(3)
	C(67)-O(67)	1.326(3)
	C(63)-C(68)	1.416(3)
Bond angles	C(42)-C(43)-N(43)	117.70(18)
	C(44)-C(43)-N(43)	119.74(18)
	C(68)-N(43)-C(43)	126.44(18)
	N(53)-C(53)-C(52)	122.10(19)
	N(53)-C(53)-C(54)	117.71(19)
	O(68)-C(67)-O(67)	121.2(2)
	N(43)-C(68)-C(63)	122.20(19)

Table 3.4. Selected hydrogen bond lengths (Å) and bond angles (°) for (*R*,*R*)-7

D-H...A	d(D-H)	d(H...A)	d(D...A)	<(DHA)
O(67)-H(67)...O(62)	0.92(3)	1.64(3)	2.490(2)	153(3)
N(43)-H(43)...O(62))	0.86	1.88	2.574(2)	137.2
N(53)-H(53B)...O(37)	0.86	2.17	3.023(2)	170.2

CHAPTER 4 - Complexation of unsymmetrical imine ligands with divalent transition metals in the presence of the weak base TEA

4.1 Introduction

Helices are of great interest due to their similarities to bioinorganic molecules such as enzymes and proteins as well as their use in asymmetric catalysis and supermolecular chemistry. A helix can be formed either by the coordination of one or two multidentate ligands to a metal center. The former will tend to result in single-stranded helices and the latter to the formation of double-stranded helices.

There has been significant study on the formation of these types of complexes, especially on single-stranded helices. Most ligands consist of nitrogen and oxygen donating polyaromatic ligands. The ligand doesn't necessarily have to be chiral. An achiral ligand of right geometry, flexibility/rigidity and size can still create a helix. However, a chiral ligand is needed to be able to control the handedness of the final complex (*M* or *P* form). Figure 4.1 shows some of the most common ligands used in the formation of single stranded helices.[50]

Figure 4.1. The structure of some common nitrogen and oxygen donating ligands that form single-stranded helices.
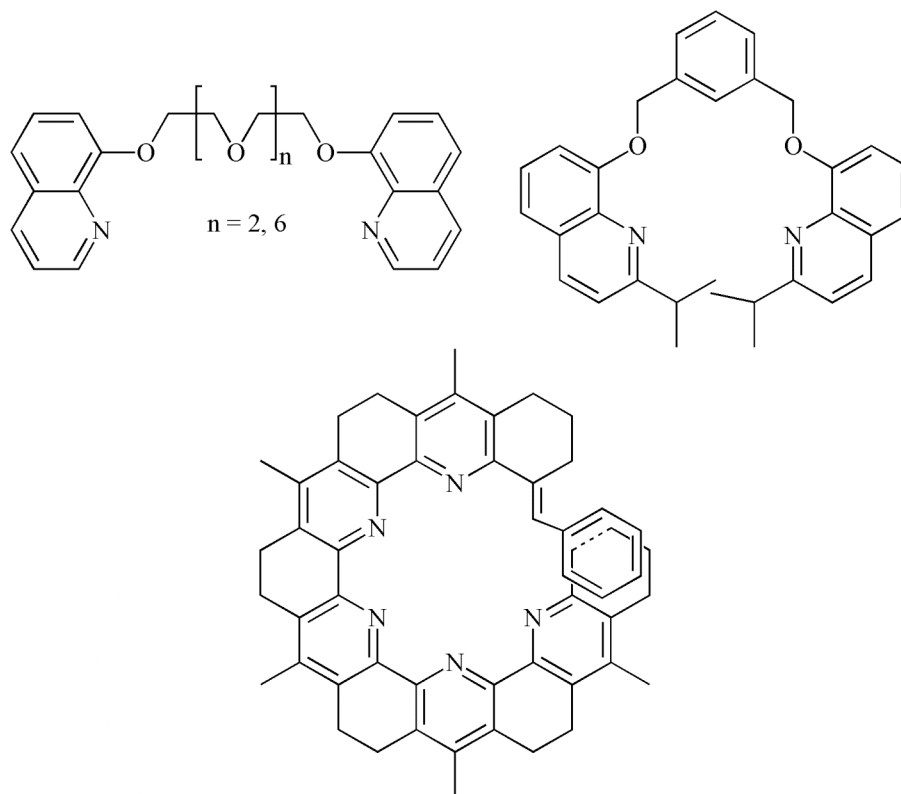
Double-stranded helices are also fairly well explored, although not in the same degree as the mono-stranded helices. In fact, there are still some challenges in the prediction of complexation of double-stranded helices, especially for tridentate ligands in combination with octahedral metal centers.[72]

Love and coworkers have shown that the formation of a double-stranded helix is favored over its dinuclear analogue (helicate) when the stoichiometry between the Schiff-base ligands and the metal complex is mismatched. Using the ligand in excess will favor the formation of the helix while a 1:1 metal/ligand ratio will result in the formation of a double-stranded helicate (Figure 4.2).[73]

Figure 4.2. Controlling the formation of double-stranded helicates and single-stranded helices by changing the metal: ligand ratio.

(i) $Mn(THF)_n[N(SiMe_3)_2]_2$
(ii) < 0.5 eq. $Mn(THF)_n[N(SiMe_3)_2]_2$

[Mn(L)]₂
double-stranded helicate

Mn(LH)₂
single-stranded helices
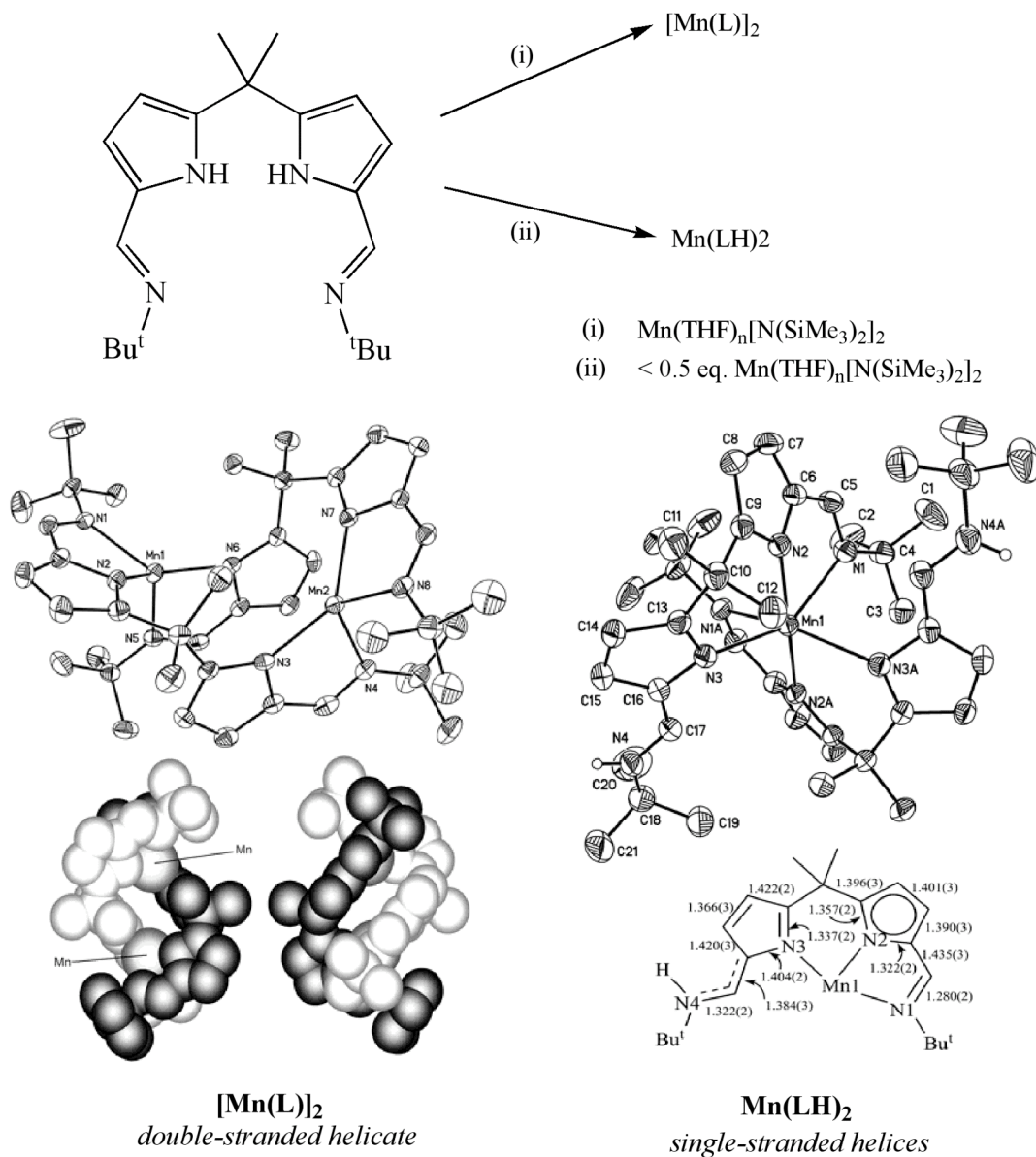
Dey and coworkers have reported the only existing double-stranded monohelices of an acid-functionalized salen ligand (Figure 4.3).[74] In this *facial* complex the thiolate donors are located *cis* to each other as are the phenoxides.

Figure 4.3. Reaction of benzothiazoline based 3-formylsalicylic acid ligands in combination with Cr(III) and Fe (III) results in the formation of *facial* double stranded helices.
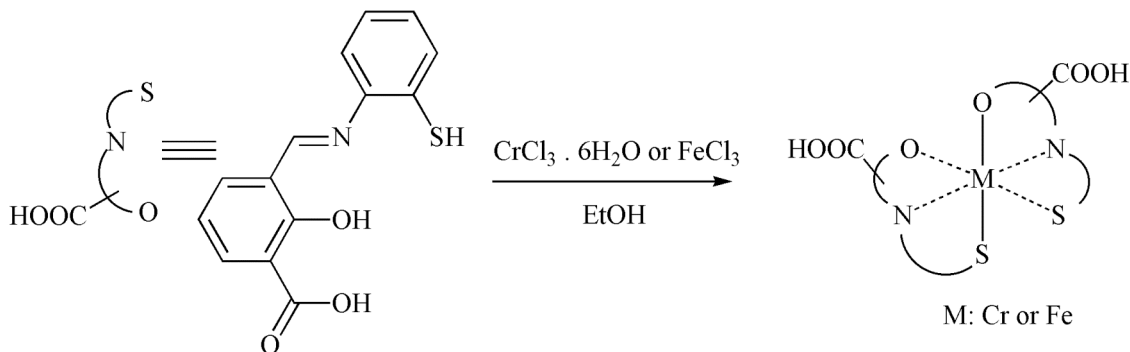
Metallations of the unsymmetrical Schiff-bases (*R,R*)-**6** and (*R,R*)-**7** have the potential of creating helices. The criterion is that the metal has to bind to the amine/imine/phenoxide pocket of the two ligand strands. It is also important that the carboxylic acid remains protonated and unavailable for metal-coordination. In that way, the ligand will have similar donating abilities as the ligand reported by Dey (Figure 4.3). The weak base TEA, will deprotonate only the phenol hydrogens and is therefore a suitable base for this analysis. However, (*R,R*)-**6** was shown to have a zwitterionic structure in solid state with an ammonium ion and a carboxylate. According to literature data, this structural configuration will result in the formation of a flat, double-stranded complex as the carboxylate has a higher coordination affinity and the ammonium groups can not act as donors.[20] However, as the solution state of the ligand indicated, the neutral and zwitterionic forms of the ligand are in equilibrium with one another. Complexation of the neutral ligand has the potential of forming a twisted helix rather than a flat complex. It was therefore of interest to see which form participates in the complexation reaction. The complexation of the symmetrical salen ligands (*R,R*)-**4** and (*R,R*)-**5** was done in the presence of a weak base, since they have the potential form twisted single-stranded

helices. In this chapter, results of the complexation of the symmetrical and unsymmetrical Schiff-base ligands (*R,R*)-**4**–**7** with divalent transition metals in triethylamine is presented.

(*R,R*)-**4**   (*R,R*)-**5**

(*R, R*)-**6**   (*R, R*)-**7**
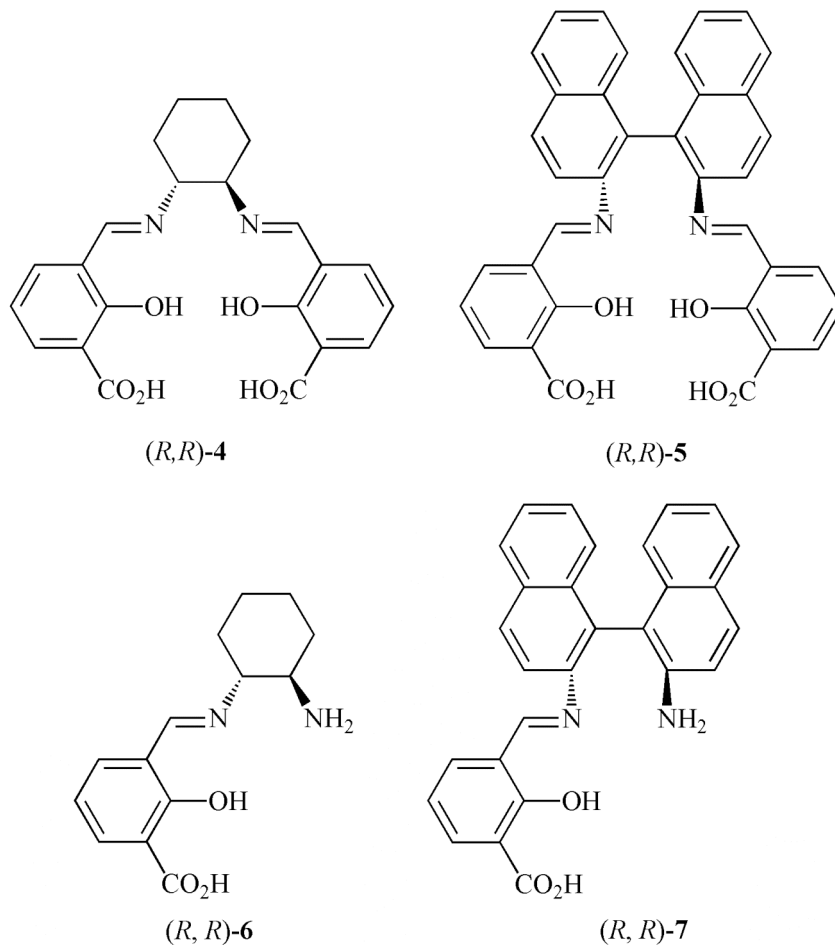
4.2 Complex synthesis

Complexation reactions are carried out by solvent-diffusion of the deprotonated ligands into a solution of the metal salts. In alcoholic solvents, crystallization stops after 1-3 days, giving yields of 46-86%. For the cyclohexyl based ligands (*R,R*)-**4** and (*R,R*)-**6**, the ligand anion is generated *in situ* by suspension of the neutral ligand in methanol and the

addition of triethylamine until clear solutions are obtained. For ligands (*R,R*)-**5** and

(*R,R*)**7**, anions are generated in ethanol with triethylamine as the base. The complexation

reaction does not occur in the absence of added base, as the neutral ligand is unreative

toward metal salts. For unsymmetrical zwitterionic Schiff-base ligands (*R,R*)-**6** and

*(R,R)***7**, tautomerization to give a neutral amine and an intramolecularly hydrogen-

bonded proton prior to complexation is likely (first step, Figure 4.4).

Reactions of the anhydrous salts $FeCl_2$, $CoCl_2$, NiX_2 (X = I, OTf) and $ZnCl_2$ with

the unsymmetrical Schiff base *(R,R)*-**6** result in the formation of **8** - **11**, respectively

(Figure 4.4). All complexes are enantiomerically pure, with each ligand having the *R, R*

configuration. These compounds are all 2:1 ligand to metal complexes with

approximately octahedral geometry and a double stranded helical structure. Crystalline

products are also isolated from copper salts, but these have a distinctly different

composition, with the metal center coordinated by the doubly deprotonated form of the

tetradentate ligand (*R, R*)-**4**. Interestingly, the same Cu(II) product, **12**, is isolated

whether Cu(OTf) or Cu(OTf)$_2$ is used in the reaction (Figure 4.4). Disproportionation of

Cu(I) (which is in excess) is implicated in the former case.

Figure 4.4. Synthesis of metal complexes of (*R,R*)-6 by solvent diffusion.
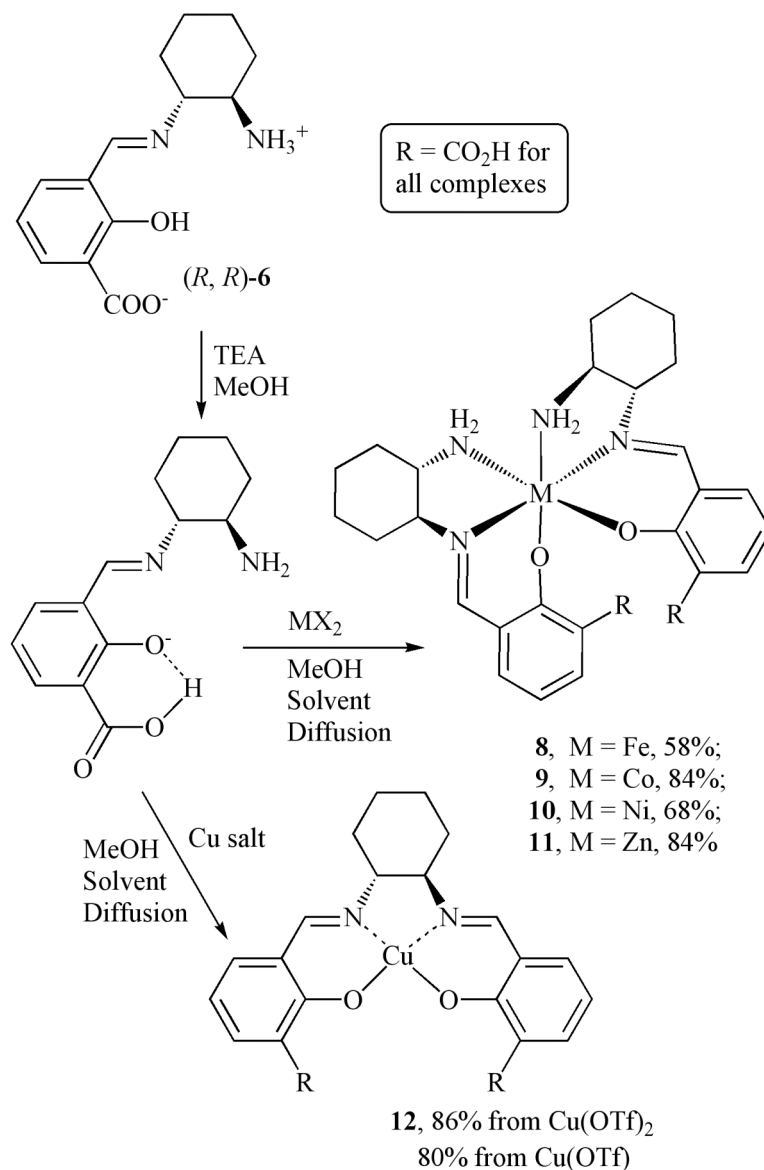
Reactions of the unsymmetrical Schiff base (*R,R*)-**7** with Cu(OTf)$_2$ resulted in a ligand reduction and promoted the binding of the symmetrical ligand (*R,R*)-**5** (Figure 4.5). In this case, TEA deprotonated both the phenols and the carboxylic acid which in turn creates two different binding pockets for the metal. As a result, complex **13** has a 2:1 metal to ligand ratio.

Figure 4.5. Synthesis of metal complexes of (*R,R*)-7 by solvent diffusion.
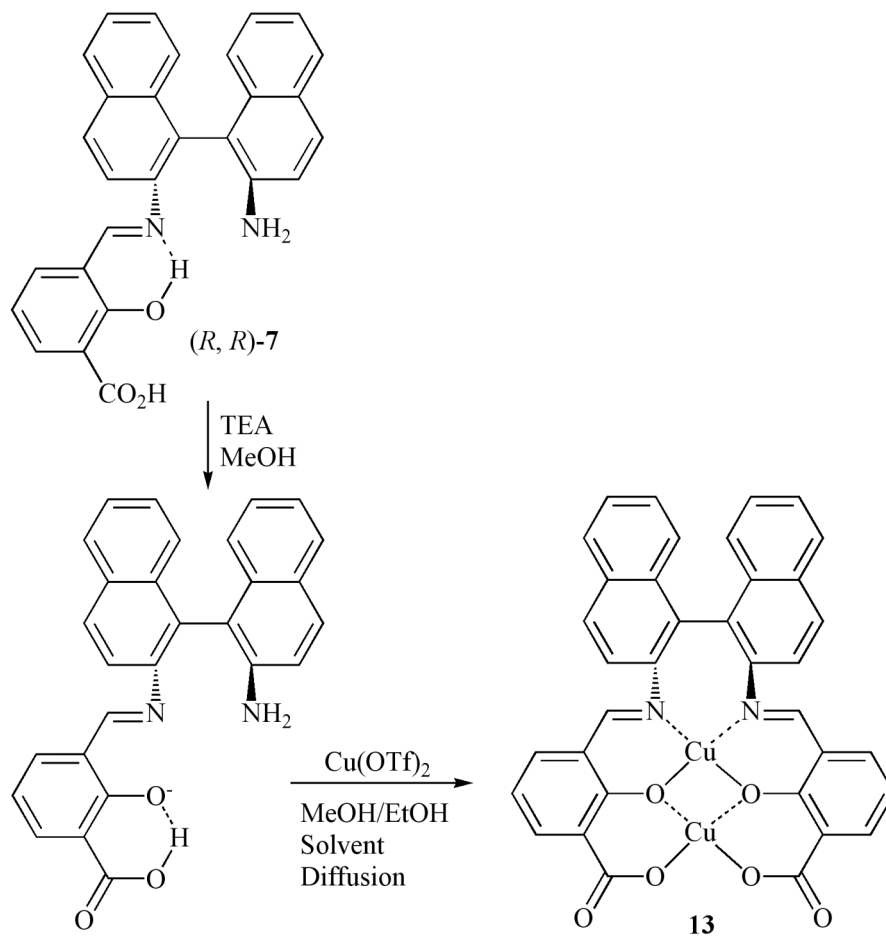
Complexation of the symmetrical salen ligand (*R,R*)-**4** with FeCl$_2$ using TEA as the base, resulted in a completely different product (Figure 4.6). In this case two symmetrical salen ligands assemble to form a cage structured hexa-metallic complex, **14**.

Figure 4.6. Synthesis of Fe-complex of (*R,R*)-4 by solvent diffusion.

S: Methanol
S': Triply bridging methoxide
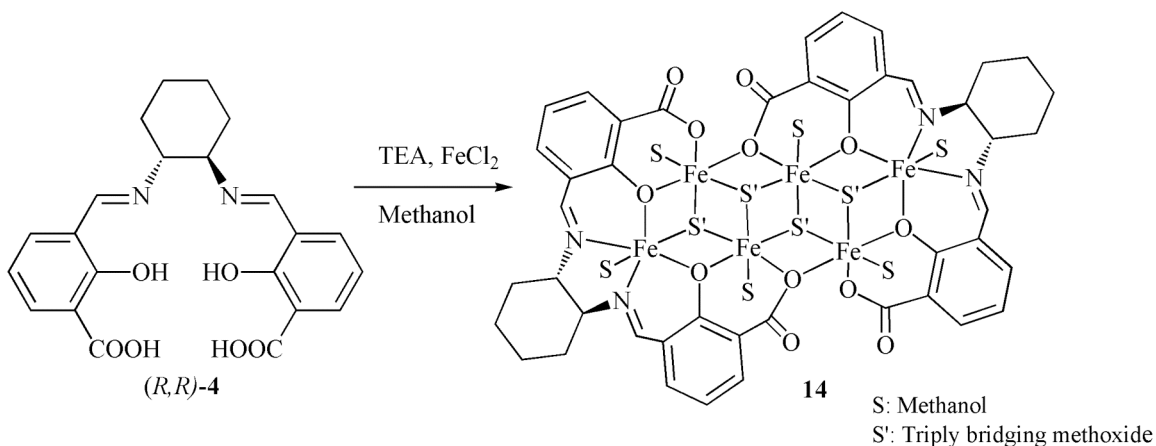
4.3 Solid state analysis of transition metal helices and copper complexes

Selected bond lengths and angles for complexes **8**-**11** are provided in Table 4.1. It is evident that the re is little structural difference between the complexes, suggesting that the steric constraints of the ligand strongly direct the observed structure, regardless of the metal ion present. The crystal structures all indicate the formation of double-stranded mononuclear complexes. This is accomplished by the *meridional* coordination of two (*R*, *R*)-**6** ligands. Figure 4.7 shows the structure of the zinc(II) complex, **11**. The structures of **8**-**10** are so similar that they are shown separately. The ligand in no longer in a zwitterionic form and is coordinated to the zinc *via* a neutral amine nitrogen, an imine nitrogen and a phenoxide. The two ligands have a 65.9° angle between them, based on the phenyl planes. This is a significant deviation from the 90° angle expected in the absence of steric interactions or chiral directing groups. The primary factor at play here is the directing nature of the chiral cyclohexyl groups, which push the phenyl groups toward each other and close down the interplanar angle between them. The nonlinear C–

O–Zn linkages can readily accommodate this arrangement, and there is not a significant steric penalty due to the planar nature of the phenyl groups. The result is a molecule with *M* helicity and a pitch angle of 65.9˚, as described by the phenyl groups. This is significantly different from the structures of most other *mer*-[M(ABC)$_2$] systems, where there is little deviation from octahedral geometry.[75-79] Only in cases where these is significant steric congestion are the there significant differences from ideal 90˚ and 180˚ angles.[75-79]

Figure 4.7. Structure of the zinc(II) complex, 7: a) thermal ellipsoid plot (50%), b) view down the C_2 axis of the molecule with the approximate directions of view for the space filling plots (c and d) shown.

7
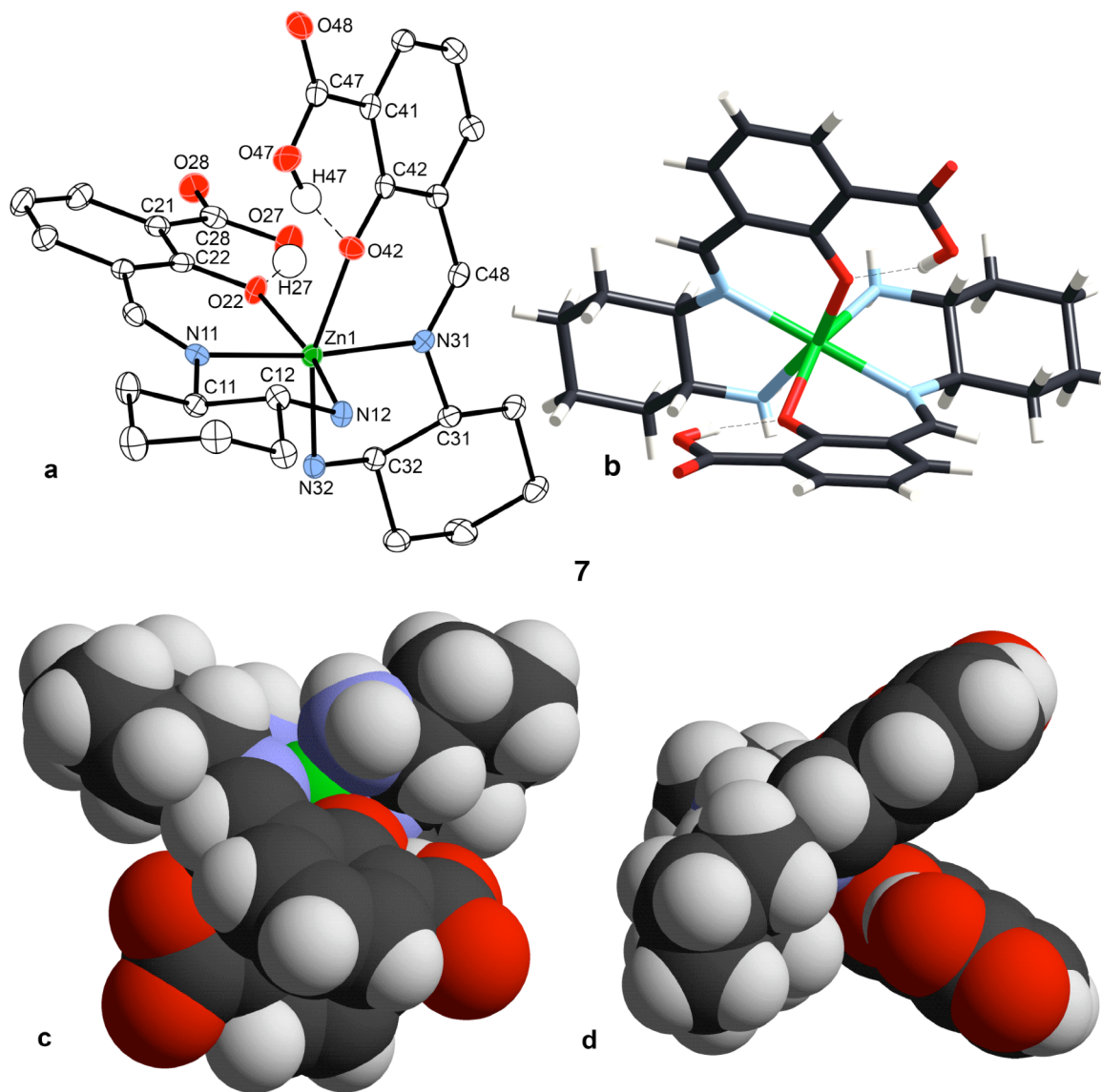
Table 4.1. Selected bond distances (Å) and bond angles (°) for 8-11.

		8 (M = Fe)	**9** (M = Co)	**10** (M = Ni)	**11** (M = Zn)
Bond Angles	O(22)-M-O(42)	95.60(3)	92.70(7)	95.30(11)	92.59(6)
	O(22)-M-N(11)	82.64(2)	88.29(7)	87.78(11)	85.70(6)
	O(42)-M-N(11)	92.11(3)	93.44(7)	93.59(11)	93.34(6)
	O(22)-M-N(31)	94.86(2)	88.74(7)	88.25(11)	88.89(6)
	O(42)-M-N(31)	85.70(3)	85.44(7)	84.50(11)	82.24(6)
	N(11)-M-N(31)	176.51(3)	176.78(8)	175.41(12)	172.86(7)
	O(22)-M-N(12)	158.28(3)	169.65(7)	167.42(11)	164.86(6)
	O(42)-M-N(12)	95.39(3)	84.86(8)	85.32(13)	84.20(7)
	N(11)-M-N(12)	78.28(3)	81.83(8)	79.65(12)	79.74(7)
	N(31)-M-N(12)	104.61(3)	101.06(8)	104.30(12)	105.27(7)
	O(22)-M-N(32)	84.19(3)	91.49(7)	92.78(12)	94.17(7)
	O(42)-M-N(32)	164.47(3)	166.54(7)	161.86(11)	161.00(6)
	N(11)-M-N(32)	103.24(3)	99.47(7)	102.95(12)	104.85(7)
	N(31)-M-N(32)	78.86(3)	81.87(8)	79.53(12)	80.16(7)
	N(12)-M-N(32)	90.12(3)	93.16(8)	90.30(13)	93.55(7)
Bond Distance	M- O(22)	2.1284(6)	2.0474(17)	2.049(3)	2.0874(15)
	M- O(42)	2.0385(6)	2.0851(16)	2.077(3)	2.1535(15)
	M- N(11)	2.1537(7)	2.0383(19)	2.088(3)	2.1223(17)
	M- N(31)	2.1326(7)	2.0437(18)	2.094(3)	2.1244(17)
	M- N(12)	2.2100(7)	2.094(2)	2.143(3)	2.1482(19)
	M- N(32)	2.1952(7)	2.115(2)	2.153(3)	2.1517(19)

Table 4.2. Hydrogen bonding distances (Å) and angles (°) for complexes 8-11.

		D-H…A	D-H (Å)	H…A (Å)	D…A (Å)	D HA (°)
M = Fe, **8**	1	O(27)-H(27)…O(22)	0.984(15)	1.488(15)	2.4216(8)	156.2(13)
	2	O(47)-H(47)…O(42)	0.842(16)	1.719(16)	2.5046(9)	154.3(18)
	3	N(32)-H(32)…O(48)*	0.885(14)	2.197(14)	3.0723(10)	169.9(13)
M = Ni, **9**	1	O(27)-H(27)…O(22)	0.88(3)	1.68(3)	2.482(2)	152(3)
	2	O(47)-H(47)…O(42)	0.85(3)	1.60(3)	2.423(2)	165(3)
	3	N(32)-H(32)…O(48)*	0.83(3)	2.26(3)	3.092(3)	173(2)
M = Co, **10**	1	O(27)-H(27)…O(22)	0.91(5)	1.59(5)	2.479(4)	163(5)
	2	O(47)-H(47)…O(42)	0.87(5)	1.56(5)	2.416(4)	168(5)
	3	N(32)-H(32)…O(48)*	0.87(5)	2.20(5)	3.072(4)	176(4)
M = Zn, **11**	1	O(27)-H(27)…O(22)	0.78(3)	1.74(3)	2.490(2)	160(3)
	2	O(47)-H(47)…O(42)	0.89(3)	1.55(3)	2.424(2)	165(3)
		N(32)-H(32)…O(48)*	0.80(3)	2.27(3)	3.059(2)	171(3)

The crystal structures of **8**-**11** reveal that the individual molecules are arranged in *M*-helical strands, formed by N–H---O interactions between molecules (Figure 4.8). Table 4.2 (entry 3) lists the intermolecular hydrogen bonding distances and angles of the complexes. Hydrogen bonding interactions between the amine donors and the carboxylic acid acceptors of adjacent molecules produces one-dimensional *M*-helices of molecules along the crystallographic *b*-axis. Only one of the ligand strands forms such hydrogen bonds. The other strand is not involved in any intermolecular bonding and forms angled "blades" in the helix. There is no hydrogen bonding between the helical strands.

Figure 4.8. Crystal packing diagram for 11, showing adjacent helical strands of hydrogen-bonded molecules, b) shows only the ligand strand participating in the helix formation.

a

b
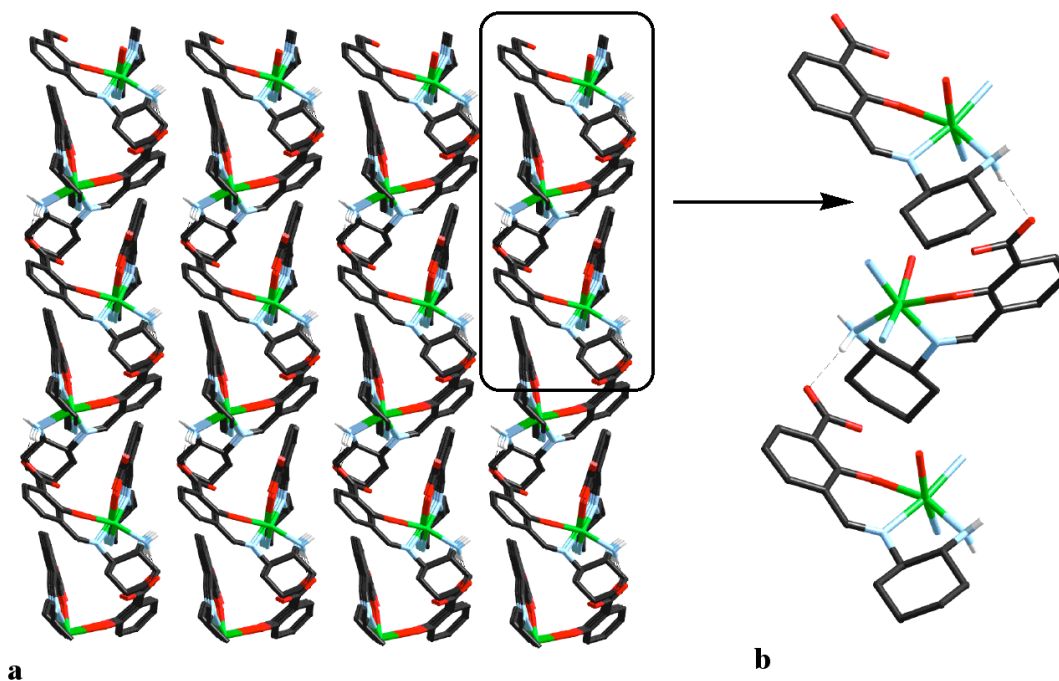
Reaction of (R, R)-**2** with copper salts resulted in a completely different structure than seen for the other metals examined. Figure 4.9 shows the structure of **12** and Table 4.3 contains selected bond distances and angles. Surprisingly, the copper is complexed to the dianion of the tetradentate ligand (R, R)-**4**, which has reformed from (R, R)-**6**. The result is a salen type of complex with terminal carboxylic acid groups, the protons of which are hydrogen-bonded to the phenoxide donors (Table 4.4). There is an additional hydrogen bond for each molecule between an acid group and a methanol of solvation. The coordination at copper is square planar, with only slight deviation from planarity. There are two very similar molecules in the asymmetric unit that are rotated 180° with respect to one another and stacked parallel. The molecules are cupped away from one another, resulting a breaking of the otherwise C_2 symmetry. Bond lengths and angles are very similar for the two independent molecules.

Figure 4.9. Thermal ellipsoid plot (50% probability) and tube representation of the iron(II) complex 12.

12
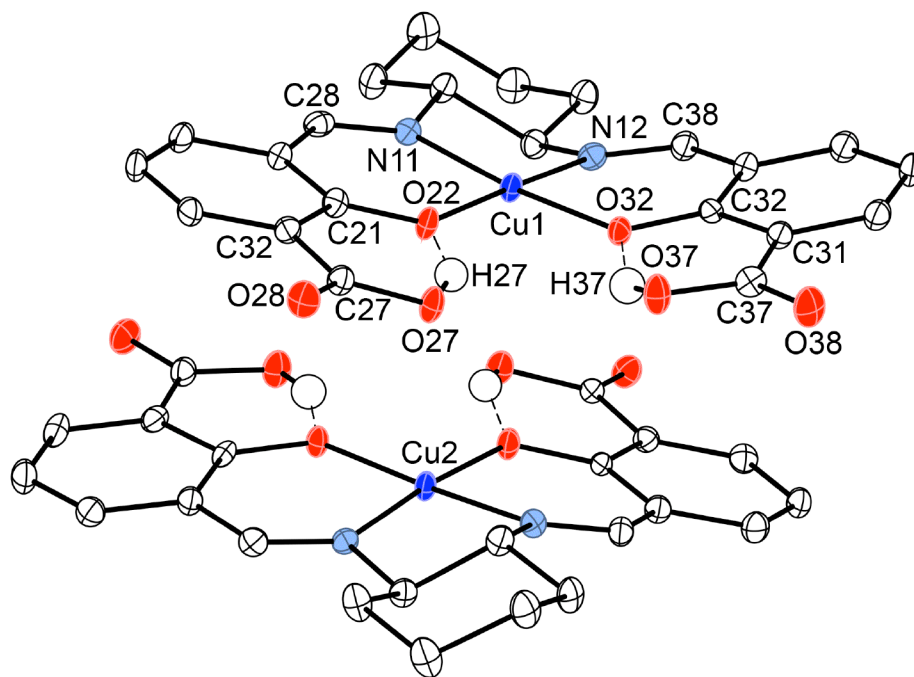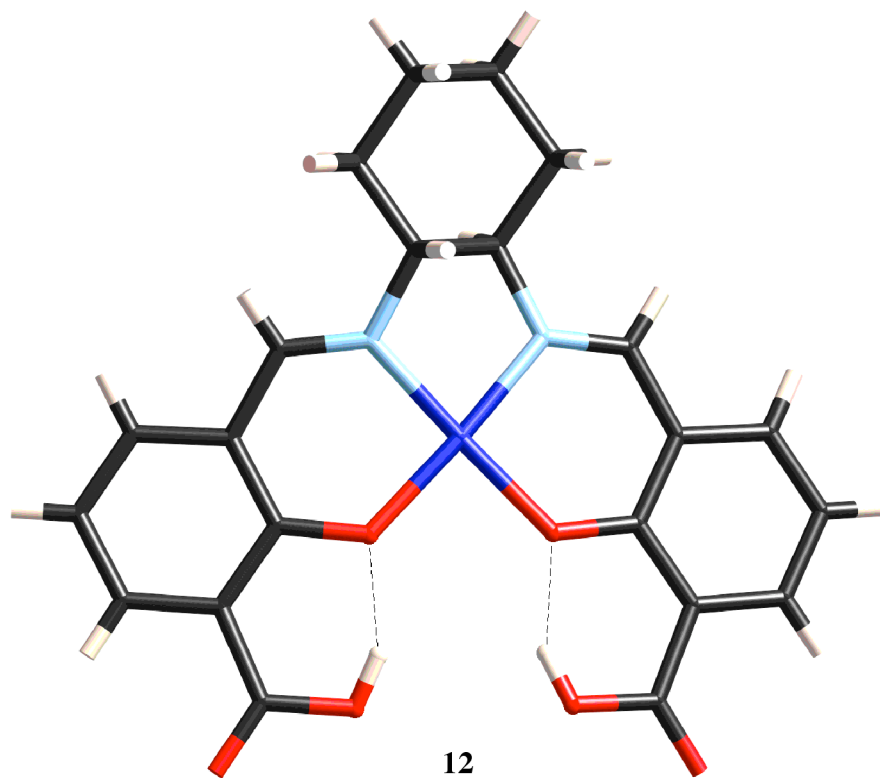
Table 4.3. Selected bond distances (Å) and bond angles (°) for 12.

	D-H…A	D-H (Å)	H…A (Å)	D…A (Å)
	Cu-O(22)	1.909(2)	O(22)-Cu-O(32)	89.30(9)
Complex 1	Cu-O(32)	1.929(2)	O(22)-Cu-N(12)	176.92(10)
	Cu-N(12)	1.932(3)	O(32)-Cu-N(12)	92.26(10)
	Cu-N(11)	1.943(3)	O(22)-Cu-N(11)	93.58(10)
			O(32)-Cu-N(11)	174.49(10)
			N(12)-Cu-N(11)	85.08(11)
	Cu-O(22)	1.908(2)	O(22)-Cu-O(32)	88.80(9)
Complex 2	Cu-O(32)	1.920(2)	O(22)-Cu-N(12)	174.49(9)
	Cu-N(12)	1.936(3)	O(32)-Cu-N(12)	93.43(9)
	Cu-N(11)	1.938(3)	O(22)-Cu-N(11)	92.38(10)
			O(32)-Cu-N(11)	176.06(9)
			N(12)-Cu-N(11)	85.74(11)

Table 4.4. Hydrogen bonding distances (Å) and angles (°) for complexes 12.

	D-H…A	D-H (Å)	H…A (Å)	D…A (Å)	DHA (°)
	O(27)-H(27)…O(22)	0.84	1.73	2.486(4)	149.4
Complex 1	O(37)-H(37)…O(32)	0.84	1.73	2.493(3)	149.6
	O(S1)-H(S1)…O(38)	0.84	1.99	2.811(3)	164.9
	O'(27)-H'(27)…O'(22)	0.84	1.70	2.476(4)	152.8
Complex 2	O'(37)-H'(37)…O'(32)	0.84	1.72	2.498(3)	152.3
	O'(S1)-H'(S1)…O'(38)	0.84	2.01	2.839(3)	166.6

Figure 4.10. Thermal ellipsoid plot (50% probability) and tube representation of the iron(II) complex 13.
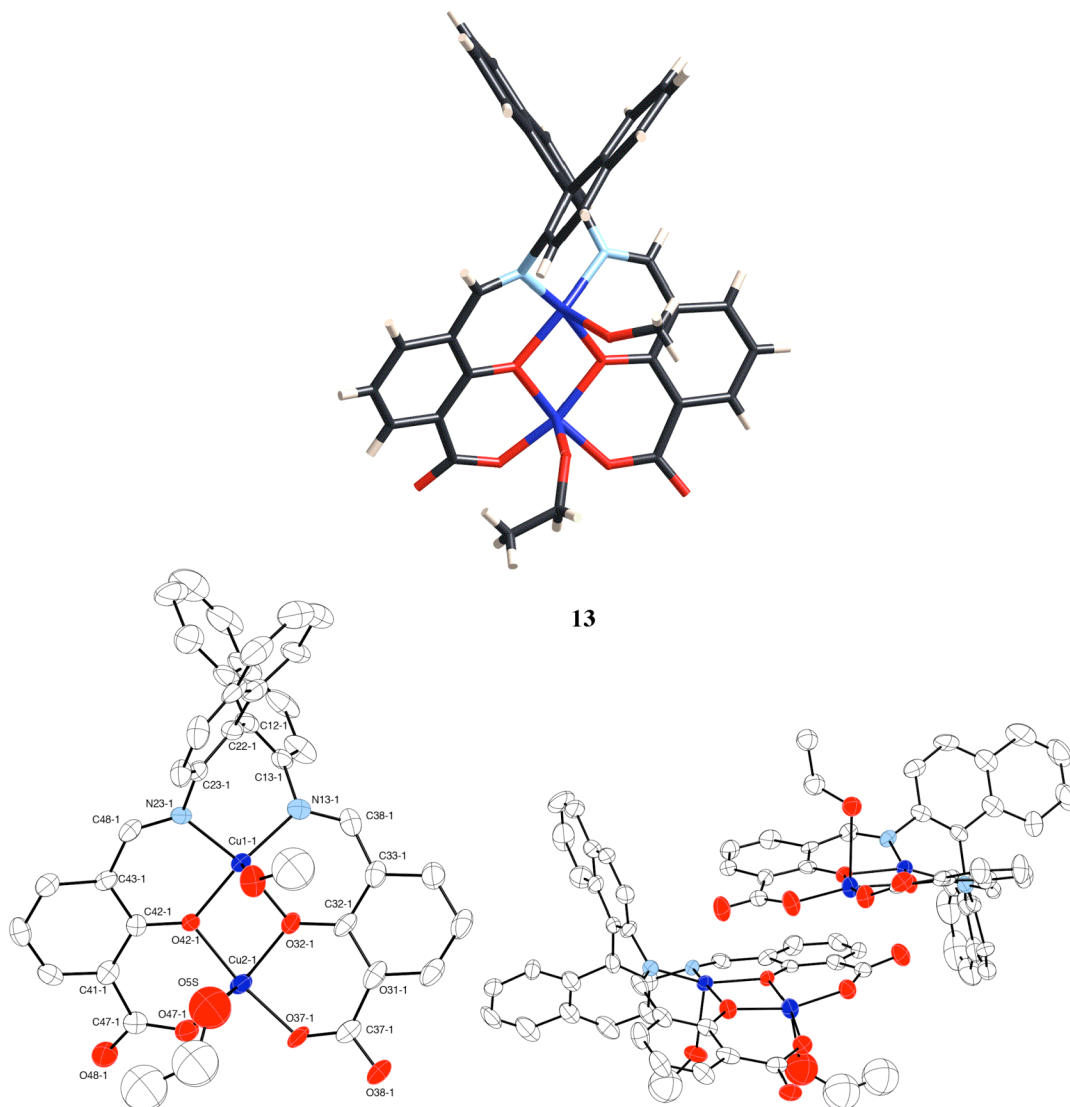
Figure 4.10 shows the crystals structure of the binaphthyldiamine-based complex **13**. As seen for its cyclohexyldiamine analogue, (*R,R*)-**7** converts to the salen ligand (*R,R*)-**5** when metallated with Cu(OTf)$_2$ in the presence of TEA. In this case, TEA has deprotonated both the phenols and the carboxylic acids. The result is a dinuclear complex where one copper metal is located in the salen pocket of the complex and the second in

the salan pocket (carboxylate/phenoxide). There are two solvent molecules present in the coordination sphere of the copper centers. A methanol occupies the apical position of the metal center located in the salen pocket and an ethanol molecule occupies that of the copper in the salan pocket. The two copper centers have square-pyramidal geometries. Similar to the copper complex **12**, there are two similar molecules in the unit cell that are rotated 180˚ with respect to one another and stacked parallel. Table 4.5 shows some of the selected bond lengths and bond angles for complex **13**.

Table 4.5. Selected bond lengths (Å) and bond angles (°) for 13

Bond lengths	Cu11-O421	1.9404(18)
	Cu11-O321	1.951(2)
	Cu11-N131	1.963(2)
	Cu11-N231	1.968(3)
	Cu21-O471	1.880(2)
	Cu21-O371	1.910(2)
	Cu21-O321	1.9287(19)
	Cu21-O421	1.953(2)
Bond angles	O421-Cu11-N131	158.53(11)
	O321-Cu11-N131	90.14(10)
	N131-Cu11-N231	103.30(11)
	O471-Cu21-O371	95.96(10)
	O371-Cu21-O321	92.29(9)
	O371-Cu21-O421	170.96(8)

Figure 4.11 shows the crystal structure of **14**. As was the case with the binaphthyl salen ligand, both phenolic hydrogens and carboxylic hydrogens have been deprotonated by TEA. The anionic donors coordinate to the six iron centers that are present in the complex. Four triple bridging methoxides along with six methanol molecules combined with the six metal centers to create attached semi-cages as the core of the complex. All

iron centers have an octahedral configuration and posses a 2+ charge which along with the four negatively charge methoxides, four phenoxides and four carboxylates create a neutral complex. A more detailed description of this complex along with the selected bond distances and bond angles is reported in chapter 5.

Figure 4.11. Structure of the iron(II) complex, 14**.**
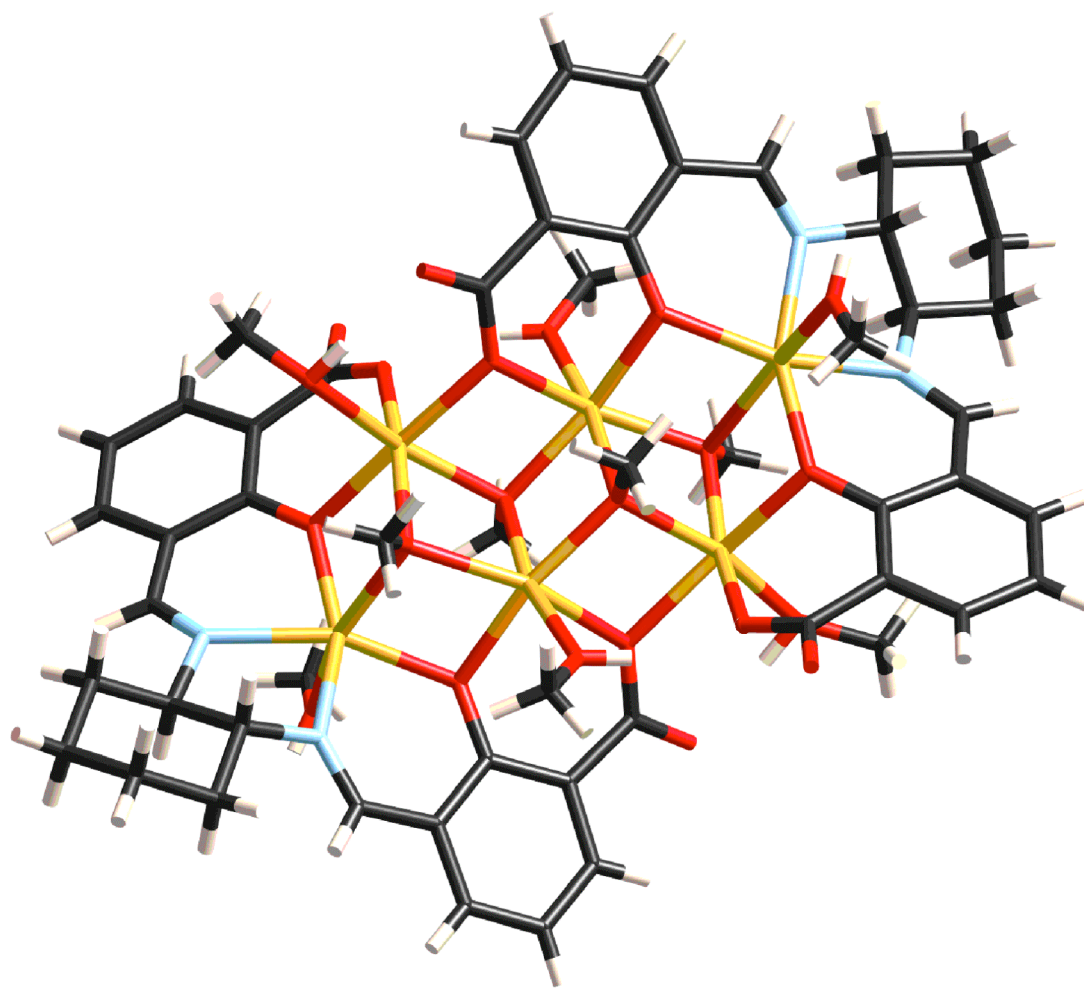
14

CHAPTER 5 - Complexation of unsymmetrical acid-functionalize imine ligands with divalent transition metals in the presence of the strong base NaOMe

5.1 Introduction

During recent years, significant studies have been devoted to the synthesis and analysis of cage related complexes.[53-58,80-82] In biological systems, cubane structures have been detected in proteins participating in electron transfer (ET) reactions. They have the ability to efficiently act as electron shufflers while minimizing unwanted redox reactions.[53] Some examples are the active sites of iron proteins or ferredoxins ($Fe_4S_4^{n+}$)[53] and photosystem II (Mn_3Ca-cubanes)[55]. In addition to their biological activities, cubanes with superparamagnetic behavior are prone to have interesting solid-state properties as well. For example, they can be used for magnetic hysteresis and to help investigate the occurrence of quantum tunneling of magnetization.[82] Quantum-mechanical tunneling of magnetized particles can help with magnetic storage.[83] Also, the magnetic exchange between two or more paramagnetic metal centers can give rise to the development of single-molecule magnets (SMMs).[54-56,58,81-82] SMMs have possible application as very small memory devices and data storage systems.[56]

The metal centers used in the design of artificial cages are preliminary Mn(III,IV), Fe(II,III), Cr(III) and V(III).[82] These metal cubanes have shown to be good candidates as single-molecule magnets. However, in the recent years, cubes containing Co(II), Ni(II) and Zn(II) have also been reported.[58,80-82] The bridging ligands in these cages usually consist of hydroxo, alkoxo, azido, sulfido or iminato groups.[82] Few studies have been

done on larger organic ligands as bridging groups, although these complexes also have been shown to have supermagnetic qualities. The most prominent work is done by Oshio *et al.*, where Fe(II) cubanes were created from chelating Schiff-base ligands and methanol molecules (Figure 5.1).[82]

Figure 5.1. The organic Schiff-base ligands used in the formation of Fe(II)-cubanes.
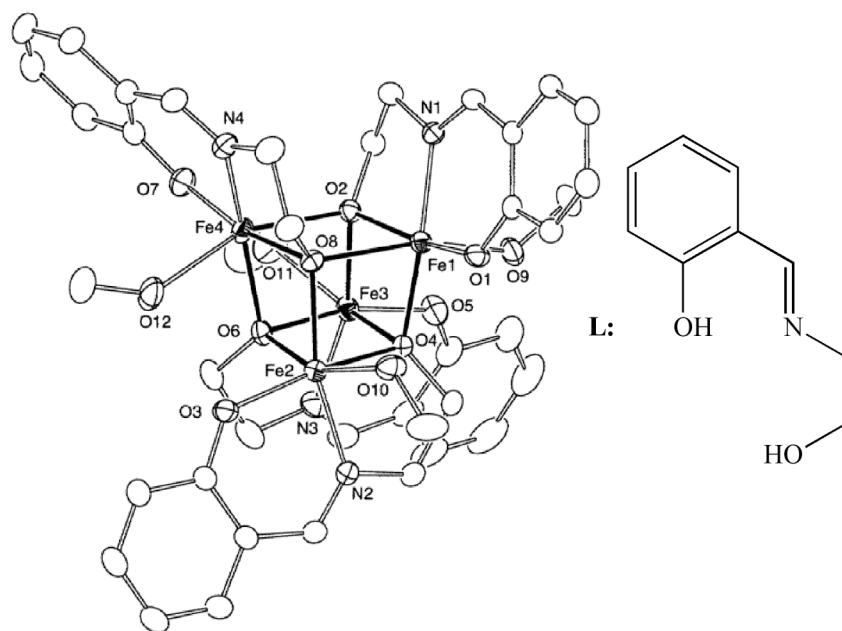
Also Robson[81] and Williams[54] have recently reported the formation of cubanes using organic frameworks. Robson managed to get the same cubanes forming with divalent Zn, Mn and Co metal salts (Figure 5.2). Williams' cubane have a C_2-axis through the center of the complex (Figure 5.3).

Figure 5.2. The structure of $[Zn\{(C_5H_4N)_2(SO_3)C(O)\}_4]$.

L:
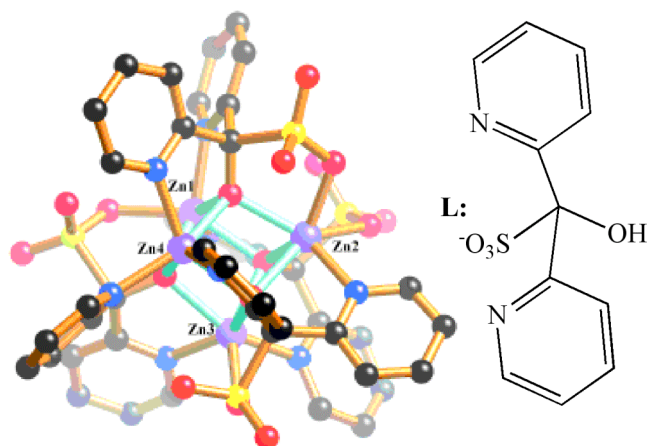
Figure 5.3. Co(II) cubanes synthesized by Williams and coworkers. Chiral ligand resulted in the present of a C_2-axis in the final cubane.

L:
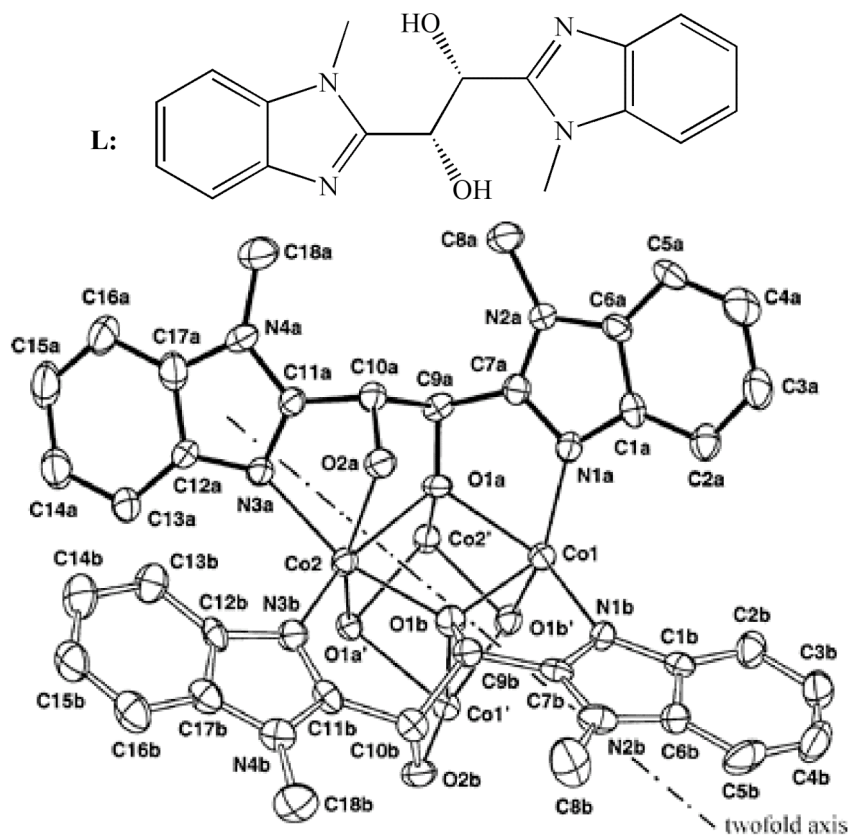
Considering the cubane-type structures that have been reported to date, the symmetrical and unsymmetrical Schiff-base ligands (*R,R*)-**4** and (*R,R*)-**6** should also be capable of forming cubane complexes if the right reaction conditions are met. Additionally, these ligands have been the potential of utilizing carboxylate-bridges. Carboxylate-bridged diiron units have shown to have important biological activities, as they are an active components of a number of oxygen-dependent metalloenzymes.[84]

Although there have been many data reported on metallation of symmetrical and unsymmetrical Schiff-bases similar to (*R,R*)-**4** and (*R,R*)-**6**, there have not been any reports of the formation of cubane structures utilizing these types of ligands. What has been reported are dinuclear complexes of either the symmetrical or unsymmetrical 3-formylsalicylic Schiff-base ligands (Figure 5.4).[41,60-62]

Figure 5.4. Complexation of related Schiff-bases in the presence of a strong base.
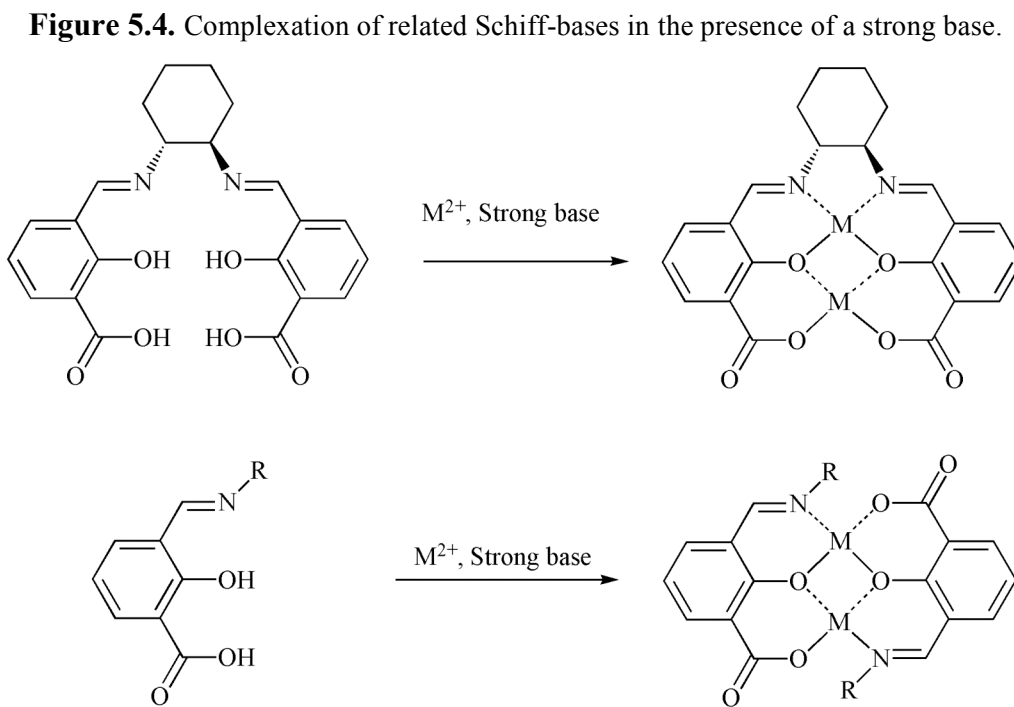
The chelating effect of triply bridging methoxides has been shown to be a crucial detail in the formation of cubanes structures.[55,80,81] The most significant work has been carried out by Robson *et. al*.[55,80,81] There, tri-substituted methoxide ligands and citric acid were demonstrated to generate cubane-related metal complexes. Figure 5 shows the general structure of the reaction of citric acid with divalent Mg, Mn, Fe, Co, Ni and Zn.[55]

Figure 5.5. Structure of $(M^{II})_4(cit)_4^{8-}$ where M= Mg, Mn, Fe, Co, Ni and Zn. X, Y and Z can be oxygen, nitrogen or sulfur donor groups. The black line represents the S_4 axis.
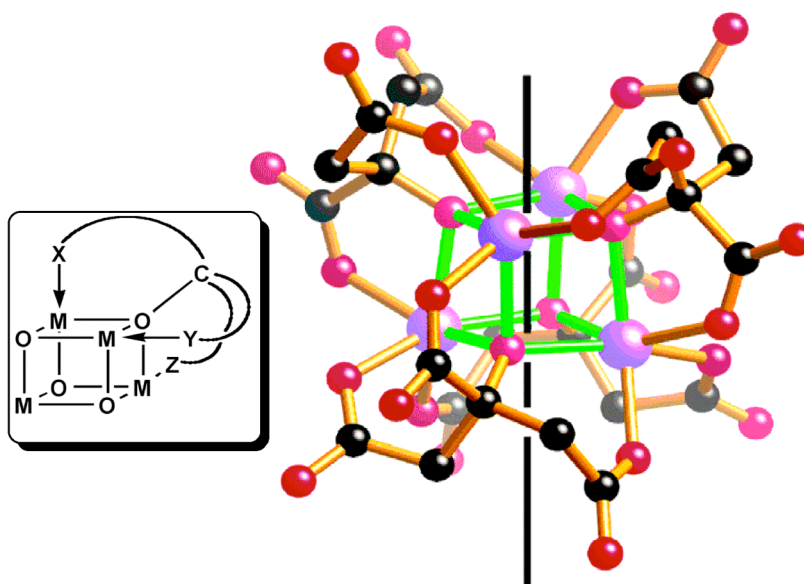
Lippard and coworkers have reported the effect of bridging alkoxides in the formation of cubane structures of iron acetate (Figure 5.5).[53,85,86]

Figure 5.6. The effect of bridging alkoxides (methoxide) molecules in the formation of cubanes. Some of the triply bridging methoxides are highlighted for clarity.
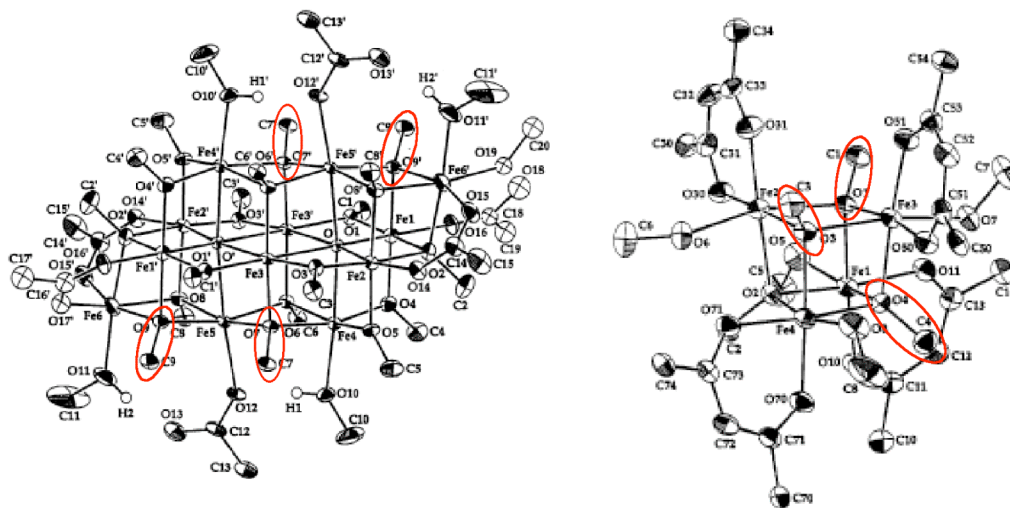
Thus far, Schiff-base ligands similar to (*R,R*)-**4** and (*R,R*)-**6**, have not been metallated in the presence of alkoxides. The strong base used is usually potassium hydroxide and the reaction has been carried out in aprotic solvents such as methylene chloride or chloroform. Complexation under conditions where methoxide/methanol are present would be favorable for the formation of cubane like structures. This was already shown in the reaction of (*R,R*)-**4** with Fe(II)/ TEA in methanol (Chapter 4).

In the following chapter, complexation of the symmetrical and unsymmetrical Schiff-bases (*R,R*)-**4** and (*R,R*)-**6** with a series of divalent metals (Fe, Co, Ni, Cu) in the presence of methoxides is presented.

5.2 Complex Synthesis

Complexations of (*R,R*)-**4** and (*R,R*)-**6** were carried out by solvent-diffusion of the deprotonated ligands into a solution of the metal salts. The ligand is combined with four

equivalents of sodium methoxide and dissolved in methanol. The solution is then layered on a saturated solution of the metal salt in methanol. Crystallization was stopped after 3-4 days, giving yields of 27-61%.

Ligand (R,R)-**4** was metallated with anhydrous $FeCl_2$ to give the hexanuclear complex **14** rather than the dinuclear complex **15** (Figure 5.7). The result is similar to the reaction of (R,R)-**4** with $FeCl_2$ using TEA as the base. The complex, **14** was afforded as dark red block crystals in high yield (52%). The result supports our hypothesis of the importance of methoxide/methanol molecules in the formation of cubane complexes. Further structural details will be discussed in section 5.3.

Figure 5.7. Metallation of ligand (R,R)-4 with iron(II) chloride/NaOMe.
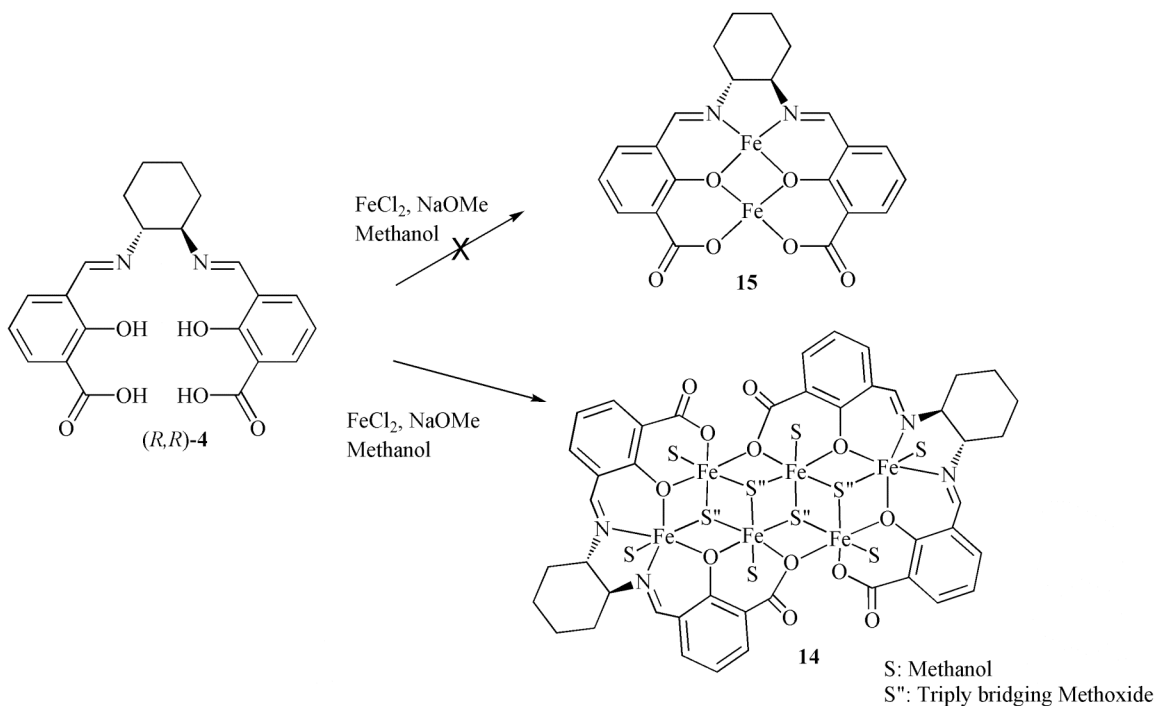
Figure 5.8 shows the results of metallation of (*R,R*)-**4** with anhydrous CoI$_2$. Dark rose block crystals were obtained after two days of crystallization. The complex **16**, is analogous to that seen for iron(II).

Figure 5.8. Metallation of Metallation of ligand (*R,R*)-4 with cobalt(II) iodide/NaOMe.

S: Methanol
S": Triply bridging Methoxide
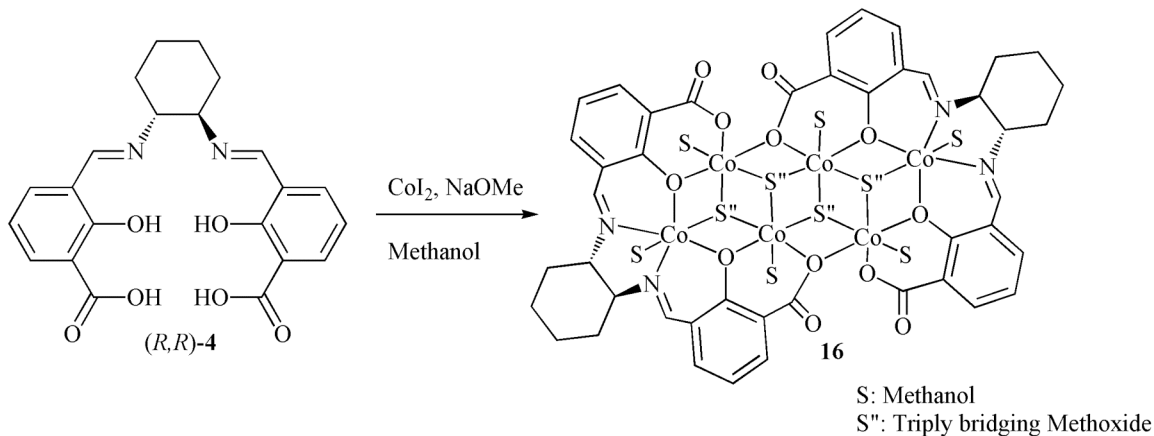
In further studies, the unsymmetrical Schiff-base ligand (*R,R*)-**6** was reacted with divalent metal salts. Interestingly, metallation of ligand *(R,R)*-**6** with iron(II) chloride in sodium methoxide resulted in the same structure as **14** rather than complex **17**. For this complex to form, the unsymmetrical Schiff-base ligand, (*R,R*)-**6** must undergo disproportionation to form the symmetrical Schiff-base, (*R,R*)-**4** and cyclohexyldiamine. Again, the dark red block crystals were obtained in moderate yield (61%) after three days.

Figure 5.9. .Metallation of ligand (*R,R*)-6 with iron(II) chloride/ NaOMe.

17

14

S: Methanol
S": Triply bridging Methoxide
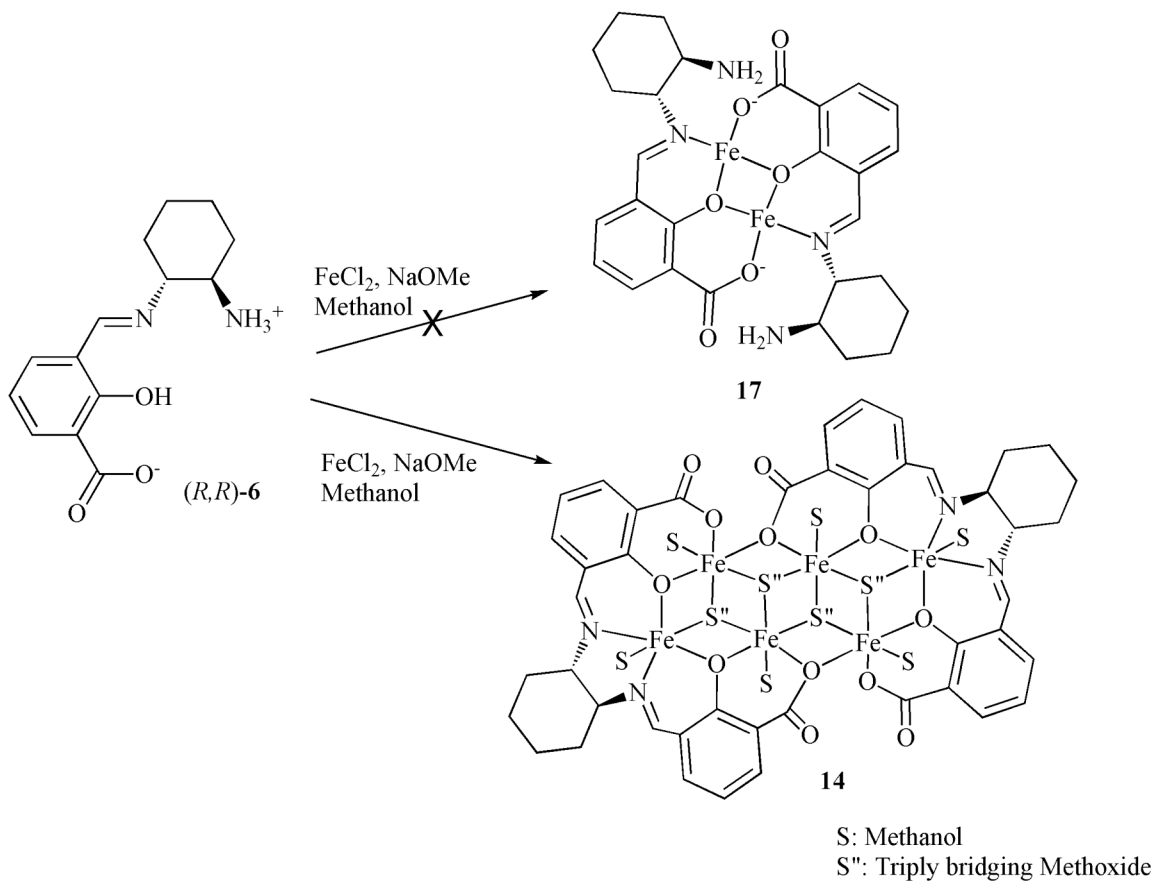
Figure 5.10 shows the result of complexation of (*R,R*)-**6** with anhydrous CoI$_2$. The complex **18** is different from that seen with the symmetrical Schiff-base ligand, **16**. The red colored crystals were obtained after three days in only low-moderate yield (47%).

Figure 5.10. Metallation of ligand (*R*,*R*)-6 with cobalt(II) iodide/ NaOMe.
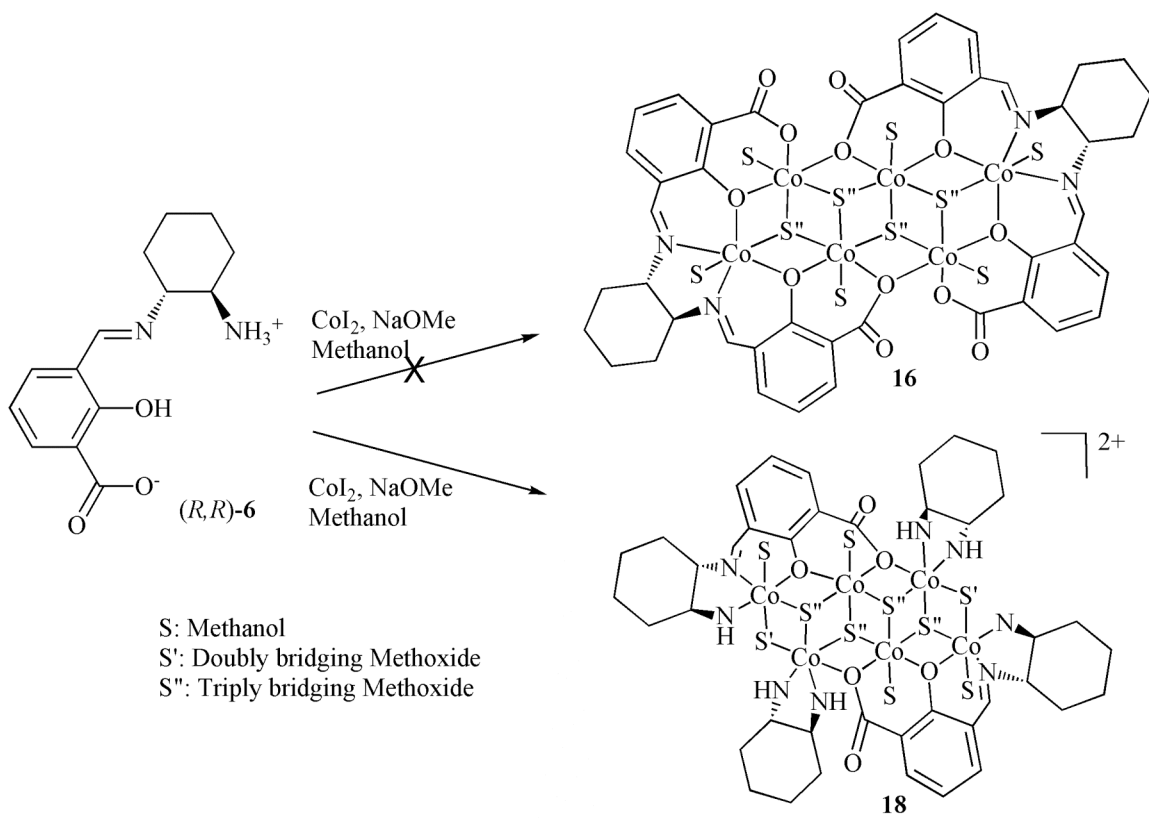
The ligand, (*R*,*R*)-**6** was also metallated with anhydrous NiI$_2$ to form long orange needles after 3 days of crystallization. Yet again, compound **21**, has a somewhat different structure than the anticipated **19** and **20** (Figure 5.11).

Figure 5.11. Metallation of ligand (*R,R*)-6 with nickel(II) iodide/ NaOMe.

S: Methanol
S': Doubly bridging Methoxide
S": Triply bridging Methoxide
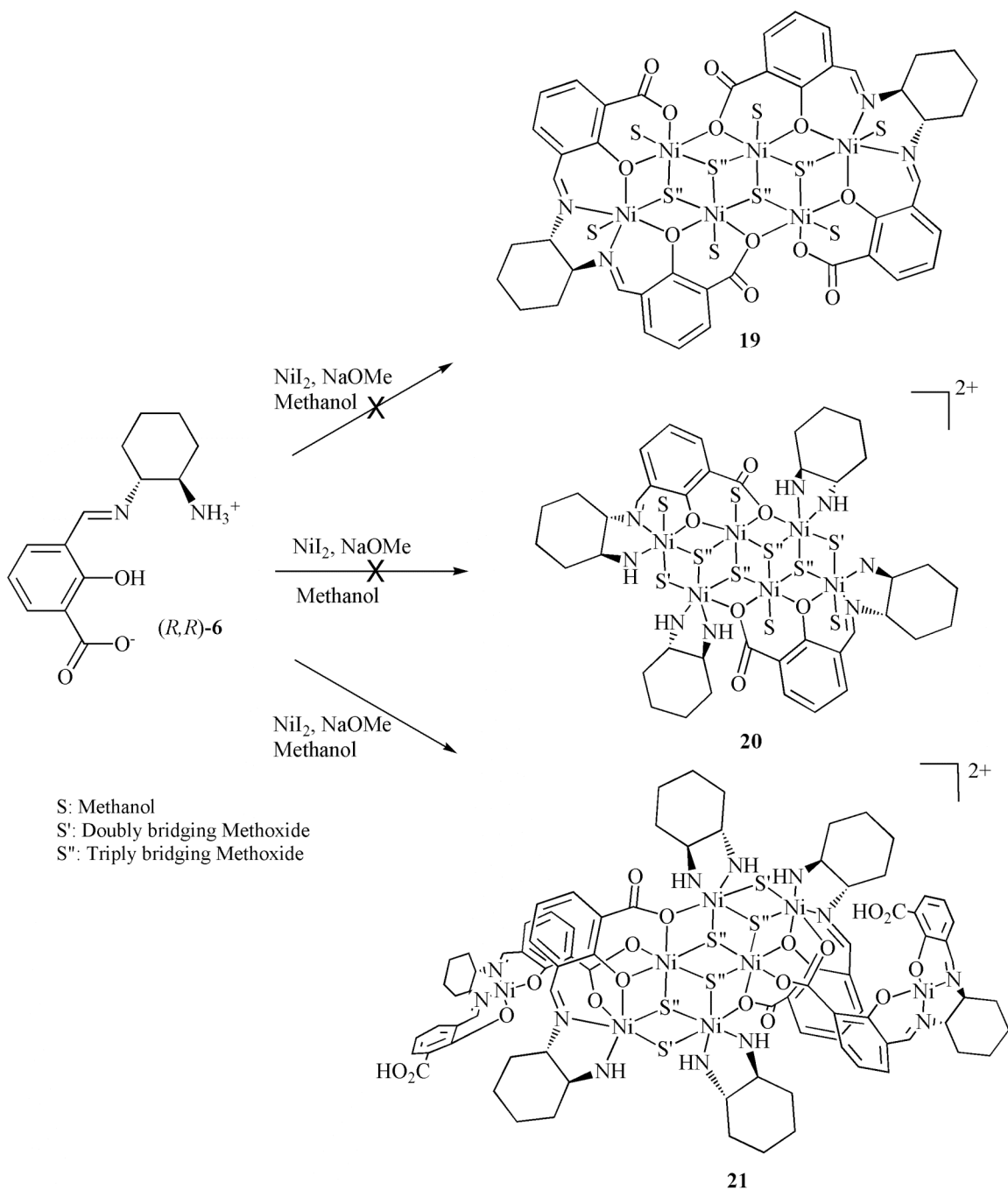
Lastly, complexations of (*R,R*)-**6** with anhydrous copper(II)triflate salts were carried out. Immediately after solvent layering, green colored crystals started to form at the interface of the two layers. After three days of diffusion, three types of crystals could

be detected in the tube. Green colored crystals at the interface, small purple colored crystals one inch below the initial interface and large maroon colored block crystals further down in the crystallization tube. The purple compound was, due to its small quantity, not analyzed. The green crystals and the maroon crystals on the other hand were analyzed by X-ray diffraction as complexes **22** and **23** respectively (Figure 5.12).

Figure 5.12. Metallation of ligand (*R,R*)-6 with nickel iodide/ NaOMe.
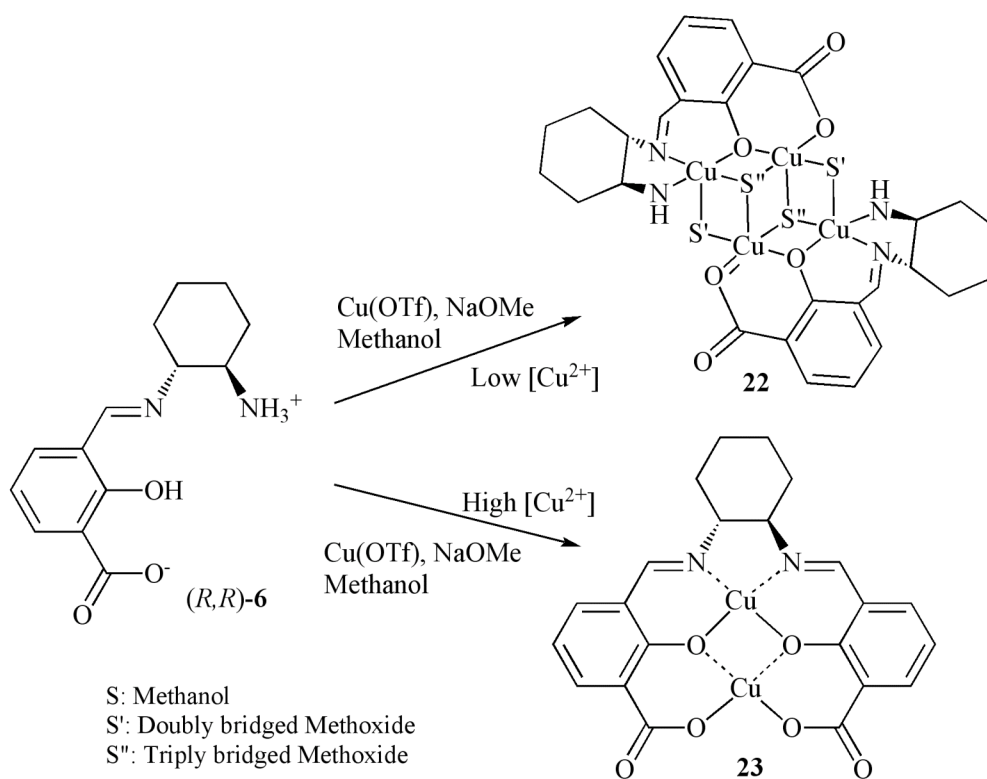
The two complexes differ in their ligand structures. In **22** the unsymmetrical Schiff-base ligand remains the same while undergoing oxidation in **23**. A powerful clue was gathered from this reaction. The positions of the two crystals reflect on the metal concentration of the reaction; the further down in the tube, the higher metal to ligand ratio. It appears that the higher the metal concentration, the more readily the

disproportionation of the unsymmetrical ligand can occur. Figure 5.13 estimates the location of each crystal formation for complexes **14**, **18**, **21**, **22** and **23** for their respective crystallizations.

As indicated in figure 5.13 the iron and nickel complexes **14** and **21** both form at or slightly underneath the solvent interface, which suggests a relatively high metal to ligand concentration (the metal was used in excess). In both cases, the unsymmetrical Schiff-base ligand has converted to the symmetrical salen ligand. The cobalt complex, **18** on the other hand was formed were the metal concentration is as its lowest; far above the interface of the two layers. This is the only cubane structure where the unsymmetrical Schiff-base ligand is observed as the chelating ligand.

Figure 5.13. Crystallization of compounds 14, 18, 21-23.
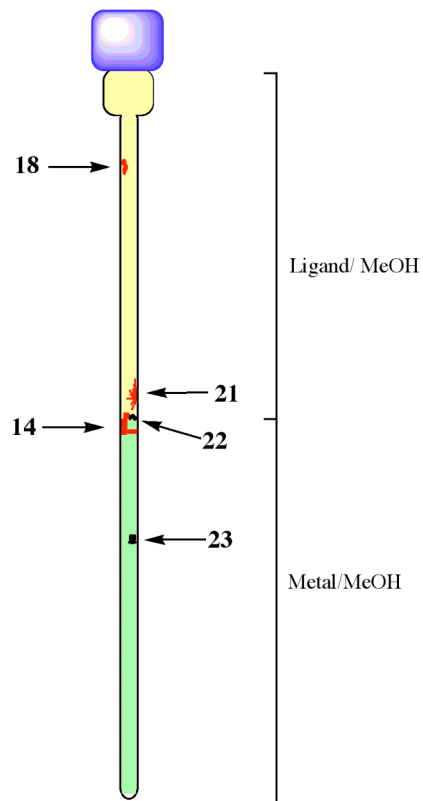
5.3 Structural analysis of transition metal cubanes and copper complexes

The obtained crystals were characterized by X-ray crystallographic analysis. The crystal structure of **14** is shown in figure 5.14. This structure is obtained by metallation of both the symmetrical and unsymmetrical Schiff-base ligands (*R,R*)-**4** and (*R,R*)-**6** with iron chloride in sodium methoxide and the metallation of (*R,R*)-**4** with iron chloride in triethylamine (Chapter 4). A hexanuclear complex containing four face-shared defected cubanes is the result. The complex consist of two salen ligands, four triply bridged methoxides, six solvent methanol molecules and six divalent metal centers. The crystal structure clearly shows both salen ligands being fully deprotonated and acting as multidentate ligands. The overall complex is neutral.

The similar cobalt analogue, **16** is depicted in figure 5.15. Both complexes **14** and **16** are enantiomerically pure, with each ligand having the (*R, R*) configuration. The overall complex has a pseudo-center of inversion located in the middle of the structure, giving rise to three different metal environments. The first environment consists of two metal ions that are located in the salen pocket of the Schiff-base ligands. These have a triply bridging methoxide and a methanol solvent occupying the same coordination plane of the octahedral metal. The other two metal environments are created by the remaining four metal ions outside the salen pockets. Two metal ions have a carboxylate oxygen, a phenoxide oxygen and two triply bridging methoxides on one coordination plane and a methanol and a triply bridging methoxide on the second coordination plane. The remaining two metal ions bind to a phenoxide oxygen from ligand 1, a carboxylate oxygen from ligand 2, a triply bridging methoxide and a methanol on one coordination

plane and a carboxylic oxygen (ligand 1) and a triply bridging methoxide on the second coordination plane. The three metal environments are indicated as (*), ( ) and (^), respectively (Figures 5.14 and 5.15). The complex adopts a face-shared tetra-cubane structure where each cubane has one missing vertex. The six metal centers occupy six vertices of the tetra-cubane core. The two cages closest to the Schiff-base ligands have two phenoxide oxygens and two triply bridging methoxides in the remaining four vertices. These two cages are connected via two carboxylate oxygens of each Schiff-base ligand, which in turn create a tetra-cubane. There are no metal-metal bonds present in the complex, so all the metals occupy opposite corners of the cube vertices.

Table 5.1 and 5.2 depicts selected bond length and angles for cubanes **14** and **16**, respectively. The angles provided suggest all metal centers have a disordered octahedral configuration.

Figure 5.14. Thermal ellipsoid plot (50% probability) and tube representation of the iron(II) complex 14. (*), ( ) and (^) indicate the three different metal environments.

14
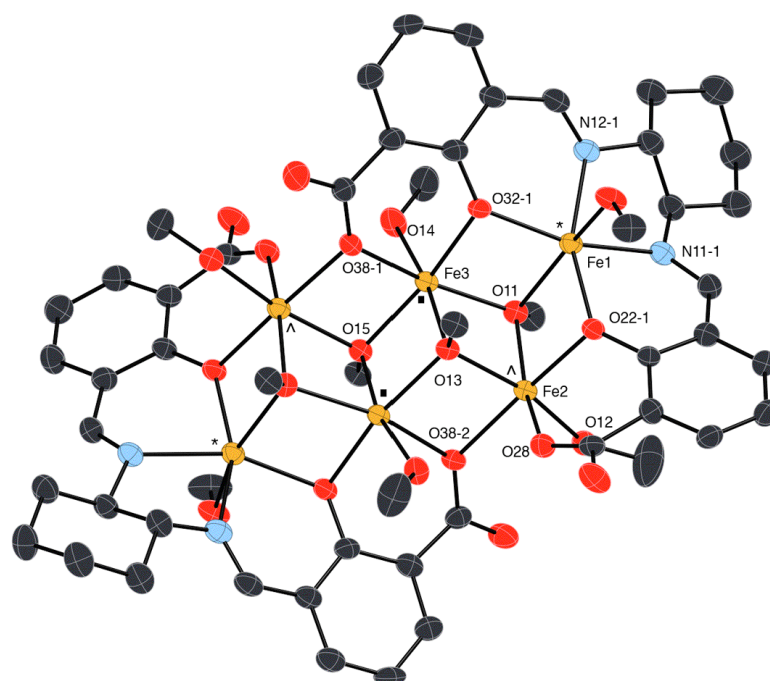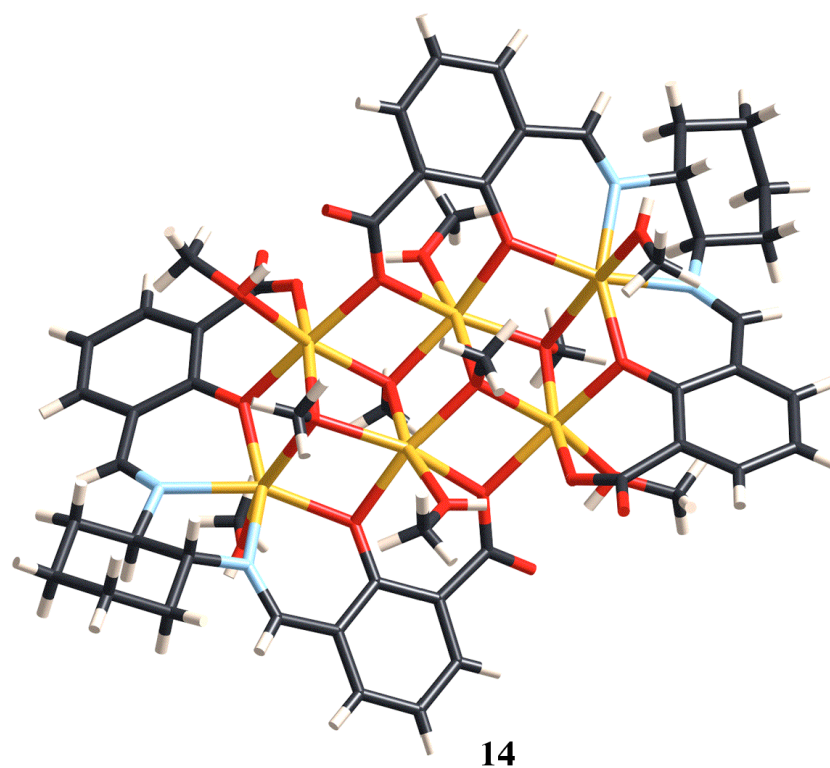
Table 5.1. Selected bond lengths (Å) and bond angles (°) for **14**.

Bond lengths	Fe(1)-O221	2.0352(18)
	Fe(1)-O321	2.0598(19)
	Fe(1)-N111	2.120(2)
	Fe(1)-N121	2.139(2)
	Fe(1)-O(10)	2.200(2)
	Fe(1)-O(11)	2.2344(18)
	Fe(2)-O(11)	2.0755(17)
	Fe(2)-O281	2.0861(18)
	Fe(2)-O221	2.0975(18)
	Fe(2)-O(13)	2.1221(18)
	Fe(2)-O(12)	2.126(2)
	Fe(2)-O382	2.1504(18)
	Fe(3)-O(15)	2.0431(18)
	Fe(3)-O321	2.0586(17)
	Fe(3)-O(11)	2.0982(18)
	Fe(3)-O381	2.1016(19)
	Fe(3)-O(14)	2.105(2)
	Fe(3)-O(13)	2.1551(17)
Bond angles	O221-Fe(1)-O321	117.66(7)
	O221-Fe(1)-N111	83.71(8)
	O221-Fe(1)-O(10)	86.53(7)
	O221-Fe(1)-O(11)	78.26(7)
	O(10)-Fe(1)-O(11)	159.32(7)
	O(11)-Fe(2)-O281	161.31(7)
	O(11)-Fe(2)-O221	80.59(7)
	O221-Fe(2)-O(13)	93.38(7)
	O281-Fe(2)-O382	87.61(7)
	O(13)-Fe(2)-O382	82.60(7)
	O(15)-Fe(3)-O321	168.41(7)
	O321-Fe(3)-O(11)	83.82(7)
	O321-Fe(3)-O381	84.53(7)
	O321-Fe(3)-O(14)	91.64(8)
	O(14)-Fe(3)-O(13)	172.25(8)

Figure 5.15. Thermal ellipsoid plot (50% probability) and tube representation of the Co(II) complex 16. (*), ( ) and (^) indicate the three different metal environments

16
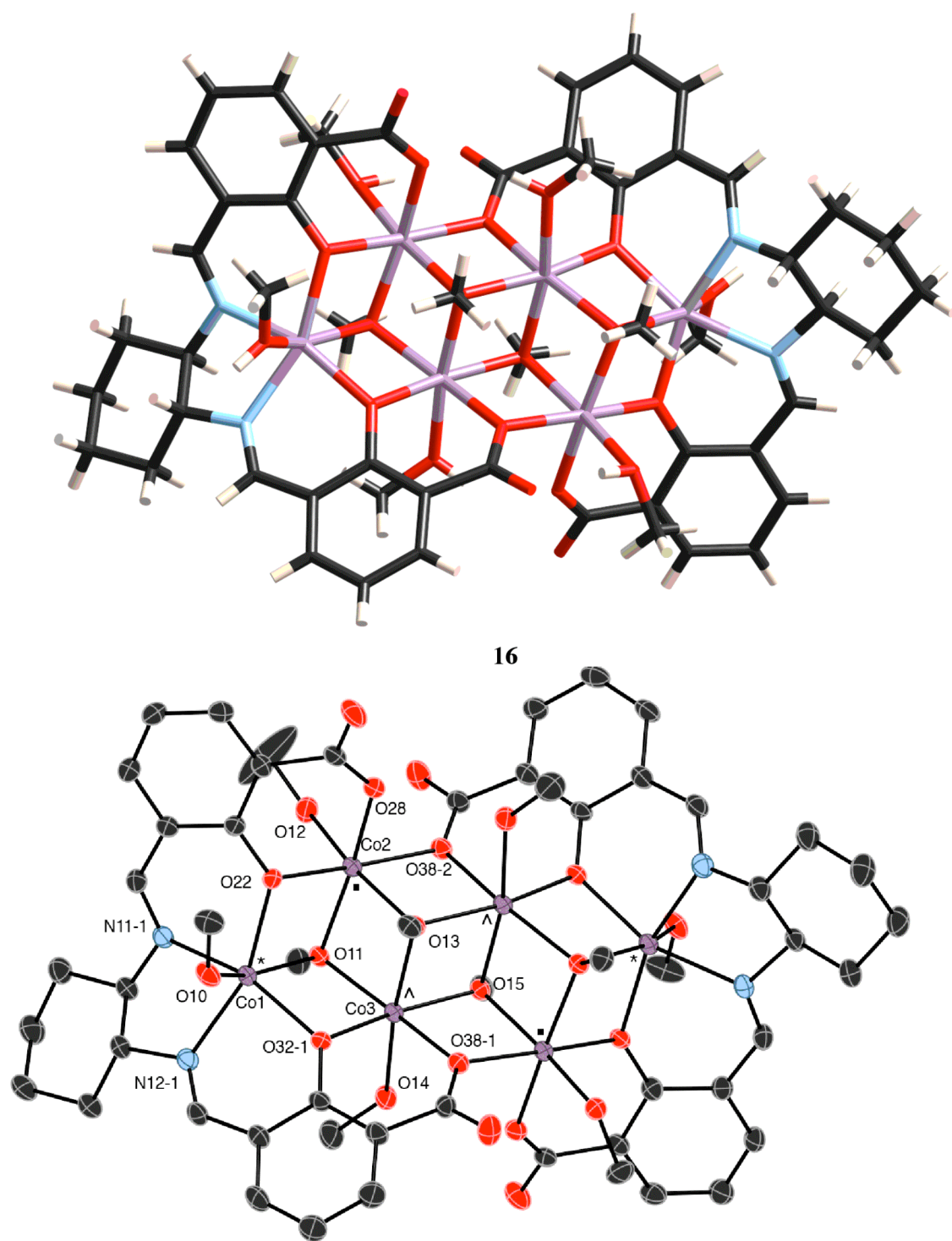
Table 5.2. Selected bond lengths (Å) and bond angles (°) for 16

Bond lengths	Co(1)-O221	2.0568(19)
	Co(1)-O321	2.0487(16)
	Co(1)-N111	2.097(2)
	Co(1)-N121	2.100(2)
	Co(1)-O(10)	2.172(2)
	Co(1)-O(11)	2.2395(18)
	Co(2)-O(12)	2.1434(19)
	Co(2)-O281	2.071(2)
	Co(2)-O221	2.0465(18)
	Co(2)-O(13)	2.0831(17)
	Co(2)-O(11)	2.0727(19)
	Co(2)-O382	2.1364(18)
	Co(3)-O(15)	2.0536(17)
	Co(3)-O321	2.0351(18)
	Co(3)-O(11)	2.0690(16)
	Co(3)-O381	2.0800(18)
	Co(3)-O(14)	2.082(2)
	Co(3)-O(13)	2.1009(19)
Bond angles	O321-Co(1)-N121	84.97(8)
	O221-Co(1)-N121	158.88(8)
	N121-Co(1)-O(10)	82.80(9)
	N111-Co(1)-N121	78.41(9)
	O(10)-Co(1)-O(11)	157.31(7)
	O221-Co(2)-O281	84.77(8)
	O281-Co(2)-O(11)	164.12(8)
	O221-Co(2)-O(13)	95.14(7)
	O221-Co(2)-O382	172.86(8)
	O221-Co(2)-O(12)	98.92(7)
	O321-Co(3)-O(15)	168.17(7)
	O321-Co(3)-O(11)	82.72(7)
	O321-Co(3)-O381	86.63(7)
	O(15)-Co(3)-O(14)	89.58(8)
	O321-Co(3)-O(13)	93.93(7)

The crystal structure of cobalt complex **18** is depicted in figure 5.16. The structure shows the same cage core as seen in complexes **14** and **15**. Again, six cobalt centers occupy the same vertices as previously seen. However, the coordination geometry of the central face-shared tetra-cubane is slightly different. Here, the remaining vertices are occupied by doubly (a total of two) and triply (a total of four) bridging methoxides. Phenoxides and carboxylates of the deprotonated unsymmetrical Schiff-base ligand complete the coordination spheres of the metals.

Complex **18** possesses a pseudo-center of inversion, which creates two different cubane environments. One cubane environment consists of, beside the three cobalt metal centers, one doubly bridging methoxide, two triply bridging methoxides and one ligand phenoxide oxygen. There are two cubanes sharing this coordination geometry and they are closest to the two unsymmetrical Schiff-base ligands. The remaining face-shared cubanes each consist of three cobalt metals, three triply bridging methoxides and one carboxylate oxygen. In addition to the two fully deprotonated unsymmetrical Schiff-base ligands and the methoxide ions, two cyclohexyldiamine molecules also act as chelates to create three different cobalt environments. Two cobalt centers are located in the pseudo-salen pocket of the unsymmetrical Schiff-base ligands. These cobalt ions have a disordered square-pyramidal coordination geometry. The basal positions are occupied by a doubly bridging phenoxide oxygen, an imine nitrogen, an amine nitrogen and a triply bridging methoxide. A doubly bridging methoxide is coordinated to the apical position. The second cobalt environment, corresponding to two cobalt centers, consist of the two amine nitrogens of the cyclohexyldiamine ligand. Furthermore, the ligand binds to two triply bridging methoxide, a doubly bridging methoxide and a doubly bridging

carboxylate oxygen of the second unsymmetrical Schiff-base ligand. The third and final cobalt environment is located in the pseudo-phenoxide/carboxylate pocket of the Schiff-base ligand, coordinating to the phenoxide and carboxylate oxygens of the same Schiff-base ligand and two triply bridging methoxides on one coordination plane and a third triply bridging methoxide and a methanol molecule on the second coordination plane of the octahedral cobalt center. Two iodine anions counter balance the positive charge of the cationic complex. Table 5.3 shows selected bond length and bond angles for **18**.

Figure 5.16. Thermal ellipsoid plot (50% probability) and tube representation of the Co(II) complex 18. The two iodine anions are shown in the thermal ellipsoid plot only. (*), ( ) and (^) indicate the three different metal environments.
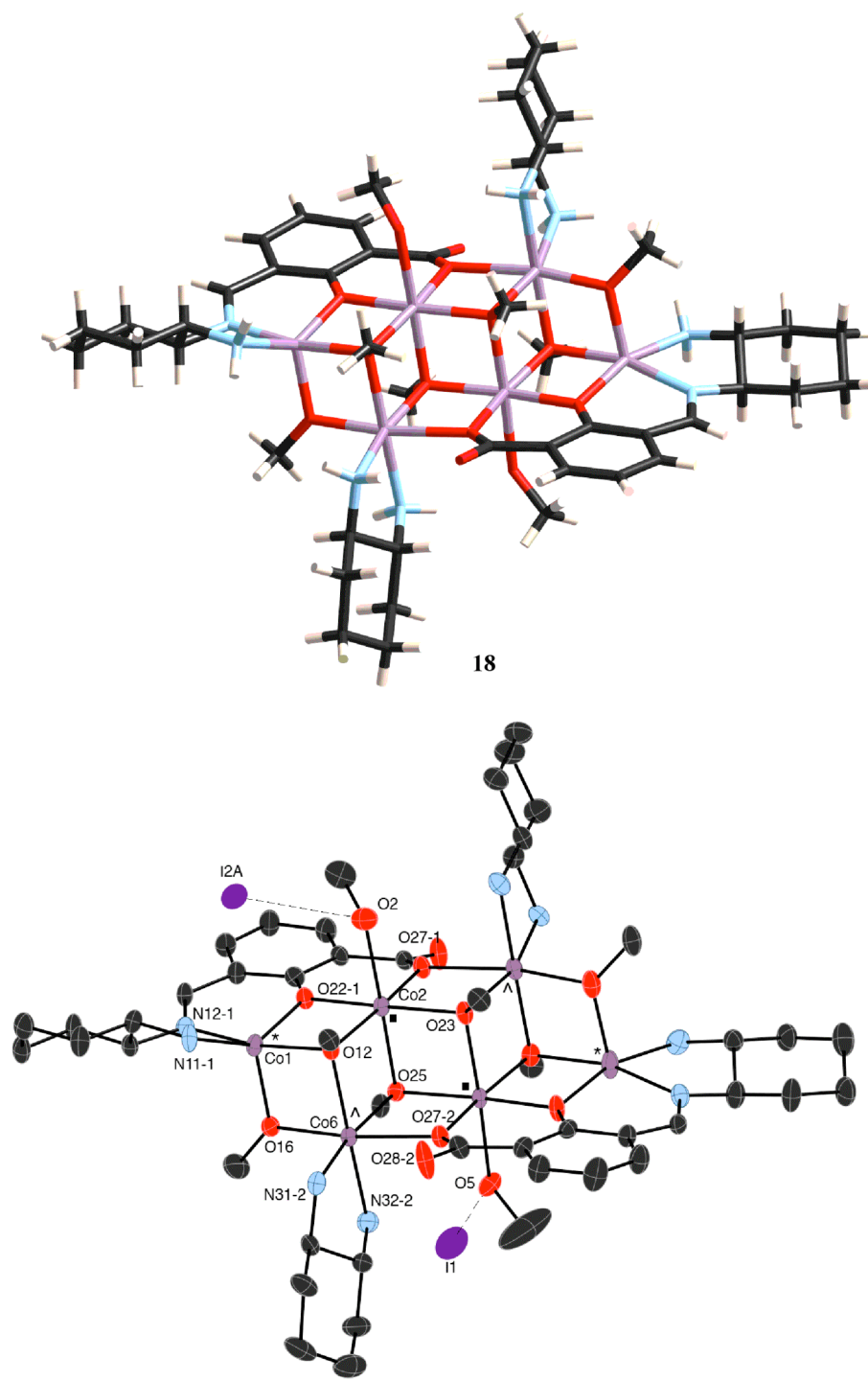
Table 5.3. Selected bond lengths (Å) and bond angles (°) for 18.

Bond lengths	Co(1)-O(16)	1.932(3)
	Co(1)-O221	2.018(3)
	Co(1)-N111	2.052(3)
	Co(1)-N121	2.098(3)
	Co(1)-O(12)	2.109(3)
	Co(2)-O(23)	2.041(3)
	Co(2)-O(12)	2.049(3)
	Co(2)-O271	2.055(3)
	Co(2)-O221	2.061(3)
	Co(2)-O(25)	2.131(3)
	Co(2)-O(2)	2.219(3)
	Co(6)-O(16)	2.019(3)
	Co(6)-O(25)	2.101(3)
	Co(6)-N312	2.119(4)
	Co(6)-O(12)	2.132(3)
	Co(6)-N322	2.136(4)
	Co(6)-O272	2.266(3)
Bond angles	O(16)-Co(1)-N111	103.98(13)
	O221-Co(1)-N111	88.31(13)
	N111-Co(1)-N121	81.15(13)
	N111-Co(1)-O(12)	170.32(13)
	O(23)-Co(2)-O221	169.29(12)
	O(12)-Co(2)-O221	84.06(11)
	O271-Co(2)-O221	86.95(11)
	O(25)-Co(2)-O(2)	177.43(12)
	O221-Co(2)-O(2)	88.05(13)
	O(16)-Co(6)-N312	94.98(13)
	O(25)-Co(6)-N312	169.12(13)
	N312-Co(6)-N322	81.41(14)
	N312-Co(6)-O272	91.74(12)
	N312-Co(6)-O(12)	100.46(12)

The crystal structure of the Ni complex **21**, with the unsymmetrical Schiff-base ligand (*R,R*)-**4** reveals a very complicated coordination environmental (Figure 5.17). The complex possesses similar face-shared tetra-cubane core as seen in the previous cases, but the ligands are of a much more complex nature. Beside the usual doubly and triply bridging methoxides, the organic ligands consist of two cyclohexyldiamine, two completely deprotonated unsymmetrical Schiff-base ligands and two partially deprotonated symmetrical salen ligands. The latter binds to the cubane through one of its carboxylate moieties where both oxygens act as coordinating ligands. The other carboxylic acid group remains protonated and does not participate in any form of complexation. Besides the six pseudo-octahedral nickel centers creating the cubanes in the core of the complex, there are two square-planar nickel centers located in the salen pockets of the two symmetrical Schiff-base ligands. The overall complex is cationic and is balanced with two iodine counter ions.[87] As in the previous cases, the complex has a pseudo-center of inversion.

Figure 5.17. Thermal ellipsoid plot (50% probability) and tube representation of the Ni(II) complex 21. The two iodine anions are shown in the thermal ellipsoid plot only.

21

With focus on the cubane core

With focus on the salen moiety
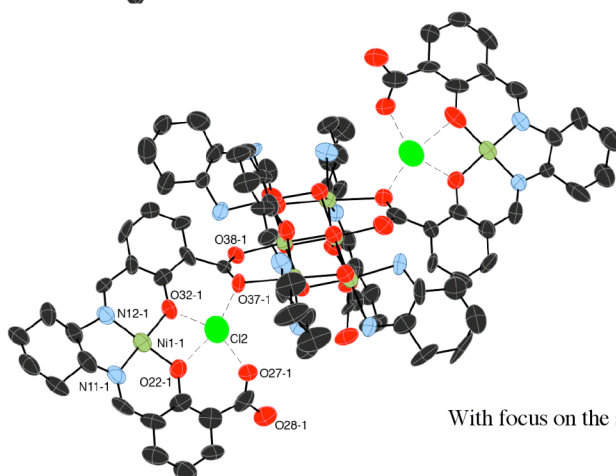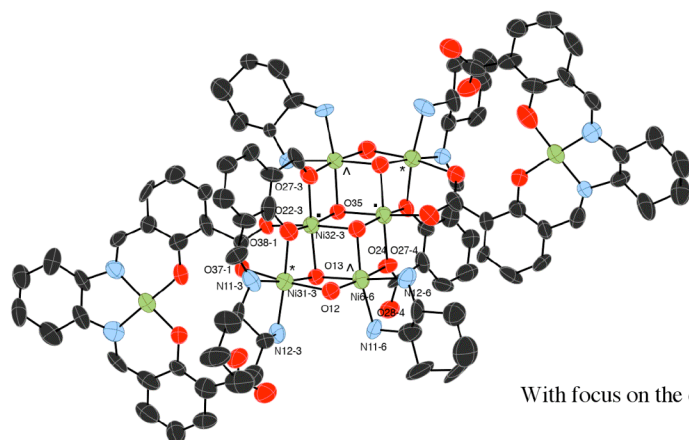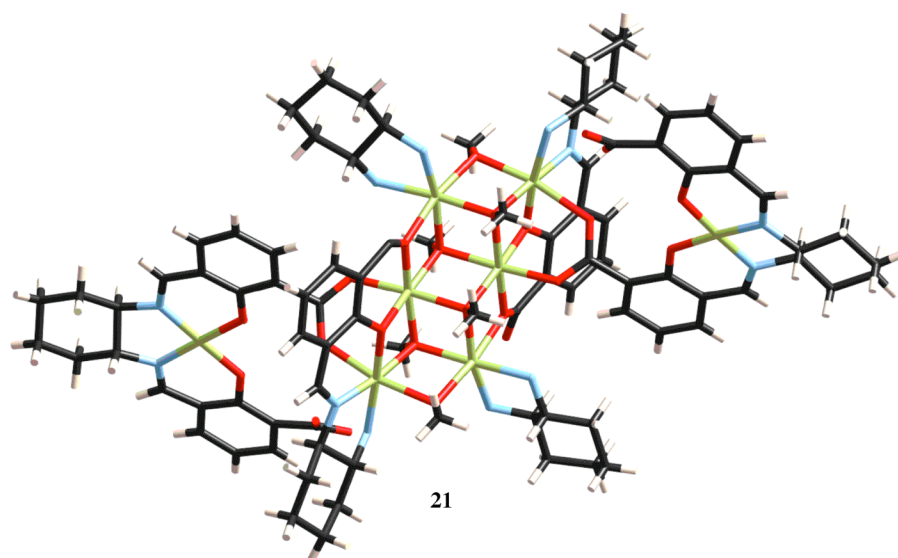
Figure 5.18 shows the crystal structure of the Cu(II) complex **22**. Selected bond lengths and angles are depicted in table 5.4. The tetranuclear complex shows a similar face-shared cubane structure as seen for Fe(II), Co(II) and Ni(II) complexes. However, in this case, there are only two cubanes held together by two triply and two doubly bridging methoxides. Two doubly bridging phenoxide oxygens occupy the two remaining vertices. There are two different copper environments consisting of two copper centers each. One is located in the pseudo-salen pocket of the fully deprotonated unsymmetrical Schiff-base ligand binding to a phenoxide oxygen, imine nitrogen, amine nitrogen and two methoxide ligands. The second is located in the pseudo-phenoxide/carboxylate pocket of the ligand coordinated to one of the carboxylic oxygens, a phenoxide oxygen and three methoxide ligands. The four coppers centers all have square-pyramidal geometries. There is a weak metal-metal bond present between the two copper centers of the distance 3.003 Å.

Figure 5.18. Thermal ellipsoid plot (50% probability) and tube representation of the Cu(II) complex 22. (*) and ( ) indicate the two different metal environments. The Cu-Cu bond is not shown.


22
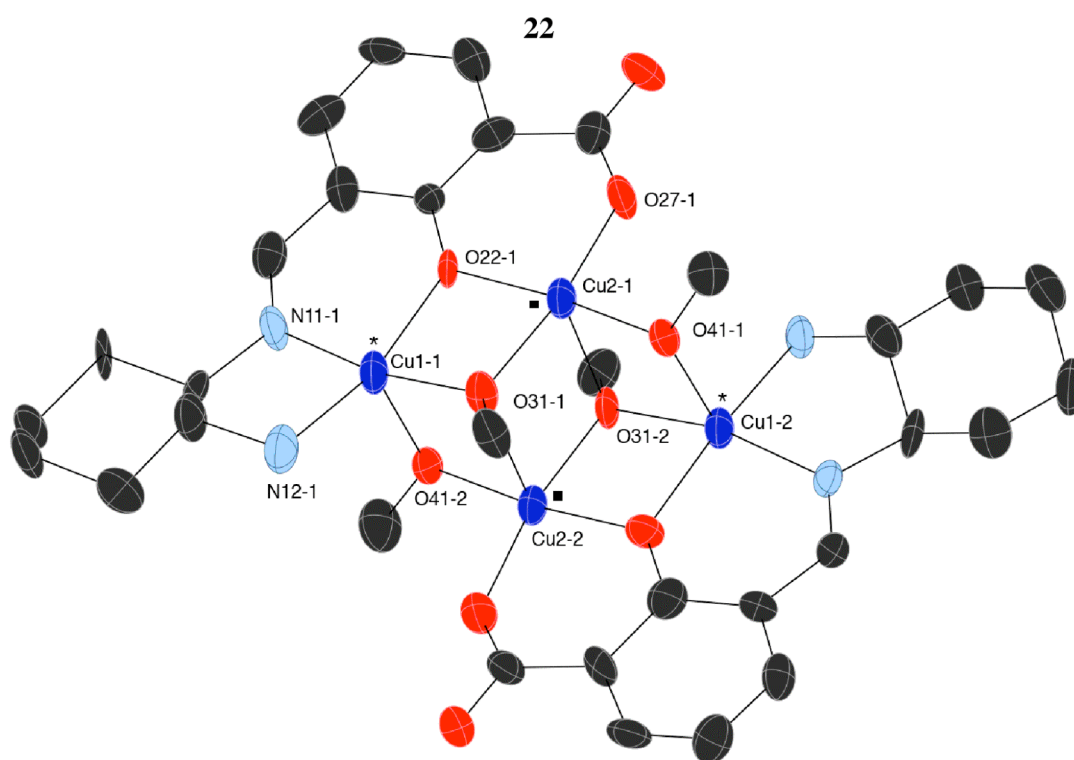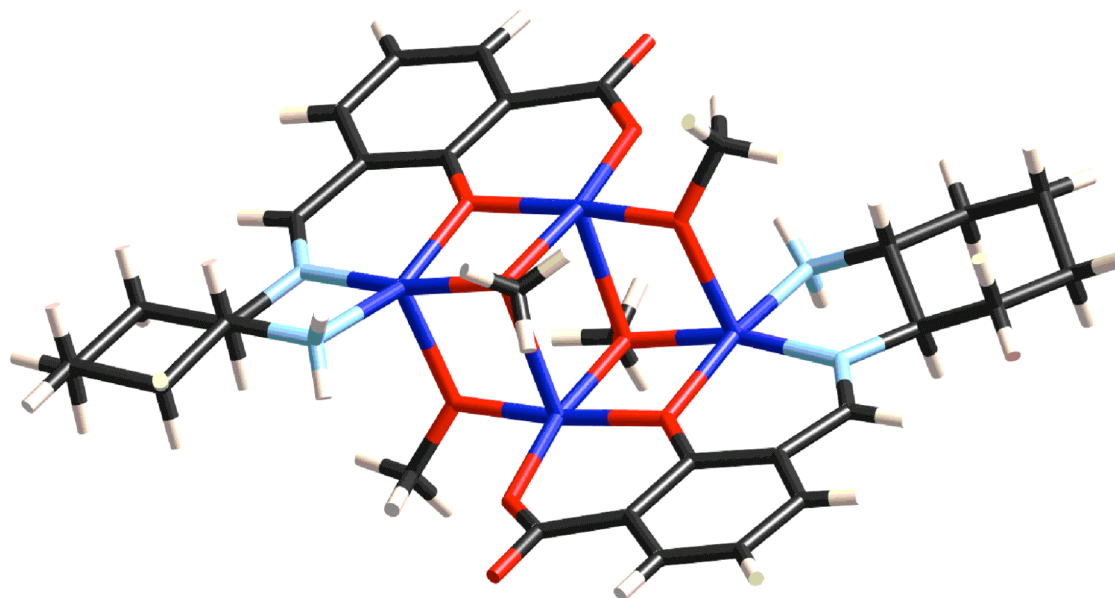
Table 5.4. Selected bond lengths (Å) and bond angles (°) for 22.

Bond lengths	Cu11-O311	1.905(9)
	Cu11-N111	1.905(11)
	Cu11-O221	1.976(9)
	Cu11-N121	2.020(12)
	Cu11-O412	2.193(10)
	Cu11-Cu21	3.0025(18)
	Cu21-O411	1.877(9)
	Cu21-O271	1.904(9)
	Cu21-O311	1.951(9)
	Cu21-O221	1.959(9)
	Cu21-O312	2.414(10)
Bond angles	O311-Cu11-N121	103.3(4)
	N111-Cu11-N121	85.4(5)
	O221-Cu11-N121	162.0(4)
	N121-Cu11-O412	102.8(4)
	O411-Cu21-O221	174.0(4)
	O271-Cu21-O221	92.3(4)
	O311-Cu21-O221	78.6(4)
	O221-Cu21-O312	94.2(4)

Figure 5.19 shows the crystals structure of the salen-copper complex **23**. These were the maroon colored crystals that were obtained at higher copper concentrations. As seen in previous reactions with excess copper (chapter 4), the unsymmetrical Schiff-base ligand disproportionates to form its symmetrical salen analogue. The dinuclear complex has two copper ions, one each in salens and phenoxide/carboxylate pockets of the ligand. This structure has been previously reported as the result of the symmetrical salen ligand with excess copper ions. The complex chirality is inherent from the chiral ligand (*R,R*)-**6** and the complex has a C_2 symmetry. Each copper center has a square-planar geometry.

The crystal packing of **23** shows the presence of non-covalent bonding in the crystal lattice (Figure 5.20). There are two types of non-covalent bonding present;

hydrogen-bonding and π-π* stacking. Hydrogen bonding between the carboxylate oxygens and the cyclohexyldiamine hydrogens of adjacent molecule creates a zigag pattern in the crystal lattice. The complex is further stabilized through π-π* interaction between two adjacent benzyl moieties with a distance of 3.6 Å.

Figure 5.19. Thermal ellipsoid plot (50% probability) and tube representation of the Cu(II) complex 23.

23
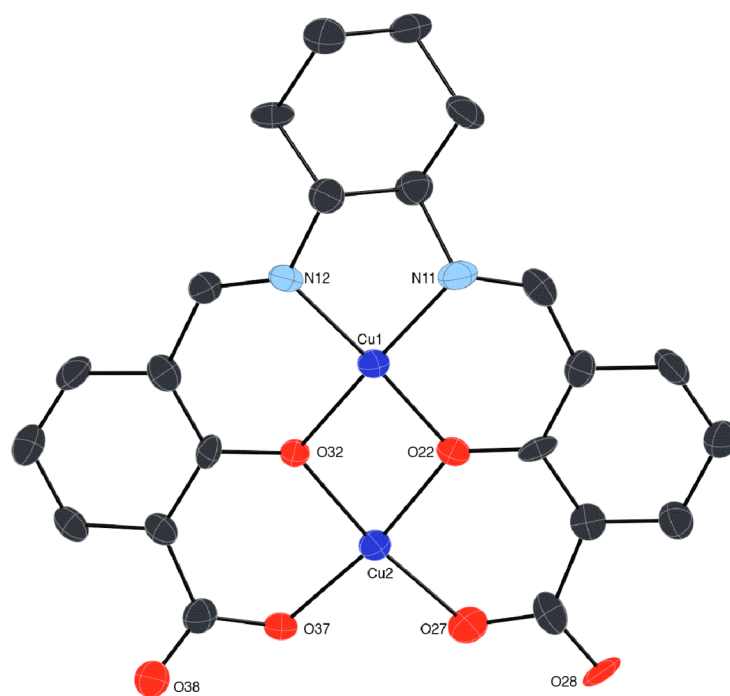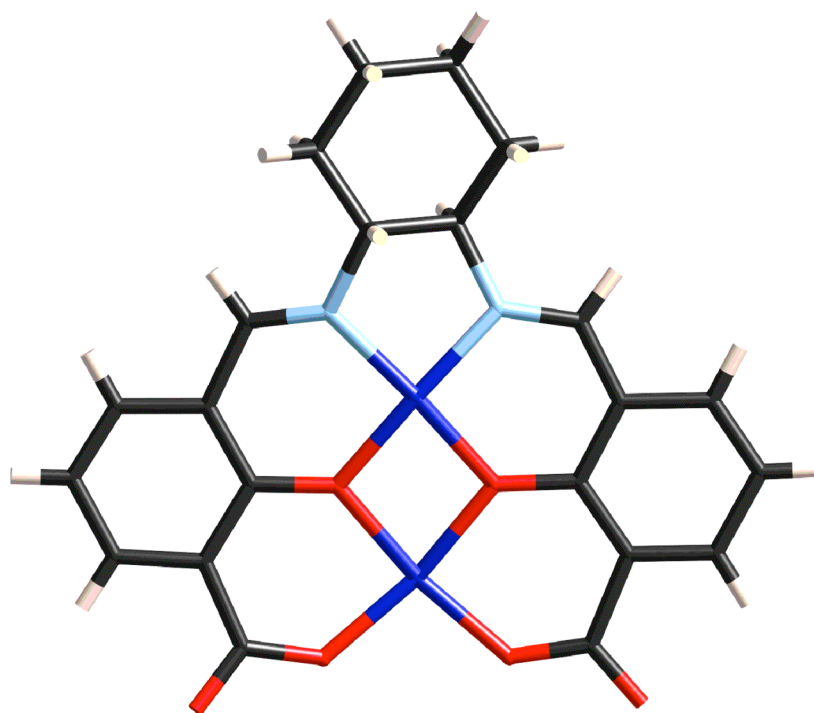
Figure 5.20. Crystal packing of 23. a) show the effect of hydrogen bonding between the carboxylic oxygens and cyclohexyldiamine hydrogens of two adjacent complexes. b) shows the effect of π-π* stacking on the formation of helices.
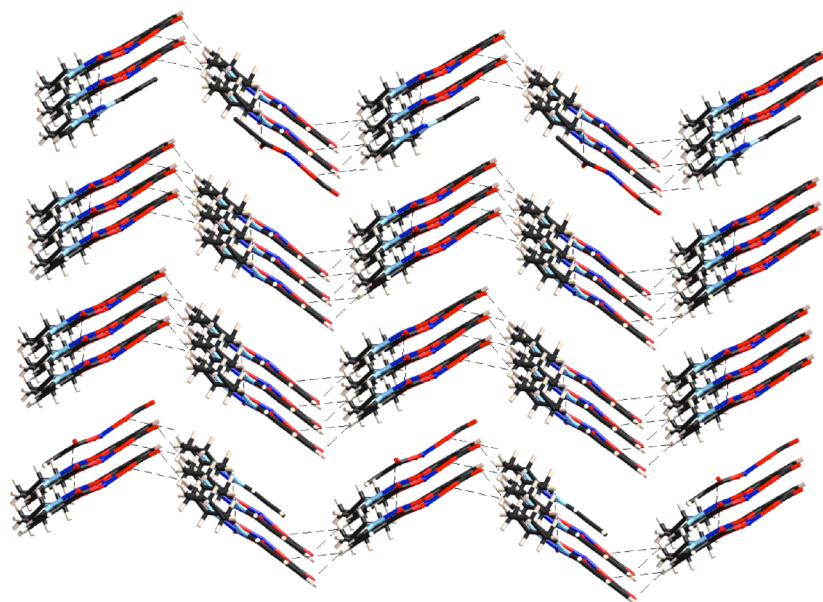
a
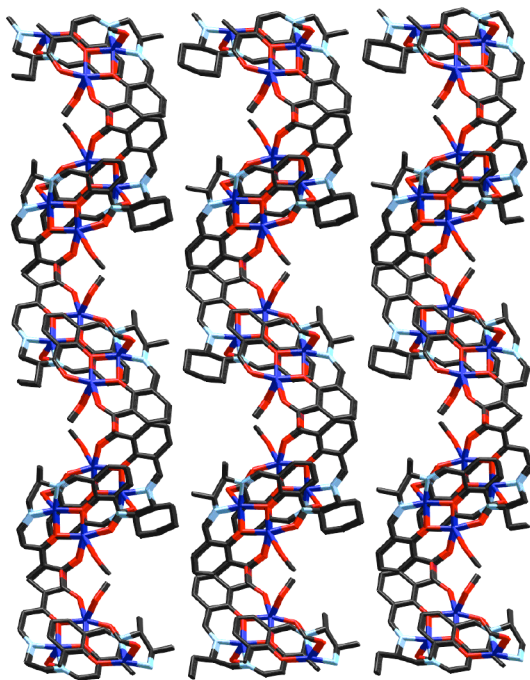
b

CHAPTER 6 - Conclusion and future work

6.1 Conclusions

This work was initiated with a desire to discover and predict the complexation modes of a series of acid-functionalized Schiff-base/salen ligands. Though not every anticipated ligand/complex could be synthesized, significant knowledge about the complexation modes of 3-formylsalicylic based Schiff-base ligands was gathered.

6.1.1 Macrocycles

Though it was the initial focus, none of the designed macrocycles could be synthesized in the lab. Many different approaches and strategies, too many to mention here, were applied, but none resulted in the formation of the desired cycles. In general, methods such as dilution techniques, template techniques, protecting functional groups and different synthetic routes were applied. Finally, it was agreed that though salen ligands are famous for their straightforward and trivial synthesis, the making of their macrocyclic analogues is very challanging (Figure 6.1).[26]

Figure 6.1. Unsuccessful attempts at synthesizing four target macrocycles.
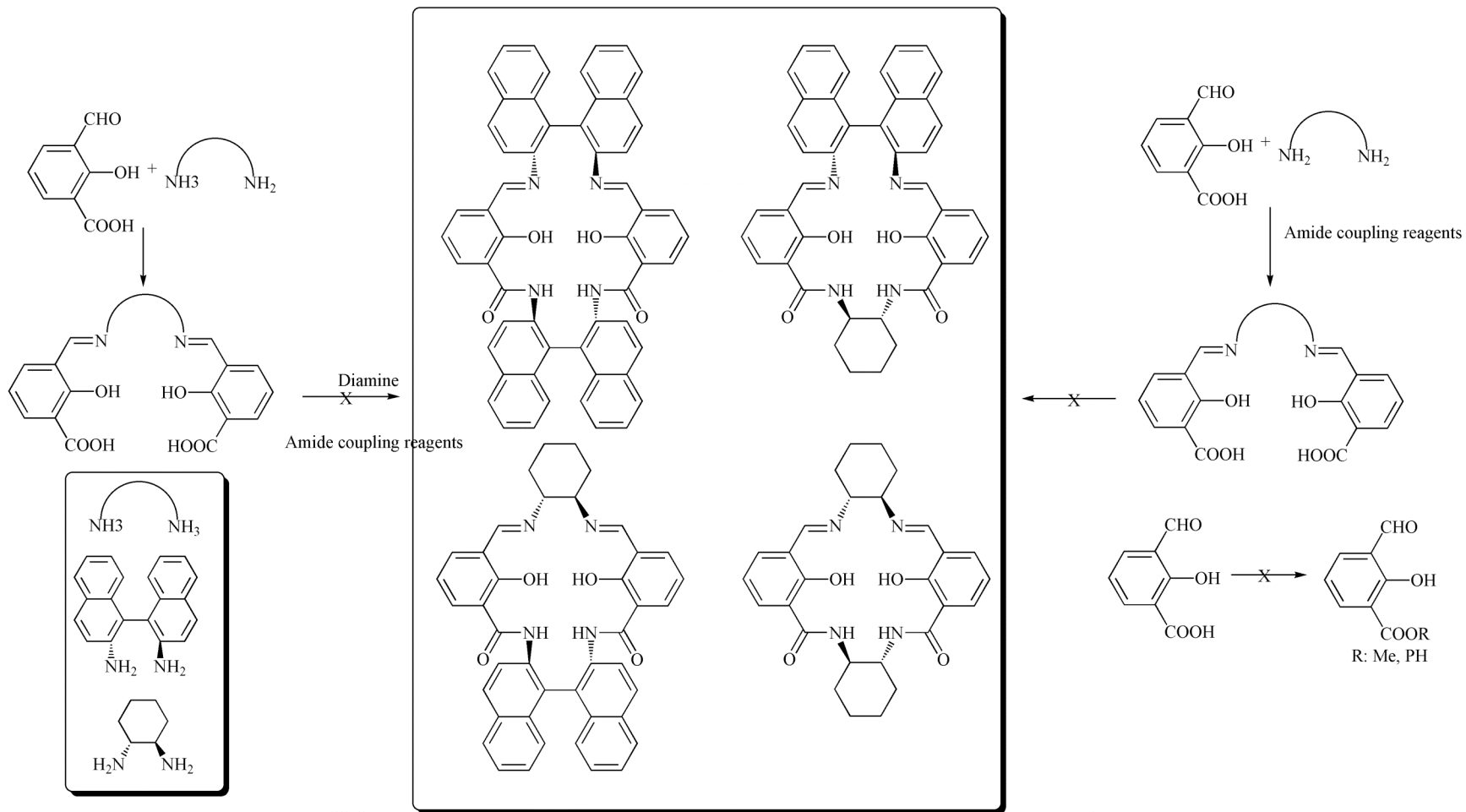
6.1.2 Acyclic diimine systems

As anticipated, the synthesis of these ligands was very straightforward. Both the cyclohexyldiamine and the binaphthyldiamine analogs of the salen complexes were obtained in excellent yields through the Schiff-base condensation of the diamines with two equivalents of 3-formylsalicylic acid. Complexation was done with divalent transition metals using both TEA and NaOMe as the reaction base. The synthesis/crystallization was done in various solvents ranging from DMSO to chloroform. However, crystals could only be obtained when methanol was used as the reaction solvent. When using TEA as the base, only the reaction of the cyclohexyldiamine based salen ligand (R,R)-**4** with $FeCl_2$ resulted in crystals suitable for X-ray analysis. Interestingly, the result showed the formation of a cubane-type structure where both the phenols and carboxylic acids were deprotonated. The same results were obtained when NaOMe was used as the base for the reaction. However, in this case crystals could be grown from reaction with both $FeCl_2$ and CoI_2. In all cases methanol and methoxide molecules helped to create defect face-shared tetra cubanes (Figure 6.2). As predicted, the presence of methanol/methoxide molecules pushed the structure to adopt a cubane structure rather than a mono- or dinuclear salen complex. Literature data suggests the formation of single stranded mono- or dinuclear salen complexes is favored in aprotic solvents such as DMSO or DMF.[20] Since no crystals could be obtained in non-polar systems, it can only be concluded that the presence of methanol/methoxide does indeed favor the formation of cubane-type structures.

Figure 6.2. Complexation of (*R*,*R*)-4 with FeCl$_2$ and CoI$_2$ using NaOMe as the base (TEA and NaOMe for Fe(II)) in methanol resulted in the formation of cubane-type structures. The stick diagram represents the Co(II) complex.
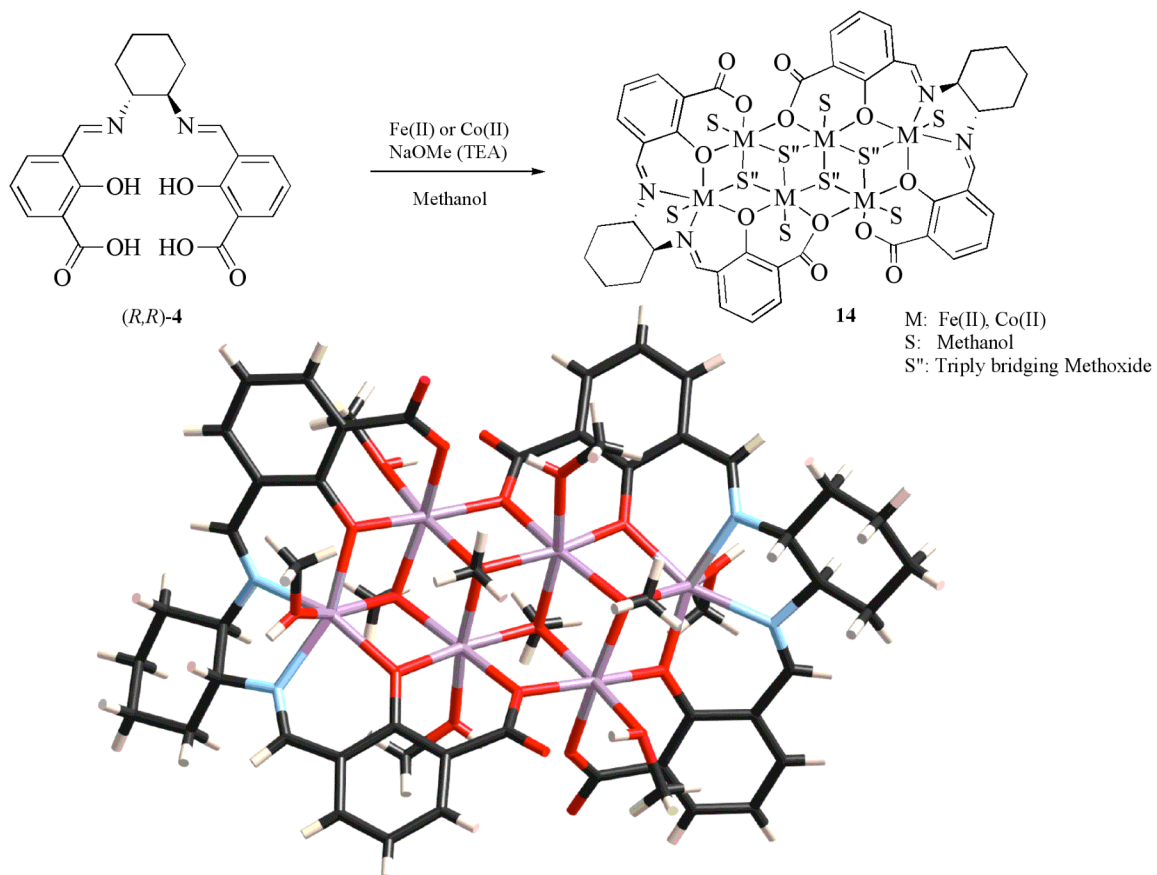
Reactions of the binaphthyl base ligand (*R*,*R*)-**5**, with metal salts in the presence of both bases gave a complicated mixture of products. Reactions were carried out using both traditional batch synthetic techniques and solvent diffusion techniques.

Table 6.1. Solvents used in the complexation/ crystallization of all complexes. (*) indicates triple layering as neither the deprotonated ligand or the metal ion was soluble in the solvents

Ligand layer	Metal layer
DMSO	Methanol
Methanol	Ethanol
Ethanol	*tert*-butanol
Pyridine	DMF
Acetonitrile	THF
Toluene	Nitrobenzene
Ethylene dichloride	
Benzyl chloride	
Methylene chloride	
Chloroform	
Diethyl ether*	
Hexane*	

Table 6.1 shows the combination of solvents used in the complexation reaction/ crystallization steps for BINAM based ligands. In most cases, the BINAM molecule itself was the isolated product indicating that the reaction must have undergone hydrolysis. As in all other cases, the reaction was carried under inert atmosphere using dried and degassed solvents. As a result, it was concluded that the BINAM based salen ligands, though fairly stable on their own, are too sensitive to partake in complexation reactions.

Three single stranded salen complexes were obtained although not from anticipated ligands. The three involved the monoimine ligands of both cyclohexyldiamine (*R,R*)-**6**, and binaphthyldiamine (*R,R*)-**7**, in combination with Cu(II) and Cu(I) salts (figure 6.3 and 6.4). The strength of the base determined if the final product is a mono- or dinuclear complex. Successful synthesis with the BINAM ligand were only obtained when TEA was used as the base.

Figure 6.3. Reaction of (*R,R*)-6 resulted in the formation of mononuclear salen ligands when reacted with either Cu(OTf)₂ or Cu(OTf) using TEA. The reaction with NaOMe resulted in the formation of the dinuclear salen complex instead.
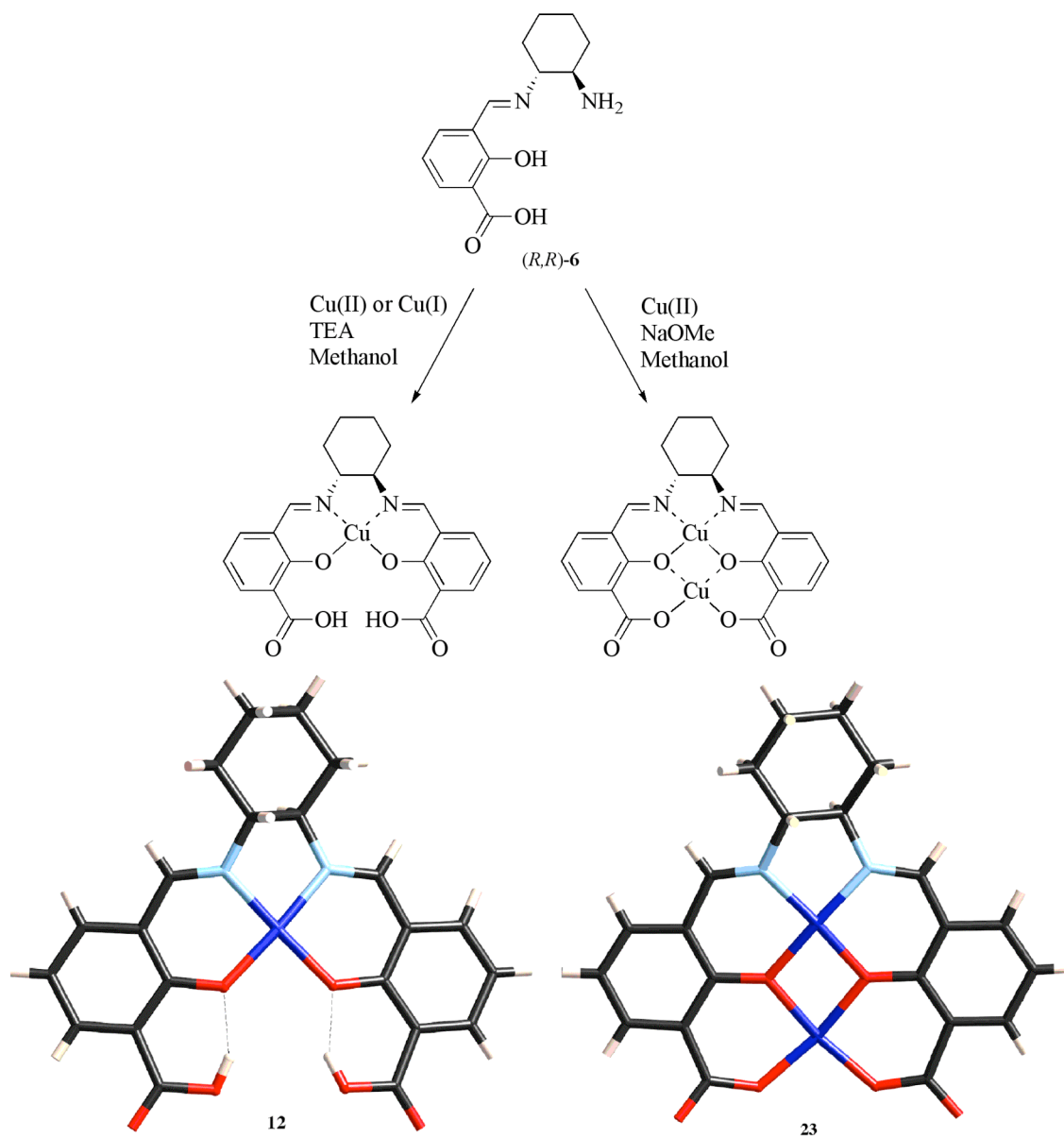
Figure 6.4. Complexation of (*R,R*)-7 with Cu(OTf)$_2$, TEA in a mixture of MeOH/EtOH resulted in the formation of a dinuclear salen complex.
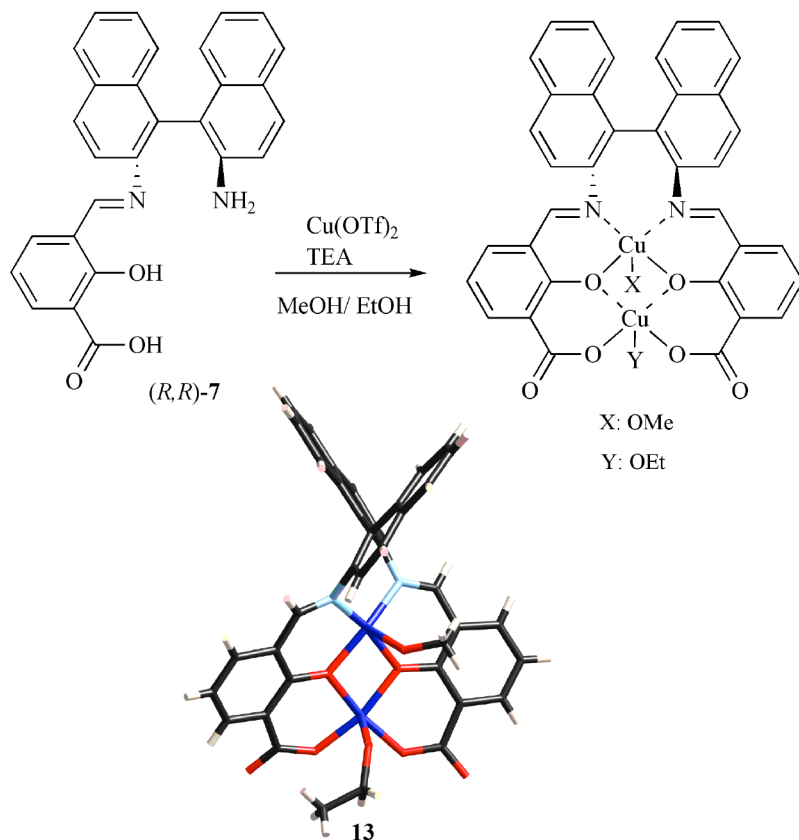
6.1.3 Acyclic monoimine systems

Monoimine Schiff-bases were synthesized from both cyclohexyldiamine and binaphthyldiamine using a 1:1 ratio of 3-formylsalicylic acid and (1*R*, 2*R*)-diaminocyclohexane and (*R*)-1,1'-binaphthyl-2,2'-diamine, respectively. The former exists as a zwitterion at room temperature with a carboxylate- and an ammonium ion functional group. The BINAM Schiff-base on the other hand remains as a neutral compound since binaphthylamine is not basic enough to deprotonate the carboxylic acid. The more basic cyclohexylamine, on the other hand, does not have any problems carrying out this deprotonation.

Metallation of the cyclohexyl based monoimine in the presence of TEA, divalent transition metals and methanol resulted in the exclusive formation of double stranded monohelices (Figure 6.5). The complexes are of a (*M*) *mer*-configuration. The crystals are further stabilized through intramolecular hydrogen bonding between the neutral carboxylic acid hydrogen and the phenolic oxygens. The crystals pack in such way that a hydrogen-bonded helical extended structure is formed. The noncovalent bonds are between the amine hydrogens of one complex and the carboxylate oxygen of an adjacent complex. Here, hydrogen bonding has been proven to increase the chances of a helix formation.

Figure 6.5. Complexation of (*R,R*)-6 with FeCl$_2$, CoI$_2$, NiI$_2$ and ZnCl$_2$, in methanol using TEA resulted in the formation of double stranded helices. These helices pack to form hydrogen bonded extended structures.
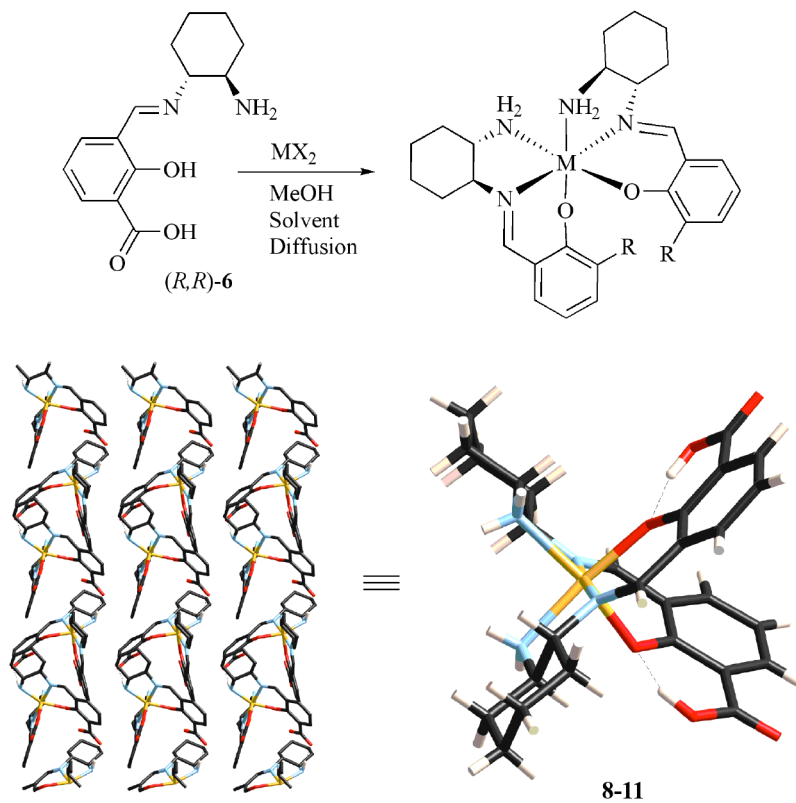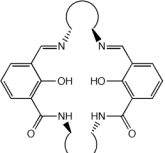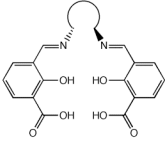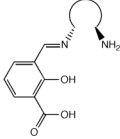
Metallation of this ligand in the presence of the strong base sodium methoxide resulted in completely different complexes. NaOMe fully deprotonates the acidic protons of the ligand. As a result, both phenoxides and carboxylates were capable of metal binding. Metallation with Fe(II), Co(II) and Ni(II) resulted in defect face shared tetra-cubane structures (Figure 6.6). Although the cubane core was very similar for all complexes, the ligands creating the cubane structure varied between the three metal salts. For Fe(II), the ligand has been converted to its diimine analog. Co(II)-cubanes had monoimine Schiff-base ligands and free cyclohexyldiamine as the organic chelating groups. In the case of Ni(II), a mixture of diimines, monoimines and free cyclohexyldiamine could be seen. A clue, however, was the location of the grown crystals. As the metal concentration increases, the conversion of the monoimine ligand to its symmetrical diimine analog becomes more likely. When Cu(II) triflate was used in moderate excess, metallation resulted in the formation of a mono-stranded dinuclear complex. The dimeric form of this complex has a defect, face shared di-cubane structure. Cubane structures were obtained only when methanol was used as the reaction solvent. Changing the solvent to any other of the above mentioned (Table 6.1), did not result in crystal formation. Once again, metallation of the BINAM monoimine ligands resulted in no isolated product. Figure 6.7 summarizes the results of all the reactions.

Figure 6.6. Complexation of (*R,R*)-6 with FeCl$_2$, CoI$_2$, NiI$_2$ and Cu(Otf)$_2$ in methanol with added resulted in the formation of cube-type structures
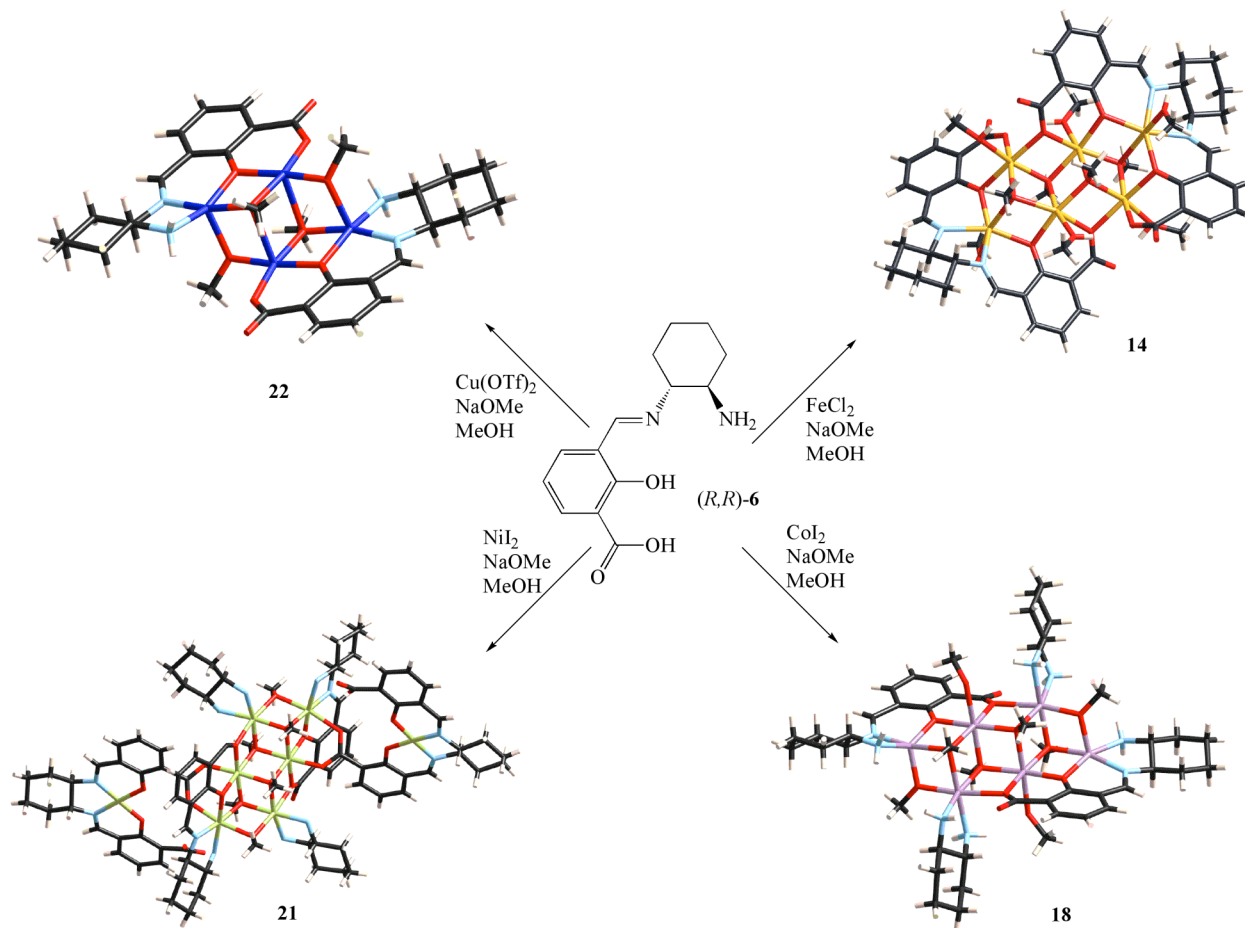
Figure 6.7. Summary and conclusion of work.

Ligand	Weak Base (TEA)	Strong base (NaOMe)	Fully deprotonated ligand Solvent: Methanol
Macrocycle	Predicted: M(II) is expected to bind to the salen pocket of the macrocycle. TEA is not basic enough to deprotonate the carboxylic acids.	Predicted: M(II) is expected to bind to the both the salen and the salan pocket of the macrocycle.	—
	Reaction outcome: None of the macrocyclic ligand could be synthesized.		
Diimine	Predicted: M(II) is expected to bind to the salen pocket of the macrocycle. TEA is not basic enough to deprotonate the carboxylic acids.	Predicted: M(II) is expected to bind to the both the salen and the salan pockets of the macrocycle.	Predicted: A fully deprotonated ligand in methanol have the potential of forming a cubane-type cages.
	Reaction outcome: No crystals could be isolated in any solvents other than methanol. Diamagnetic Zn complexes showed the presence of many different products (NMR). All attempts to crystallize the products failed.		Reaction outcome: Cubane-type cages Metals: Fe(II) and Co(II) Base: Both NaOMe and TEA resulted in acomplete deprotonation of the ligand. Comment: Only the CHDA based ligand could be analyzed as no crystals were obtained for the BINAM based ligand.
Monoimine	Predicted: Considering the pKa's of the functional groups, it is believed TEA will only deprotonated the phenolic hydrogen. However, in the case of CHDA, the amines have the potential of deprotonation the carboxylic acid creating an ammonium ion and a carboxylate. CHDA: M(II) is expected to bind to the phenoxide/carboxylic acid pocket of two *cis* located (H-bonding ability) ligands. BINAM: M(II) is expected to bind to the phenoxide/imine/amine pocket of two *cis* located ligands. The chirality of the backbone is believed to promote the formation of helices.	Predicted: A fully deprotonated ligand of this kind is expected to form a dinuclear, double stranded complex. There are two possibilities for hydrogen bonding; between two adjacent amines or between an amine and a carboxylate. The latter is believed to be more likely since the carboxylate has a higher pKa than an amine. Therefore it is predicted the final double strand will have a *trans* configuration.	Predicted: A fully deprotonated ligand in methanol has the potential of forming a cubane-type cages.
	Reaction outcome: Helices & mononuclear Salen complexes Helices: Fe(II), Co(II), Ni(II), Zn(II) Salen complexes: Cu(II) and Cu(I) Ligand: CHDA based Comment: The CHDA based ligand did indeed form a zwitterion with an ammonium group and a carboxylate. However, the ligand acted as a neutral ligand upon complexation with amines and carboxylic groups. The metal coordinated to the phenoxide/imine/amine pocket of the two ligand strands. These are located *cis* to each other but there are no H-bonding between the amine groups. The reason for a *cis* configuration can be due to the chirality of the ligand. Furthermore, this chirality is the reason for the helix formation rather than a flat double stranded complex. When Cu(II) and Cu(I) salts were used, a mono-nuclear salen complex was achieved. No crystals were obtained for the BINAM based ligand.	Reaction outcome: No crystals could be obtained on solvents other than methanol.	Reaction outcome: Cubanes & dinuclear Salen complexes Cubanes: Fe(II), Co(II), Ni(II),Cu(II) Salen Complexes: Cu(II) (highly excess) Base: TEA Ligand: CHDA based for cubanes CHDA and BINAM based for Salen complexes. Comment: The cubanes formed had similar metal-oxygen core. The essential oxygen linkers mostly came from methanol/methoxide ligands and the deprotonated phenoxide and carboxylate oxygens. All cubanes beside Cu(II) formed defected face-shared tetracubanes. The organic ligands surrounding the core varied significantly from metal to metal. It was suggested that the metal concentration played an important factor in the ligand oxidation process. Dinuclear salen complexes were obtained when Cu(II) salts were used in excess. Both CHDA and BINAM based ligands resulted in similar complexation outcome. This was the only case were crystals of a BINAM based complex was analyzed.

139

6.2 Future work

An increased understanding of the forces determining the advanced process of metal binding and molecular self-assembly is going to be a great tool in the synthesis of new catalytic systems. However, as most catalysts operate under homogeneous conditions, investigating the solid-state structures of the complexation product, is not sufficient. Extensive studies of solution structures of these complexes are necessary. For instance, a helix may only show one handedness (*M* or *P*) in the solid state while interconverting between the two forms in solution state. This complex, if used as a chiral catalyst will not yield a high enantiomeric excess, as each configuration will form products of different chirality.

Some of these complexes have already been shown to have some catalytic activities with no applied chirality. It was discovered that the addition of a mixture of Zn(II), Fe(II) and Ni(II) helices (**8**, **10** and **11**) in pyridine to methylene chloride will activate the C-Cl bond to form pyridinium ionic solids (Figure 6.8). The metal complexes are heated in pyridine, cooled down and added to methylene chloride. After three days at RT, crystals of the pyridinium salt starts to from. Further investigation of this catalytic reaction is needed. However, the first results indicate that the complex is activated by the addition of pyridine, probably through a substitution reaction where the amine group of the ligand is replaced by the pyridine. This activation can be confirmed using VT-NMR techniques and UV analysis. NMR techniques can also be used to investigate the catalytic reaction.

Figure 6.8. Catalytic activity of complexes 8 (Fe(II)), 10 (Ni(II)) and 11 (Zn(II)).
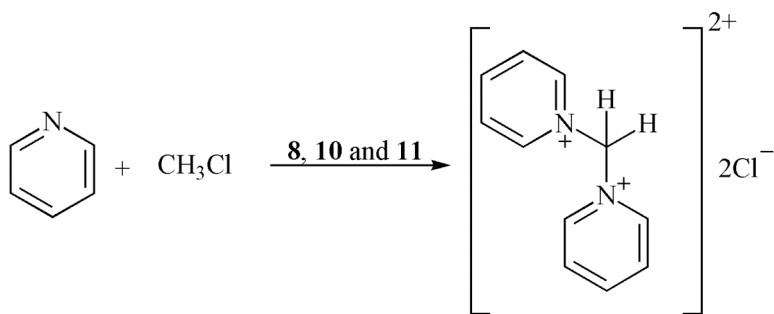
For cubane-type structures, the magnetic properties of these complexes need to be investigated. Also, creating cubanes containing different metal centers in the same core is highly attractive. Systems where different metal salts are mixed with the deprotonated ligand have the potential of forming these mixed-nuclei complexes. Other information that can be gathered from such experiments is the preference for the ligands towards the metal salt.

Experimental Section

General Methods

All reactions were carried under inert atmospheres (nitrogen or argon). Solvents used in complexation reactions were dried and degassed prior to vacuum transfer into reaction vessels. Methanol was dried over magnesium and triethylamine (TEA) was dried over calcium hydride. ACS reagent grade methanol was used without further purification for ligand syntheses. NMR solvents were dried over 4Å molecular sieves. Complexation reactions were carried out using solvent diffusion crystallization techniques in 7 mm OD borosilicate tubing. 3-FSA was prepared according to the methods of Duff and Bills.[17] (1*R*,2*R*)-diaminocyclohexane (DAC) was resolved according to literature procedures.[18] ^{1}H and ^{13}C NMR were obtained on a Varian 400 MHz or Bruker 800 MHz spectrometer employing residual solvent protons as an internal standard. Crystallographic data was collected using either a Bruker SMART 1000 CCD, a Bruker-AXE SMART APEX CCD or a κAPEX 2II diffractometer. Electrospray Ionization spectra were acquired on a LCT Premier (Waters Corp., Milford MA) time of flight mass spectrometer. The instrument was operated at 10,000 resolution (W mode) with dynamic range enhancement that attenuates large intensity signals. Optical rotations were measured using a Perkin-Elmer 241 polarimeter. Electronic spectra are acquired on a Hewlett-Packard 8453 spectrometer, using a 1.00 cm path length quartz cell.

3,3'-[(1R,2R)-1,2-cyclohexanediylbis(nitrilomethylidyne)]bis[2-hydroxybenzoic acid], **(R,R)-4**. A solution of 3-formylsalicylic acid (1.55 g, 9.33 mmol) and (1R,2R)-diaminocyclohexane (0.53 g, 4.67 mmol) in methanol (15 mL) was heated to reflux for 4 h under argon. The resulting yellow precipitate was collected by filtration to give (R,R)-**4** (1.845g, 96% yield). ^{1}H NMR (DMSO-d_6, 400MHz): δ 1.40 (m, 2H), 1.83 (m, 4H), 2.18 (d, 2H), 4.26 (d, 2H), 6.66 (t, 2H), 7.64 (d, 2H), 8.03 (d, 2H), 8.76 (s, 2H, H-N=), 13.11 (br), 15.98 (br). ^{13}C NMR (CDCl$_3$, 200MHz): δ 19.22, 24.16, 33.51, 114.96, 115.81, 119.89, 141.06, 141.75, 168.07, 169.98, 176.69. $[\alpha]_{25°}$ = -8.50° in ethanol. MS (m/z): [M + Na]$^+$ calcd for C$_{22}$H$_{22}$N$_2$O$_6$·Na$^+$, 433.1375; found, 433.1389 (3.2 ppm).

3,3'-[(1R,2R-binaphthalenediylbis(nitrilomethylidyne)]bis-[2-hydroxybenzoic acid], (R,R)-5.

A solution of 3-formylsalicylic acid (1.00 g, 6.02 mmol) and (R)-[1,1'-binaphthalene]-2,2'-diamine (0.815 g, 2.866 mmol) in methanol (20 mL) was heated to reflux for 4 h under argon. The resulting orange precipitate was collected by filtration to give (R, R)-**5** (1.42, 2.43 mmol, 81% yield). ^{1}H NMR (DMSO-d_6, 400MHz): δ 6.72 (t, 2H), 7.09 (d, 2 H), 7.39 (d, 2H), 7.57 (d, 2H), 7.62 (d, 2H), 7.89 (d, 2H), 8.16 (m, 4H), 8.40 (d, 2H), 9.37 (s, 2H), 14.16(br, 4H). ^{13}C NMR (DMSO-d_6, 50MHz): δ 116.87, 117.42, 118.49, 118.72, 125.56, 125.94, 127.34, 128.53, 129.12, 131.68, 132.76, 133.13, 138.64, 139.17, 161.17, 168.10, 170.07.

3-(((1R,2R)-2-aminocyclohexylimino)methyl)-2-hydroxybenzoic acid, (R, R)-6. A solution of (R,R)-**4** (1.65 g, 4.03 mmol) and (1R, 2R)-diaminocyclohexane (0.46 g, 4.03 mmol) in methanol (20 mL) was heated to 40-50° C for 4 h under argon. The resulting white precipitate was collected by filtration to give (R, R)-**6** (1.93 g, 91% yield). $[\alpha]^D_{25}$ = -3.04° in ethanol. UV-VIS (nm, pyridine); 261, 341, 368. ^{1}H NMR of **6a** (DMSO-d_6, 400MHz): δ1.32-2.05 (m, 8H), 3.16 (m, 2 H), 6.58 (t, 1H), 7.2 (br, ~ 3H), 7.75 (d, 1H), 7.82 (d, 2H), 8.75 (s, 1H), 18.02 (br), ^{1}H NMR of **6b** (DMSO-d_6, 400 MHz): δ1.15-1.95 (m, 8H), 3.1-3.2 (m, 2 H), 4.1 (br, ~2 H), 6.50 (t, 1H), 7.61 (d, 1H), 7.71 (d, 1H), 8.61 (s, 1H). ^{13}C NMR (DMSO-d_6, 50 MHz): δ 22.96, 28.46, 31.88, 32.31, 53.57, 70.44, 113.76, 120.08, 121.55, 128.71, 132.28, 158.18, 164.62, 170.00 MS (m/z): [M + Na]$^+$ calc for $C_{14}H_{18}N_2O_3 \cdot Na^+$, 285.1215; found, 285.1224 (3.2 ppm).

 (R,R)- 2-[3N-iminosalicylic acid] binaphthylamine, (R,R)-7. A solution of (R,R)-**5** (0.67 g, 1.15 mmol) and (R)-[1,1'-binaphthalene]-2,2'-diamine (0.67 g, 1.15 mmol) in methanol (15 mL) was heated to 40-50° C for 4 h under argon. The resulting red precipitate was collected by filtration to give (R, R)-**7** (0.97 g, 2.24 mmol, 81% yield). ^{1}H NMR of **7a** (DMSO-d_6, 800 MHz): δ 4.7 (br), 6.57 (d, 1 H), 6.71 (tr, 1H), 7.12 (d, 1H), 7.23 (d, 1H), 7.27 (d, 1H), 7.47 (d, 1H), 7.62 (d, 1H), 7.76 (m, 2H), 7.82 (d, 1H), 7.99 (d, 1H), 8.15 (d, 1H), 8.31 (d, 1H), 8.33 (d, 1H), 9.56 (s, 1H), 15 (br, 2H). ^{13}C NMR (DMSO-d_6, 400 MHz): δ 114.79, 116.24, 116.52, 118.61, 120.99, 121.94, 126.47, 126.73, 126.94, 127.89, 128.12, 128.37, 128.61, 128.78, 130.51, 132.76, 133.09, 133.42, 133.76, 139.79, 140.27, 160,27, 167.24, 175.19.

General Metallation Procedure A

The following procedure was carried out in a glove box with a nitrogen atmosphere. Methanol (1 mL) was added to an excess amount of metal salt (~15 equivalents). After 10 minutes of vigorous shaking the solution/suspension was filtered and any residual metal salt was dried and weighed in order to determine the amount dissolved. The ligands were separately added to methanol (1 mL). Dry triethylamine was added dropwise to the dissolved ligand until a clear solution was obtained (~0.1 mL added). The solution was filtered to eliminate any particles. The solution containing the ligand was layered on top of the solution of metal salt, and the tube was sealed. Crystals were usually obtained after 1-3 days at ambient temperature. The crystals were isolated and washed with cold methanol (5 × 1 mL), and the product was dried *in vacuo*. Yields ranged from 56-86% based on the amount of ligand used.

General Metallation Procedure B

The following procedure was carried out in a glove box with a nitrogen atmosphere. Metal solutions were prepared according to procedure A, The ligands and four equivalents of NaOMe were separately added to methanol (1 mL). The solution was filtered to eliminate any particles. The solution containing the ligand was layered on top of the solution of metal salt, and the tube was sealed. Crystals were usually obtained after 3-4 days at ambient temperature. The crystals were isolated and washed with cold methanol (5 × 1 mL), and the product was dried *in vacuo*. Yields ranged from 27-61% based on the amount of ligand used.

Fe(II)-(*R,R*)-6 complex (8). Anhydrous FeCl$_2$ (0.1204 g 0.949 mmol) and (*R,R*)-**6** (0.0315 g 0.120 mmol) were combined following the general procedure A. After 3 days, 0.020 g (0.035 mmol, 58% yield) of red crystals were obtained. MS (*m/z*): [M + H]$^+$ calcd for C$_{28}$H$_{34}$N$_4$O$_6$Fe·H$^+$, 579.1906; found, 579.3683.

Co(II)-(*R,R*)-6 complex (9). Anhydrous CoI$_2$ was used as the metal salt according to procedure A. After 24 h, 0.025 g (0.043 mmol, 68% yield) of pink crystals were obtained from 0.034 g (0.128 mmol) of (*R,R*)-**6** and 0.077 g (0.247 mmol) of CoI$_2$. MS (*m/z*): [M + Na]$^+$calcd for C$_{28}$H$_{32}$N$_4$O$_6$Co·Na$^+$, 603.1630; found, 603.1624 (1.0 ppm).

Ni(II)-(*R,R*)-6 complex (10). Method A. Anhydrous Ni(OTf)$_2$ was used as the metal salt and the reaction was set up following procedure A. After 48 h, 0.036 g (0.062 mmol, 84% yield) of yellow crystals were obtained from 0.038 g (0.145 mmol) of (*R,R*)-**6** and 0.058 g (0.161 mmol) of Ni(OTf)$_2$. Method B. Anhydrous NiI$_2$ was used as the metal salt. After 48 h, 0.042 g (0.072 mmol, 73% yield) of yellow crystals were obtained from 0.052 g (0.198 mmol) of (*R,R*)-**6** and 0.099 g (0.318 mmol) of NiI$_2$. MS (*m/z*): [M + H]$^+$ calcd for C$_{28}$H$_{34}$N$_4$O$_6$Ni·H$^+$, 581.1910; found, 581.1893 (2.9 ppm).

Zn(II)-(*R,R*)-6 complex (11). Anhydrous ZnCl$_2$ was used as the metal salt. The reaction was set up following procedure A. After 48 h, 0.038 g (0.065mmol, 84% yield) of yellow crystals were obtained from 0.040 g (0.152 mmol) of (*R,R*)-**6** and 0.150 g (1.100 mmol) of ZnCl$_2$. ^{1}H NMR (DMSO-d_6, 400 MHz): δ 1.05-2.18 (m, 14 H), 3.16-4.34 (m, 10H), 6.79 (t, 1H), 7.62 (d, 1H), 8.03 (d, 1H), 8.45 (s, 1H). ^{13}C NMR (DMSO-d_6, 50MHz): δ 24.05, 27.64, 33.85, 48.62, 55.53,

63.79, 115.46, 121.47, 122.59, 124.33, 139.78, 165.48, 170.00, (the C=N carbon is broadened due to the quadropolar effect of ^{14}N) MS (m/z): [M + H]$^+$ calcd for $C_{28}H_{34}N_4O_6Zn\cdot H^+$, 587.1848; found, 587.1864 (2.7 ppm).

Cu(II)-(R,R)-4 complex (12). Method A. Anhydrous Cu(OTf)$_2$ was used as the metal salt. The reaction was set up following procedure A. After 24 h, 0.039 g (0.077 mmol, 86% yield) of maroon crystals were obtained from 0.047 g (0.179 mmol) of (R R)-**6** and 0.078 g (0.217 mmol) of Cu(OTf)$_2$. Method B. Anhydrous Cu(OTf)·C$_6$H$_5$CH$_3$ was used as the metal salt. After 24 h, 0.032 g (0.063 mmol) of maroon crystals were obtained from 0.041 g (0.157 mmol) of (R,R)-**6** and 0.043 g (0.083 mmol) of copper(I) trifluoromethanesulfonate toluene adduct, (CF$_3$SO$_3$)Cu·C$_6$H$_5$CH$_3$, 80% yield. ^{1}H and ^{13}C NMR spectra for this paramagnetic compound were unresolved. MS (m/z): [M + H]$^+$ calcd for $C_{22}H_{20}N_2O_6Cu\cdot H^+$, 472.0696; found, 472.0717 (4.4 ppm).

Complex (13). METHOD A. A saturated solution of anhydrous Cu(OTf)$_2$ and (R,R)-**7** (0.0095g, 0.022 mmol) were combined following the general procedure A. After a week, green colored crystals were obtained. The reaction yield could not be calculated as the quantity of the crystals was too small. METHOD B. This reaction was according to regular batch synthesis. TEA was added dropwise to a mixture of (R,R)-**7** (0.06 g, 0.139 mmol) in methanol (10 ml) until a clear yellow solution was obtained. To this was added Cu(OTf)$_2$ (0.114 g, 0.365 mmol). Green precipitate started to form immediately. After 16 of stirring under room temperature, the solution was filtered to give **13**, as a green solid (0.033 g, 61% yield). (MW: 777.00)

Complex (14). METHOD A. A saturated solution of anhydrous $FeCl_2$ and (*R,R*)-**4** (0.0298 g, 0.073 mmol) were combined following the general procedure A. After 2 days, 0.028 g (0.017 mmol, 52% yield) of red crystals were obtained. (MW: 1464.23). METHOD B. A saturated solution of anhydrous $FeCl_2$ and (*R,R*)-**4** (0.026 g, 0.063 mmol) were combined following the general procedure B. After 2 days, 0.032 g (0.015 mmol, 59% yield) of red crystals were obtained. METHOD C. A saturated solution of anhydrous $FeCl_2$ and (*R,R*)-**6** (0.014 g, 0.0533mmol) were combined following the general procedure B. After 2 days, 0.012 g (0.08 mmol, 61% yield) of red crystals were obtained.

Complex (16). A saturated solution of anhydrous CoI_2 and (*R,R*)-**4** (0.026 g, 0.063 mmol) were combined following the general procedure B. After 2 days, 0.017 g (0.011 mmol, 36% yield) of rose-colored crystals were obtained. (MW: 1482.76).

Complex (18). A saturated solution of anhydrous CoI_2 and (*R,R*)-**6** (0.014 g, 0.0533mmol) were combined following the general procedure B. After 3 days, 0.011 g (0.068 mmol, 51% yield) of red crystals were obtained. (MW: 1606.65).

Complex (21). A saturated solution of anhydrous NiI_2 and (*R,R*)-**6** (0.014 g, 0.0533mmol) were combined following the general procedure B. After 3 days, 0.009 g (0.036 mmol, 27% yield) of orange needles were obtained. (MW: 2473.31).

Complex (23). A saturated solution of anhydrous $Cu(OTf)_2$ and (*R,R*)-**6** (0.014 g, 0.0533mmol) were combined following the general procedure B. After a few hours, 0.002g (0.046 mmol, 28% yield) of maroon colored were obtained. (MW: 533.48). Complex 24 was obtained from the same reaction. However, no yields can be reported on this complex as the quantity was too small.

References

1. Masar, M. S.; Gianneschi, N.C.; Oleveri, C.G.; Stern, C. L.; Nguyen, S. T.; Mirking, C. A. *J. Am. Chem. Soc.* **2007**, *129*, 10149.

2. Rao, M.L.N.; Houjou, H.; Hiratani, K. *Chem. Commun.* **2002**, 420.

3. Thompson, A.; Dolphin, D. *J. Org. Chem.* **2000**, *65*, 7870.

4. Hannon, M.J.; Painting, C.L.; Jackson, A.; Hamblin, J.; Errington, W. *Chem. Commun.* **1997**, 1807.

5. Ma, C.; Han, Y.; Zhang, R. *J. Inorg. Organomet. Polym.* **2007**, *3*, 541.

6. Amendola, V.; Fabbrizzi, L.; Linati, L.; Mangano, C.; Pallavicini, P.; Pedrazzini, V.; Zema, M. *Eur. J. Chem.* **1999**, *5*, 3679.

7. He, Z.; He, C.; Wang, Z.; Gao, E.; Liu, Y.; Yan, C. *Dalton Trans.* **2004**, 502.

8. Fleming, J. S.; Psillakis, E.; Couchman, S. M.; Jeffery, J. C.; McCleverty, J. A.; Ward, M. D. *Dalton Trans.* **1998**, 537.

9. Xavier, K. O.; Chako, J.; Yusuff, K. K. M. *J. Mol. Catal. A: Chem.* **2002**, 275.

10. Carbonaro, L.; Isola, M.; Liuzzo, V.; Marchetti, F.; Balzano, F.; Pomelli, C. S.; Raffaelli, A. *Eur. J. Chem.* **2001**, 353.

11. Cui, Y.; Ngo, H. L.; White, P. S.; Lin, W. *Inorg. Chem.* **2003**, *42*, 652.

12. Reid, S. D.; Blake, A. J.; Wilson, C.; Love, J. B. *Inrog. Chem.* **2006**, *45*, 636.

13. Psillakis, E.; Jeffery, J. C.; McCleverty, J. A.; Ward, M. D. *J. Chem. Soc. Dalton Trans.* **1997**, 1645.

14. Rice, C. R.; Worl, S.; Jeffery, J. C.; Paul, R. L.; Ward, M. D. *J. Chem. Soc., Dalton Trans.* **2001**, 550.

15. Vazques, M.; Bermejo, M. R.; Fondo, M.; Garcia-Deibe, A.; Gonzalez, A. M.; Pedrido, R. *Eur. J. Inorg. Chem.* **2002**, 465.

16. Charbonniere, L. J.; Williams, A. F.; Frey, U.; Merbach, A. E.; Kamalaprija, P.; Schaad, O. *J. Am. Chem. Soc.* **1997**, *119*, 2488.

17. Erxleben, A.; Schumacher, D. *Eur. J. Inorg. Chem.* **2001**, 3039.

18. Heo, J.; Jeon, Y.; Mirkin, C. A. *J. Am. Chem. Soc.* **2007**, *129*, 7712.

19. Tefler, S. G.; Kuroda, R.; Lefebvre, J.; Leznoff, D. B. *Inorg. Chem.* **2006**, *45*, 4592.

20. Erxleben, A. *Inorg. Chem.* **2001**, *40*, 208.

21. Vazquez, M,; Bermejo, M. R.; Fondo, M,; Gonzalez, A. M.; Mahia, J,; Sorace, L.; Gatteschi, D. *Eur. J. Inorg. Chem.* **2001**, 1863.

22. Li, Z.; Jablonski, C. *Inorg. Chem.* **2000**, *39*, 2456.

23. Franceschi, F.; Guillemot, G.; Solari, E.; Floriani, C.; Re, N.; Birkedal, H.; Pattison, P. *Eur. J. Chem.* **2001**, *7*, 1468.

24. Vigato, P.A.; Tamburini, S. *Coord. Chem. Rev.* **2004**, 1717.

25. Lehn. J.M

26. Borisova, N. E.; Reshetova, M. D.; Ustynyuk, Y. A. *Chem. Rev.* **2007**, *107*, 46.

27. de Geest, D. J.; Noble, A.; Moubaraki, B.; Murrary, K. S.; Larsen, D. S.; Brooker, S. *J. Chem. Soc. Dalton Trans.* **2007,** 467.

28. Kim, G.; Park, D.; Tak, Y. *Catal. Lett.* **2000,** *65*, 127.

29. Furutachi, H.; Fujinami, S.; Suzuki, M.; Okawa, H. *J. Chem. Soc. , Dalton Trans.* **2000**, 2761.

30. Furutachi, H.; Ishida, A.; Miyasaka, H.; Fukita, N.; Ohbo, M.; Okawa, H.; Kiokawa, M. *J. Chem. Soc., Dalton Trans.* **1999**, 367.

31. Furutachi, H.; Okawa, H. *Inorg. Chem.* **1997**, *36*, 3911.

32. Shinoura, M.; Kita, S.; Ohba, M.; Okawa, H. *Inorg. Chem.* **2000**, *39*, 4520.

33. Kita, S.; Furutachi, H.; Okawa, H. *Inorg. Chem.* **1999**, *38*, 4038.

34. Bermejo, M. R.; Fernandez, M. I.; Gomes-Forneas, E.; Gonzalez-Noya, A.; Meneiro, M.; Perdido, R.; Rodrigues, M. J. *Eur. J. Inorg. Chem.* **2007**, 3789.

35. Okawa, H. *Inorg. Chim. Acta* **1987**, *129*, 173.

36. Okawa, H.; Kanda, W.; Kida, S. *Chem. Lett.* **1980**, 1281.

37. Bhadbhade, M. M.; Srinivas, D. *Inrog. Chem.* **1993**, *32*, 6122.

38. Sakiyama, H.; Okawa, H.; Oguni, N. *Bull. Chem. Soc. Jpn.* **1992,** *65*, 608.

39. Tuna, F.; Pascu, G. I.; Sutter, J.; Andruh, M.; Golhen, S.; Guillevis, J.; Pritzkow, H. *Inorg. Chim. Act.* **2003**, *342*, 131.

40. Andruh, M.; Ramade, I.; Codjovi, E.; Guillo, O.; Kahn, O.; Trombe, J. C. *J. Am. Chem. Soc.* **1993**, *115*, 1822.

41. Tanaka, M.; Okawa, H.; Tamura, T.; Kida, S. *Bull. Chem. Soc. Jpn.* **1974,** *47*, 1669.

42. Dey, K.; Maiti, R. K. *Indian J. Chem.; Sect. A* **1976**, *14A*, 602.

43. Ikeda, K.; Ohba, M.; Okawa, H. *J. Chem. Soc., Dalton Trans.* **2001**

44. Verma, R. K.; Mishra, B. K.; satpathy, K. C.; Mahapatra, A. *Asian J. Chem.* **1997**, *9,* 365.

45. Nag, J. K.; Das. D.; De, B. B.; Sinha, C. *J. Indian Chem. Soc.* **1998**, *75*, 496.

46. Amedola, V.; Fabbrizzi, L.; Mangano, C.; Pallavicini, P.; Roboli, E.; Zema, M. *Inorg. Chem.* **2000**, *39*, 5803.

47. Hannon, M. J.; Painting, C. L.; Alcock, N. W. *Chem Commun.* **1999**, 2023.

48. Reid, S. D.; Blake, A. J.; Kockenberger, W.; Wilson, C.; Love, J. B. *J. Chem. Soc., Dalton Trans.* **2003**, 4387.

49.   Albrecht, M. *Chem. Rev.* **2001**, *101*, 3457.

50.   Piguet, C.; Bernadinelli, G.; Hopfgartner, G. *Chem. Rev.* **1997**, *97*, 2005.

51.   Seitz, M.; Kaiser, A.; Stempfhuber, S.; Zabel, M.; Reiser, O. *J. Am. Chem. Soc.* **2004**, *126*, 11426.

52.   Seitz, M.; Kaise, A.; Powell, D. R.; Borovik, A. S.; Reiser, O. *Adv. Synth. Catal.* **2004**, *346*, 737.

53.   Lee, D.; Sorace, L.; Caneschi, A.; Lippard, S. J. *Inorg. Chem.* **2001**, *40,* 6774.

54.   Isele, K.; Gigon, F.; Williams, A. F.; Bernardinelli, G.; Franz. P.; Decurtins, S.; *J. Chem. Soc., Dalton Trans.* **2007,** 332.

55.   Hudson, T. A.; Berry, K. J.; Moubaraki, B.; Murray, K. S.; Robson, R. *Inorg. Chem.* **2006**, *45*, 3549.

56.   Oshio, H.; Hoshino, N, Ito, T.; Nakano, M. *J. Am. Chem. Soc.* **2004**, *162*, 8805.

57.   Kawagusi, H.; Matsu, T. *Chem. Commun.* **2002**, 958.

58.   Ribas-Arino, J.; Baruah, T.; Pederson, M. R. *J. Am. Chem. Soc.* **2006**, *128*, 9497.

59.   Wiznycia, A. *"The preparation and study of Bis(pyridyl-imine) and monohelical salen-type complexes of iron and zinc"* Dissertation document, Kansas State University, Manhatttan, **2006**. (a) p. 91 (b) p.31

60.   Tanaka, M.; Kitaoka, M. *Bull. Chem. Soc. Japan* **1976**, *49*, 2469.

61.   Torihara, N.; Okawa, H.; Kida, S. *Chem. Lett.* **1978**, 185.

62.   Zhang, W.; Hao, Y.; Yao, L.; Yu, Z. *Huaxue Yanjiu* **2005**, *16*, 49.

63.   (a) Larrow, J. F.; Jacobsen, E. N. *J. Org. Chem.* **1994**, *59*, 1939. (b) Brown, K. J.; Berry, M. S.; Murdock, J. R. *J. Org. Chem.* **1985**, *50*, 4345.

64.   Duff, J. C.; Bills, E. J. *J. Chem. Soc.* **1932**, 1957.

65. Williams, H. D.; Fleming, I. "Spectroscopic Methods in Organic Chemistry", The McGraw-Hill Companies, London, 5th edition. p.145-167

66. Zarembowitch, J.; Kahn, O. *Inorg. Chem.* **1984**, *23*, 589.

67. Sarkar, S.; Dey, K. *Spectrochim. Acta* **2005**, *62*, 383.

68. Jeon, Y.; Heo, J.; Mirkin. C. A. *Tetrahedron Lett.* **2007**, *48*, 2591.

69. Djedouani, A.; Bendaas, A.; Boufas, S.; Allain, M.; Bouet, G.; Khan, M. *Acta Crystallogr. Sec. E: Biol. Crystallogr.* **2007**, *E63*, 1271.

70. Childs, R.; Shaw, G. S. *J. Am. Chem. Soc.* **1988**, *110*, 3013.

71. Pi-pi

72. Knof, U.; Zelewsky von, A. *Angew. Chem. Int. Ed.* **1999**, *38*, 302.

73. Reid, S.D.; Blake, A. J.; Kocken berger, W.; Eilson, C.; Love, J. B. *J. Chem. Soc., Dalton Trans.* **2003**, 4387.

74. Dey, K.; Bhowmick, R.; Sarakr, S. *Synt. React. Inorg. Met.-Org. Chem.* **2002**, *32*, 1393.

75. Telfer, S. G.; Sato, T.; Harada, T.; Kuroda, R.; Lefebvre, J.; Leznoff, D. B. *Inorg. Chem.* **2004**, *43*, 6168.

76. Pallavicini, Op.; Amendola, V.; Fernansez, Y. D.; Ghisalberti, M.; Linani, L.; Mangano, C.; Manfredi, A. M.; Massera, C. *Dalton Trans.* **2003**, 575.

77. Zhu, H.; Liu, W.; Wang, Y.; Wang, D.; *Kristallogr. NCS* **2003**, *218*, 255.

78. Florez-Lopez, L.; Parra-Hake, M.; Somanathan, R.; Walch, P. J. *Organometallics,* **2000**, *19*, 2153.

79. Glowka, M. L.; Olczak, A.; Karolak-Wojciechowska, J.; Ciechanowska-Urbanska, E. *Acta. Cryst.* **1998**, *B54*, 250.

80. Abrahams, B. F.; Hudson, T. A; Robson, R. *J. Am. Chem. Soc.* **2004**, *126*, 8624.

81.   Abrahams, B. F.; Hudson, T. A.; Robson, R. *Eur. J. Chem.* **2006**, *12*, 7095.

82.   Oshio, H.; Hoshio, N.; Ito, T. *J. Am. Chem. Soc.* **2000**, *122*, 12602.

83.   http://stinet.dtic.mil/oai/oai?verb=getRecord&metadataPrefix=html&identifier=ADA306 382

84.   Yoon, S.; Lippard, S. J. *J. Am. Chem. Soc.* **2005**, *127*, 8386.

85.   Taft, K. L.; Papefthymiou, G. C.; Lippard, S. J. *Inorg. Chem.* **1994**, *33,* 1510.

86.   Taft, K. L.; Caneschi, A.; Pence, L. E.; Delfs, C. D.; Papefthymiou, G. C.; Lippard, S. J *J. Am. Chem. Soc.* **1993,** *115*, 11753.

87.   Crystal structure shows the presence of Cl⁻ instead of I⁻.

Appendix

Crystal Data

Table 1. Crystal data and structure refinement for (*R*,*R*)-4

Identification code	al0704m
Empirical formula	C56 H72 Fe6 N4 O24
Formula weight	1520.28
Temperature	120(2) K
Wavelength	0.71073 Å
Crystal system	Orthorhombic
Space group	P2(1)2(1)2(1)
Unit cell dimensions	a = 13.1631(14) Å $\quad$ a= 90°.
	b = 16.4553(17) Å $\quad$ b= 90°.
	c = 29.595(3) Å $\quad$ g = 90°.
Volume	6410.3(12) Å^3
Z	4
Density (calculated)	1.575 Mg/m^3
Absorption coefficient	1.403 mm^{-1}
F(000)	3136
Crystal size	0.20 x 0.15 x 0.08 mm^3
Theta range for data collection	1.38 to 30.36°.
Index ranges	-18<=h<=8, -23<=k<=23, -41<=l<=42
Reflections collected	115607
Independent reflections	19216 [R(int) = 0.0741]
Completeness to theta = 30.36°	99.6 %
Absorption correction	None
Max. and min. transmission	0.8960 and 0.7666
Refinement method	Full-matrix least-squares on F^2
Data / restraints / parameters	19216 / 2 / 810

Goodness-of-fit on F^2 1.088

Final R indices [I>2sigma(I)]   R1 = 0.0564, wR2 = 0.1250

R indices (all data)   R1 = 0.0860, wR2 = 0.1372

Absolute structure parameter   0.050(14)

Largest diff. peak and hole   2.000 and -0.558 e.Å^{-3}

Table 2. Crystal data and structure refinement for (*R,R*)-5

Identification code	al0605m
Empirical formula	C73 H50 Cl2 N4 O13
Formula weight	1262.07
Temperature	173(2) K
Wavelength	0.71073 Å
Crystal system	Monoclinic
Space group	P2(1)
Unit cell dimensions	a = 15.8949(17) Å $\alpha= 90°$.
	b = 11.0560(12) Å $\beta= 103.272(5)°$.
	c = 18.3156(18) Å $\gamma = 90°$.
Volume	3132.7(6) $Å^3$
Z	2
Density (calculated)	1.338 g/cm^3
Absorption coefficient	0.174 mm^{-1}
F(000)	1308
Crystal size	0.40 x 0.20 x 0.20 mm^3
Theta range for data collection	1.53 to 27.72°.
Index ranges	-20<=h<=20, -12<=k<=14, -23<=l<=23
Reflections collected	21849
Independent reflections	7582 [R(int) = 0.1413]
Completeness to theta = 27.72°	98.1 %
Absorption correction	None
Refinement method	Full-matrix least-squares on F^2
Data / restraints / parameters	7582 / 7 / 834
Goodness-of-fit on F^2	0.841
Final R indices [I>2sigma(I)]	R1 = 0.0823, wR2 = 0.1917
R indices (all data)	R1 = 0.2187, wR2 = 0.2478

Absolute structure parameter   0.2(3)

Extinction coefficient   0.037(3)

Largest diff. peak and hole   0.523 and -0.431 e.Å^{-3}

Table 3. Crystal data and structure refinement for (*R*,*R*)-6

Identification code	al0602
Empirical formula	C28 H36 N4 O6
Formula weight	524.61
Temperature	100(2) K
Wavelength	0.71073 Å
Crystal system	Orthorhombic
Space group	P2(1)2(1)2(1)
Unit cell dimensions	a = 6.1675(8) Å a= 90°.
	b = 11.9167(15) Å b= 90°.
	c = 18.033(2) Å g = 90°.
Volume	1325.3(3) Å^3
Z	2
Density (calculated)	1.315 Mg/m^3
Absorption coefficient	0.093 mm^{-1}
F(000)	560
Crystal size	0.24 x 0.24 x 0.18 mm^3
Theta range for data collection	2.05 to 28.37°.
Index ranges	-7<=h<=8, -15<=k<=15, -23<=l<=23
Reflections collected	10527
Independent reflections	1867 [R(int) = 0.0521]
Completeness to theta = 28.37°	97.3 %
Absorption correction	None
Refinement method	Full-matrix least-squares on F^2
Data / restraints / parameters	1867 / 0 / 184
Goodness-of-fit on F^2	1.095

Final R indices [I>2sigma(I)]   R1 = 0.0479, wR2 = 0.1163

R indices (all data)   R1 = 0.0567, wR2 = 0.1214

Absolute structure parameter   1.4(16)

Largest diff. peak and hole   0.403 and -0.219 e.Å^{-3}

Table 4. Crystal data and structure refinement for (*R*,*R*)-7

Identification code	al0601
Empirical formula	C56 H40 N4 O6
Formula weight	864.92
Temperature	446(2) K
Wavelength	0.71073 Å
Crystal system	Orthorhombic
Space group	P2(1)2(1)2(1)
Unit cell dimensions	a = 7.6898(6) Å $\alpha = 90°$.
	b = 16.4610(12) Å $\beta = 90°$.
	c = 33.257(2) Å $\gamma = 90°$.
Volume	4209.7(5) Å^3
Z	4
Density (calculated)	1.365 g/cm^3
Absorption coefficient	0.090 mm^{-1}
F(000)	1808
Crystal size	0.37 x 0.33 x 0.14 mm^3
Theta range for data collection	1.38 to 28.28°.
Index ranges	-10<=h<=9, -21<=k<=20, -43<=l<=42
Reflections collected	36266
Independent reflections	5743 [R(int) = 0.0313]
Completeness to theta = 28.28°	98.1 %
Absorption correction	None
Refinement method	Full-matrix least-squares on F^2
Data / restraints / parameters	5743 / 0 / 601
Goodness-of-fit on F^2	1.029
Final R indices [I>2sigma(I)]	R1 = 0.0411, wR2 = 0.1036
R indices (all data)	R1 = 0.0448, wR2 = 0.1067

Absolute structure parameter   0.6(10)

Largest diff. peak and hole   0.419 and -0.348 e.$Å^{-3}$

Table 5. Crystal data and structure refinement for (*R,R*)-8

Identification code	al0701m
Empirical formula	C28 H34 Fe N4 O6
Formula weight	578.44
Temperature	100(2) K
Wavelength	0.71073 Å
Crystal system	Monoclinic
Space group	P2(1)
Unit cell dimensions	a = 8.8032(4) Å $\quad$ α= 90°.
	b = 12.5533(6) Å $\quad$ β= 95.159(2)°.
	c = 12.3334(6) Å $\quad$ γ = 90°.
Volume	1357.43(11) Å^3
Z	2
Density (calculated)	1.415 g/cm^3
Absorption coefficient	0.605 mm^{-1}
F(000)	608
Crystal size	0.30 x 0.30 x 0.10 mm^3
Theta range for data collection	2.73 to 36.32°.
Index ranges	-14<=h<=14, -20<=k<=20, -20<=l<=20
Reflections collected	50859
Independent reflections	12859 [R(int) = 0.0255]
Completeness to theta = 36.32°	99.9 %
Absorption correction	Semi-empirical from equivalents
Max. and min. transmission	0.9420 and 0.8393
Refinement method	Full-matrix least-squares on F^2
Data / restraints / parameters	12859 / 1 / 370
Goodness-of-fit on F^2	1.028
Final R indices [I>2sigma(I)]	R1 = 0.0246, wR2 = 0.0648

R indices (all data)	R1 = 0.0264, wR2 = 0.0657
Absolute structure parameter	0.012(4)
Largest diff. peak and hole	0.654 and -0.282 e.Å^{-3}

Table 6. Crystal data and structure refinement for (*R,R*)-9

Identification code	al0614m
Empirical formula	C28 H34 Co N4 O6
Formula weight	581.52
Temperature	173(2) K
Wavelength	0.71073 Å
Crystal system	Monoclinic
Space group	P2(1)
Unit cell dimensions	a = 8.8100(8) Å $\alpha = 90°$.
	b = 12.4866(12) Å $\beta = 94.572(4)°$.
	c = 12.3007(12) Å $\gamma = 90°$.
Volume	1348.9(2) Å^3
Z	2
Density (calculated)	1.432 g/cm^3
Absorption coefficient	0.686 mm^{-1}
F(000)	610
Crystal size	0.35 x 0.20 x 0.08 mm^3
Theta range for data collection	1.66 to 27.89°.
Index ranges	-10<=h<=11, -15<=k<=16, -16<=l<=15
Reflections collected	9993
Independent reflections	5362 [R(int) = 0.0516]
Completeness to theta = 27.89°	97.2 %
Absorption correction	Semi-empirical from equivalents
Max. and min. transmission	1.000 and 0.629
Refinement method	Full-matrix least-squares on F^2
Data / restraints / parameters	5362 / 1 / 370
Goodness-of-fit on F^2	0.973
Final R indices [I>2sigma(I)]	R1 = 0.0465, wR2 = 0.1087

R indices (all data)   R1 = 0.0612, wR2 = 0.1193

Absolute structure parameter   0.001(16)

Largest diff. peak and hole   1.118 and -0.410 e.Å^{-3}

Table 7. Crystal data and structure refinement for (*R,R*)-10

Identification code	al0609m
Empirical formula	C28 H34 N4 Ni O6
Formula weight	581.30
Temperature	173(2) K
Wavelength	0.71073 Å
Crystal system	Monoclinic
Space group	P2(1)
Unit cell dimensions	a = 8.8657(7) Å $\alpha = 90°$.
	b = 12.5139(10) Å $\beta = 94.431(4)°$.
	c = 12.1221(9) Å $\gamma = 90°$.
Volume	1340.86(18) Å^3
Z	2
Density (calculated)	1.440 g/cm^3
Absorption coefficient	0.774 mm^{-1}
F(000)	612
Crystal size	0.35 x 0.25 x 0.20 mm^3
Theta range for data collection	1.68 to 28.29°.
Index ranges	-11<=h<=11, -16<=k<=15, -16<=l<=15
Reflections collected	12597
Independent reflections	5555 [R(int) = 0.0386]
Completeness to theta = 28.29°	95.1 %
Absorption correction	Semi-empirical from equivalents
Max. and min. transmission	1.000 and 0.753
Refinement method	Full-matrix least-squares on F^2
Data / restraints / parameters	5555 / 1 / 370
Goodness-of-fit on F^2	0.974
Final R indices [I>2sigma(I)]	R1 = 0.0395, wR2 = 0.1142

R indices (all data)   R1 = 0.0439, wR2 = 0.1197

Absolute structure parameter   0.043(14)

Largest diff. peak and hole   0.507 and -0.334 e.Å^{-3}

Table 8. Crystal data and structure refinement for (*R,R*)-11

Identification code	al0610
Empirical formula	C28 H34 N4 O6 Zn
Formula weight	587.96
Temperature	100(2) K
Wavelength	0.71073 Å
Crystal system	Monoclinic
Space group	P2(1)
Unit cell dimensions	a = 8.7802(7) Å $\quad$ α= 90°.
	b = 12.5067(10) Å $\quad$ β= 94.8560(10)°.
	c = 12.3400(10) Å $\quad$ γ = 90°.
Volume	1350.21(19) Å^3
Z	2
Density (calculated)	1.446 g/cm^3
Absorption coefficient	0.959 mm^{-1}
F(000)	616
Crystal size	0.54 x 0.12 x 0.04 mm^3
Theta range for data collection	1.66 to 28.27°.
Index ranges	-11<=h<=11, -16<=k<=16, -16<=l<=16
Reflections collected	15953
Independent reflections	6375 [R(int) = 0.0256]
Completeness to theta = 28.27°	97.6 %
Absorption correction	None
Max. and min. transmission	0.9626 and 0.6254
Refinement method	Full-matrix least-squares on F^2
Data / restraints / parameters	6375 / 1 / 370
Goodness-of-fit on F^2	1.026
Final R indices [I>2sigma(I)]	R1 = 0.0298, wR2 = 0.0707

R indices (all data)   R1 = 0.0319, wR2 = 0.0718

Absolute structure parameter   0.008(7)

Largest diff. peak and hole   0.608 and -0.204 e.Å^{-3}

Table 9. Crystal data and structure refinement for (*R,R*)-12

Identification code	al0611
Empirical formula	C23 H24 Cu N2 O7
Formula weight	503.98
Temperature	100(2) K
Wavelength	0.71073 Å
Crystal system	Monoclinic
Space group	P2(1)
Unit cell dimensions	a = 7.5321(7) Å $\alpha = 90°$.
	b = 16.0522(14) Å $\beta = 92.7830(10)°$.
	c = 17.4225(15) Å $\gamma = 90°$.
Volume	2104.0(3) Å^3
Z	4
Density (calculated)	1.591 g/cm^3
Absorption coefficient	1.089 mm^{-1}
F(000)	1044
Crystal size	0.08 x 0.12 x 0.45 mm^3
Theta range for data collection	2.34 to 28.30°.
Index ranges	-9<=h<=10, -21<=k<=21, -22<=l<=22
Reflections collected	18451
Independent reflections	9615 [R(int) = 0.0238]
Completeness to theta = 28.30°	96.1 %
Absorption correction	Semi-empirical from equivalents
Max. and min. transmission	1.000 and 0.767
Refinement method	Full-matrix least-squares on F^2
Data / restraints / parameters	9615 / 1 / 597
Goodness-of-fit on F^2	0.973
Final R indices [I>2sigma(I)]	R1 = 0.0335, wR2 = 0.0807

R indices (all data)	R1 = 0.0405, wR2 = 0.0844
Absolute structure parameter	0.009(9)
Largest diff. peak and hole	0.463 and -0.261 e.Å^{-3}

Table 10. Crystal data and structure refinement for (*R*,*R*)-13

dentification code	al0703m
Empirical formula	C38.45 H26.90 Cu2 N2 O8
Formula weight	772.00
Temperature	100(2) K
Wavelength	0.71073 Å
Crystal system	Monoclinic
Space group	P2(1)
Unit cell dimensions	a = 11.4428(7) Å α = 90°.
	b = 17.7113(13) Å β = 93.670(3)°.
	c = 16.1563(10) Å γ = 90°.
Volume	3267.6(4) Å^3
Z	4
Density (calculated)	1.569 g/cm^3
Absorption coefficient	1.361 mm^{-1}
F(000)	1574
Crystal size	0.30 x 0.25 x 0.20 mm^3
Theta range for data collection	1.71 to 29.57°.
Index ranges	-15<=h<=15, -23<=k<=22, -22<=l<=22
Reflections collected	59624
Independent reflections	15542 [R(int) = 0.0494]
Completeness to theta = 29.57°	96.4 %
Absorption correction	None
Max. and min. transmission	0.7725 and 0.6856
Refinement method	Full-matrix least-squares on F^2
Data / restraints / parameters	15542 / 7 / 879
Goodness-of-fit on F^2	1.029
Final R indices [I>2sigma(I)]	R1 = 0.0559, wR2 = 0.1320

R indices (all data)   R1 = 0.0991, wR2 = 0.1572

Absolute structure parameter   -0.009(12)

Largest diff. peak and hole 1.222 and -0.784 e.Å⁻

Table 11. Crystal data and structure refinement for (*R*,*R*)-14

Identification code	al0704m
Empirical formula	C56 H72 Fe6 N4 O24
Formula weight	1520.28
Temperature	120(2) K
Wavelength	0.71073 Å
Crystal system	Orthorhombic
Space group	P2(1)2(1)2(1)
Unit cell dimensions	a = 13.1631(14) Å α= 90°.
	b = 16.4553(17) Å β= 90°.
	c = 29.595(3) Å γ = 90°.
Volume	6410.3(12) Å^3
Z	4
Density (calculated)	1.575 Mg/m^3
Absorption coefficient	1.403 mm^{-1}
F(000)	3136
Crystal size	0.20 x 0.15 x 0.08 mm^3

Theta range for data collection   1.38 to 30.36°.

Index ranges   -18<=h<=8, -23<=k<=23, -41<=l<=42

Reflections collected   115607

Independent reflections   19216 [R(int) = 0.0741]

Completeness to theta = 30.36°   99.6 %

Absorption correction   None

Max. and min. transmission   0.8960 and 0.7666

Refinement method   Full-matrix least-squares on F^2

Data / restraints / parameters   19216 / 2 / 810

Goodness-of-fit on F^2 1.088

Final R indices [I>2sigma(I)]   R1 = 0.0564, wR2 = 0.1250

R indices (all data)   R1 = 0.0860, wR2 = 0.1372

Absolute structure parameter   0.050(14)

Largest diff. peak and hole 2.000 and -0.558 e.Å^{-3}

Table 12. Crystal data and structure refinement for (*R*,*R*)-16

Identification code	al0708m
Empirical formula	C56 H80 Co6 N4 O24
Formula weight	1546.82
Temperature	120(2) K
Wavelength	0.71073 Å
Crystal system	Orthorhombic
Space group	P2(1)2(1)2(1)
Unit cell dimensions	a = 13.1068(5) Å $\quad\quad$ $\alpha= 90°$.
	b = 16.6810(6) Å $\quad\quad$ $\beta= 90°$.
	c = 28.9025(10) Å $\quad\quad$ $\gamma = 90°$.
Volume	6319.1(4) Å^3
Z	4
Density (calculated)	1.626 g/cm^3
Absorption coefficient	1.621 mm^{-1}
F(000)	3192
Crystal size	0.20 x 0.15 x 0.08 mm^3
Theta range for data collection	1.41 to 31.51°.
Index ranges	-19<=h<=19, -24<=k<=20, -39<=l<=42
Reflections collected	90853
Independent reflections	20921 [R(int) = 0.0593]
Completeness to theta = 31.51°	99.5 %
Absorption correction	Semi-empirical from equivalents
Max. and min. transmission	0.8812 and 0.7375
Refinement method	Full-matrix least-squares on F^2
Data / restraints / parameters	20921 / 0 / 824
Goodness-of-fit on F^2	0.985
Final R indices [I>2sigma(I)]	R1 = 0.0408, wR2 = 0.0875

R indices (all data)   R1 = 0.0590, wR2 = 0.0954

Absolute structure parameter   0.009(8)

Largest diff. peak and hole   1.000 and -0.483 e.Å^{-3}

Table 12. Crystal data and structure refinement for (*R*,*R*)-18

Identification code	al0712
Empirical formula	C52.40 H99.20 Co6 I2 N8 O18.70
Formula weight	1747.98
Temperature	100(2) K
Wavelength	0.71073 Å
Crystal system	Triclinic
Space group	P1
Unit cell dimensions	a = 12.0370(13) Å $\alpha = 64.8250(10)°$.
	b = 12.4183(13) Å $\beta = 71.5110(10)°$.
	c = 13.8405(14) Å $\gamma = 82.2510(10)°$.
Volume	1775.7(3) $Å^3$
Z	1
Density (calculated)	1.635 g/cm^3
Absorption coefficient	2.306 mm^{-1}
F(000)	887
Crystal size	0.19 x 0.14 x 0.14 mm^3
Theta range for data collection	1.78 to 28.31°.
Index ranges	-15<=h<=15, -16<=k<=16, -18<=l<=18
Reflections collected	21128
Independent reflections	15913 [R(int) = 0.0166]
Completeness to theta = 28.31°	94.8 %
Absorption correction	None
Refinement method	Full-matrix least-squares on F^2
Data / restraints / parameters	15913 / 9 / 799
Goodness-of-fit on F^2	1.038
Final R indices [I>2sigma(I)]	R1 = 0.0391, wR2 = 0.1028
R indices (all data)	R1 = 0.0410, wR2 = 0.1041

Absolute structure parameter   0.045(11)

Largest diff. peak and hole   1.387 and -0.791 e.Å^{-3}

Table 13. Crystal data and structure refinement for (*R*,*R*)-22

Identification code	al0716
Empirical formula	C17 H26 Cu2 N2 O6
Formula weight	481.48
Temperature	100(2) K
Wavelength	0.71073 Å
Crystal system	Triclinic
Space group	P1
Unit cell dimensions	a = 9.2895(7) Å α= 111.875(4)°.
	b = 10.3641(10) Å β= 92.445(5)°.
	c = 11.2757(10) Å γ = 108.572(5)°.
Volume	938.77(14) Å^3
Z	2
Density (calculated)	1.703 g/cm^3
Absorption coefficient	2.302 mm^{-1}
F(000)	496
Crystal size	0.42 x 0.198 x 0.086 mm^3
Theta range for data collection	2.27 to 27.70°.
Index ranges	-9<=h<=12, -13<=k<=11, -14<=l<=12
Reflections collected	6438
Independent reflections	6438 [R(int) = 0.0000]
Completeness to theta = 27.70°	98.0 %
Absorption correction	None
Refinement method	Full-matrix least-squares on F^2
Data / restraints / parameters	6438 / 3 / 488
Goodness-of-fit on F^2	1.057
Final R indices [I>2sigma(I)]	R1 = 0.0564, wR2 = 0.1340
R indices (all data)	R1 = 0.0932, wR2 = 0.1505

Absolute structure parameter   0.01(3)

Largest diff. peak and hole   1.309 and -0.831 e.Å^{-3}

Table 14. Crystal data and structure refinement for (*R*,*R*)-23

Identification code	al0709m
Empirical formula	C24 H26 Cu2 N2 O8
Formula weight	597.55
Temperature	120(2) K
Wavelength	0.71073 Å
Crystal system	Monoclinic
Space group	P2(1)
Unit cell dimensions	a = 9.1716(3) Å α = 90°.
	b = 20.2618(6) Å β = 108.962(2)°.
	c = 13.0903(5) Å γ = 90°.
Volume	2300.60(13) Å^3
Z	4
Density (calculated)	1.725 g/cm^3
Absorption coefficient	1.904 mm^{-1}
F(000)	1224
Crystal size	0.25 x 0.10 x 0.08 mm^3
Theta range for data collection	1.64 to 30.51°.
Index ranges	-12<=h<=13, -28<=k<=28, -18<=l<=18
Reflections collected	37486
Independent reflections	12871 [R(int) = 0.0422]
Completeness to theta = 30.51°	99.8 %
Absorption correction	None
Max. and min. transmission	0.8626 and 0.6475
Refinement method	Full-matrix least-squares on F^2
Data / restraints / parameters	12871 / 1 / 665
Goodness-of-fit on F^2	1.028
Final R indices [I>2sigma(I)]	R1 = 0.0353, wR2 = 0.0747

R indices (all data)   R1 = 0.0563, wR2 = 0.0817

Absolute structure parameter   0.003(12)

Largest diff. peak and hole   0.464 and -0.546 e.Å^{-3}